Magnetic Iron Oxide Nanoparticles: Synthesis, Stabilization, Vectorization, Physicochemical Characterizations, and Biological Applications

Sophie Laurent,[†] Delphine Forge,[†] Marc Port,[‡] Alain Roch,[†] Caroline Robic,[‡] Luce Vander Elst,[†] and Robert N. Muller*,[†]

Department of General, Organic, and Biomedical Chemistry, NMR and Molecular Imaging Laboratory, University of Mons-Hainaut, B-7000 Mons, Belgium, and Guerbet, Centre de Recherche, BP 57400, 95943 Roissy CdG Cedex, France

Contents

1. Introduction

In the past decade, the synthesis of superparamagnetic nanoparticles has been intensively developed not only for its fundamental scientific interest but also for many technological applications: among others, magnetic storage media,[1] biosensing applications,[2] medical applications, such as targeted drug delivery,[3,4] contrast agents in magnetic resonance imaging (MRI),[5–12] and magnetic inks for jet printing.[13] The control of the monodisperse size is very important because the properties of the nanocrystals strongly depend upon the dimension of the nanoparticles. To understand ferrofluid behavior and to improve applications or develop new ones, careful studies related to fluid stability, control of surfactants, particle sizes, materials, and physical behavior are essential.

Superparamagnetic iron oxide nanoparticles with appropriate surface chemistry can be used for numerous *in vivo* applications, such as MRI contrast enhancement, tissue repair, immunoassay, detoxification of biological fluids, hyperthermia, drug delivery, and cell separation.[14] All of these biomedical applications require that the nanoparticles have high magnetization values, a size smaller than 100 nm, and a narrow particle size distribution. These applications also need peculiar surface coating of the magnetic particles, which has to be nontoxic and biocompatible and must also allow for a targetable delivery with particle localization in a specific area. Such magnetic nanoparticles can bind to drugs, proteins, enzymes, antibodies, or nucleotides and can be directed to an organ, tissue, or tumor using an external magnetic field.[15] A number of approaches have been described to produce magnetic nanoparticles.[16,17]

In this review, we summarize the chemical routes for the synthesis of superparamagnetic iron oxide nanoparticles

* To whom correspondence should be addressed: Department of General, Organic, and Biomedical Chemistry, NMR and Molecular Imaging Laboratory, University of Mons-Hainaut, B-7000 Mons, Belgium. Telephone/Fax: +32-65-373520. E-mail: robert.muller@umh.ac.be.
† University of Mons-Hainaut.
‡ Guerbet.

Sophie Laurent was born in 1967. Her studies were performed at the University of Mons-Hainaut (Belgium), where she received her Ph.D. degree in chemistry in 1993. She joined then Prof. R. N. Muller's team and was involved in the development (synthesis and physicochemical characterization) of paramagnetic Gd complexes and super paramagnetic iron oxide nanoparticles as contrast agents for MRI. She is currently working on the vectorization of contrast agents for molecular imaging.

Delphine Forge was born in 1982 in Belgium. Her studies were performed at the University of Mons-Hainaut, where she received her Master's degree in chemistry in 2004. At present, she is in the third year of her thesis at the NMR laboratory in the group of Professor Robert. N. Muller. Her research interests are in the optimization of the synthesis of iron oxide nanoparticles for different applications, such as MRI contrast agents, hyperthermia, cell labeling, etc. Her expertise covers the synthesis of magnetite and physical characterization methods, such as magnetometry and relaxometry, to understand the role of the different factors on the size of the nanoparticles.

Marc Port did his graduate work with Robert Lett at the University of Paris 6 (Ph.D. degree in 1995), where he achieved a new total synthesis of 19-nor-steroid. Thereafter, he did postdoctoral training in medicinal chemistry at the Institut de Chimie Pharmaceutique A. Lespagnol (Lille). In 1995, he joined Guerbet, where he is currently the head of the Drug Discovery Department. He is the co-author of more than 40 publications, including 10 patents in the field of contrast agents. Since 2004, he is also the Invited Professor in medicinal and diagnostic chemistry at the Conservatoire National des Arts et Metiers (Paris).

Alain Roch was born in 1952 in Belgium. He obtained an engineer degree in nuclear chemistry. He achieved a Master's degree in chemistry in 1987. He works under the supervision of Professor R. N. Muller and obtained his Ph.D. degree in 1994 for the development of a theoretical model that predicts the proton relaxation of superparamagnetic colloids. He works as a Senior Researcher in the NMR and Molecular Imaging Laboratory of the University of Mons-Hainaut. He is in charge of the development of the superparamagnetic relaxation theories and its use in the characterization of superparamagnetic particles.

(classic synthesis by precipitation, high-temperature reactions, reactions in steric environments, sol−gel reactions, decomposition of organometallic precursors, polyol methods, etc.), fluid stabilization (using electrostatic layer or sterical repulsion), surface modification for grafting biomolecules (different methods of particle vectorization), the different techniques for structural and physicochemical characterization [photon correlation spectroscopy (PCS), magnetometry and relaxivity profiles (NMRD curves), transmission electron microscopy (TEM) images, and X-ray diffraction (XRD)], and we give some biomedical applications (MRI, cellular targeting, hyperthermia, *in vitro* bioseparation, etc.). At the present time, magnetic iron oxide nanoparticles are routinely used as contrast agents for targeting organs (liver and spleen) or lymph nodes. New developments are focused on targeting through molecular imaging and cell tracking. A challenge is the functionalization of nanoparticle surfaces.

Another challenge is the synthesis of stealth nanoparticles able to circulate in the blood compartment for a prolonged time and bearing ligands able to facilitate their specific internalization in tumor cells.

Published reviews, up to now, have highlighted the chemical aspects, such as synthesis and characterization, along with biomedical applications, all of which aim at developing very successful contrast agents intended for molecular imaging. However, they have only in part covered physicochemical properties, important to understand the action of the particles and to improve their efficiency. Also, other reviews give generalities about particles without focusing specifically on iron oxide particles.

This review, on the other hand, constitutes a more complete view of superparamagnetic iron oxide nanoparticles. It includes greater emphasis on synthesis and characterization, delves into all physicochemical properties, and gives some examples of biomedical applications in the field of molecular imaging and cell targeting.

Caroline Robic is an engineer from the Ecole Nationale Superieure des Industries Chimiques (1999). She received her Ph.D. degree in 2002, working at the Commissariat à l'Energie Atomique (CEA) on the rheological behavior of liquid crystal polymers. Then, she did postdoctoral research at the Ecole Supérieure de Physique et de Chimie Industrielles (ESPCI), investigating the recognition of antibodies with antigens grafted in magnetic colloids. In 2005, she joined Guerbet, where she is in charge of the synthesis and physicochemical characterization of iron oxide nanoparticles.

Luce Vander Elst was born in 1955. She studied at the University of Mons-Hainaut, where she obtained her Ph.D. degree in 1984. She did postdoctoral research on the multinuclear NMR analysis of the metabolism of perfused mammalian hearts at the Medical School of Harvard University in 1986. She works as a Professor in the NMR and Molecular Imaging Laboratory of the University of Mons-Hainaut. Her research focuses mainly on high-resolution NMR and the physiso-chemical characterization of MRI contrast agents.

## 2. Synthesis of Magnetic Nanoparticles

Numerous chemical methods can be used to synthesize magnetic nanoparticles for medical imaging applications: microemulsions,[18] sol−gel syntheses,[19] sonochemical reactions,[20] hydrothermal reactions,[21] hydrolysis and thermolysis of precursors,[22] flow injection syntheses,[23] and electrospray syntheses.[24] The synthesis of superparamagnetic nanoparticles is a complex process because of their colloidal nature. The first main chemical challenge consists of defining experimental conditions, leading to a monodisperse population of magnetic grains of suitable size. The second critical point is to select a reproducible process that can be industrialized without any complex purification procedure, such as ultracentrifugation,[25] size-exclusion chromatography,[26] magnetic filtration,[9] or flow field gradient.[27] These methods have been used to prepare particles with homogeneous composition and narrow size distribution. However, the most common method for the production of magnetite nanoparticles is the chemical coprecipitation technique of iron salts.[28–32]

Robert N. Muller was born in 1948 and studied at the University of Mons-Hainaut, Belgium, from which he graduated with a Lic. Sci. degree in 1969. He obtained his Ph.D. degree in 1974 from the University of Mons-Hainaut, where he was successively appointed Assistant Lecturer and Professor. He did postdoctoral studies in Magnetic Resonance Imaging (MRI) in Paul C. Lauterbur's research group at the State University of New York at Stony Brook from 1981−1982 and was on sabbatical leave at the CERM, Florence, Italy, with Professors Ivano Bertini and Claudio Luchinat from 2002−2003. He is the co-founder of the European Workshop on Nuclear Magnetic Resonance in Medicine, vice-chairman of the European Magnetic Resonance Forum Foundation, 1991−present, president of the European Society for Magnetic Resonance in Medicine and Biology, 1987−1988, president of the Groupe de Recherche sur les Applications du Magnétisme en Médecine (GRAMM), 1998−2000, founding member of the European Society for Molecular Imaging (ESMI), editor-in-chief of the new journal *Contrast Media and Molecular Imaging* (Wiley), and member of the editorial boards of *Magnetic Resonance Materials MAGMA* (Springer) and *Investigative Radiology* (Lipincott). He published around 160 publications and 6 books. In recent years, his research interests were mainly in NMR relaxometry and spectroscopy and the development and applications of contrast agents for magnetic resonance molecular imaging.

2.1. Classical Synthesis by Coprecipitation

The coprecipitation technique is probably the simplest and most efficient chemical pathway to obtain magnetic particles. Iron oxides (either Fe_3O_4 or γFe_2O_3) are usually prepared by an aging stoichiometric mixture of ferrous and ferric salts in aqueous medium. The chemical reaction of Fe_3O_4 formation may be written as eq 1.

$$Fe^{2+} + 2Fe^{3+} + 8OH^- \rightarrow Fe_3O_4 + 4H_2O \qquad (1)$$
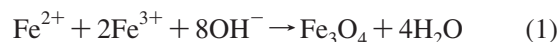
According to the thermodynamics of this reaction, complete precipitation of Fe_3O_4 should be expected at a pH between 8 and 14, with a stoichiometric ratio of 2:1 (Fe^{3+}/Fe^{2+}) in a non-oxidizing oxygen environment.[33]

However, magnetite (Fe_3O_4) is not very stable and is sensitive to oxidation. Magnetite is transformed into maghemite (γFe_2O_3) in the presence of oxygen.

$$Fe_3O_4 + 2H^+ \rightarrow \gamma Fe_2O_3 + Fe^{2+} + H_2O \qquad (2)$$
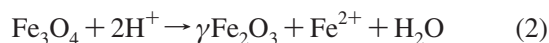
Oxidation in air is not the only way to transform magnetite (Fe_3O_4) into maghemite (γFe_2O_3). Various electron or ion transfers depending upon the pH of the suspension are involved, according to eq 2. Under acidic and anaerobic conditions, surface Fe^{2+} ions are desorbed as hexa-aqua complexes in solution, whereas, under basic conditions, the oxidation of magnetite involves the oxidation−reduction of the surface of magnetite. The oxidation of ferrous ions is always correlated with migration of cations through the lattice framework, creating cationic vacancies to maintain the charge

balance, explaining the structure of maghemite. In maghemite, iron ions are distributed in the octahedral (Oh) and tetrahedral (Td) sites of the spinel structure (formula 1), but maghemite differs from magnetite by the presence of cationic vacancies within the octahedral site. The vacancies ordering scheme is closely related to the sample preparation method and results in symmetry lowering and possibly superstructures. The vacancies can be completely random or partially or totally ordered. It has been shown, essentially from combined IR spectroscopy and X-ray diffraction, that vacancy ordering occurs only for particles exceeding 5 nm.[34]

$$Fe_3O_4 : [Fe^{3+}]_{Td}[Fe^{3+}Fe^{2+}]_{Oh}O_4$$
$$\gamma Fe_2O_3 : 0.75[Fe^{3+}]_{Td}[Fe^{3+}_{5/3}V_{1/3}]_{Oh}O_4$$

formula 1 : structure of magnetite and maghemite
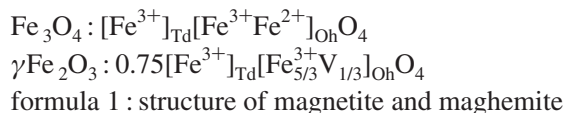
The main advantage of the coprecipitation process is that a large amount of nanoparticles can be synthesized. However, the control of particle size distribution is limited, because only kinetic factors are controlling the growth of the crystal. In the coprecipitation process, two stages are involved:[35–40] a short burst of nucleation occurs when the concentration of the species reaches critical supersaturation, and then, there is a slow growth of the nuclei by diffusion of the solutes to the surface of the crystal. To produce monodisperse iron oxide nanoparticles, these two stages should be separated; i.e., nucleation should be avoided during the period of growth.[17]

The LaMer diagram[41] illustrates the formation of mono-dispersed nano- and microparticles with the nucleation and crystal growth mechanisms. In a supersaturated solution when the nuclei form at the same time, subsequent growth of these nuclei results in the formation of particles with a very narrow size distribution.[42] In conclusion, size control of monodispersed particles must normally be performed during the very short nucleation period, because the final particle number is determined by the end of the nucleation and it does not change during particle growth. A wide variety of factors can be adjusted in the synthesis of iron oxide nanoparticles to control size, magnetic characteristics, or surface properties. A number of studies have dealt with the influence of these different factors.[43–49]

The size and shape of the nanoparticles can be tailored with relative success by adjusting pH, ionic strength, temperature, nature of the salts (perchlorates, chlorides, sulfates, and nitrates), or the Fe^{II}/Fe^{III} concentration ratio. Particles with size ranging from 2 to 17 nm can be thus obtained. The influence of different parameters (media composition, Fe^{II}/Fe^{III} ratio, injection fluxes, iron and TMAOH concentration, temperature, and oxygen) on magnetic properties and size has been studied in a basic coprecipitation process.[9]

The addition of chelating organic anions (carboxylate or α hydroxy carboxylate ions, such as citric, gluconic, or oleic acid) or polymer surface complexing agents (dextran, carboxydextran, starch, or polyvinyl alcohol) during the formation of magnetite can help to control the size of the nanoparticles. This aspect will be analyzed in the section dedicated to the stabilization by polymers. According to the molar ratio between the organic ion and the iron salts, the chelation of these organic ions on the iron oxide surface can either prevent nucleation and then lead to larger particles or inhibit the growth of the crystal nuclei, leading to small nanoparticles.

The Massart process describes the coprecipitation without molecules for stabilization. The syntheses in the presence of those kinds of molecules will be developed afterward.

The first controlled preparation of superparamagnetic iron oxide particles using alkaline precipitation of $FeCl_3$ and $FeCl_2$ was performed by Massart.[50] In the original synthesis, magnetite (Fe_3O_4) particles were roughly spherical, and their diameter measured by XRD was 8 nm.[51] The parameters of this process were carefully studied to demonstrate the influence of the base (ammonia, CH_3NH_2, and NaOH),[40,51] of the pH value, of added cations [$N(CH_3)_4^+$, $CH_3NH_3^+$, Na^+, Li^+, K^+, and NH_4^+] and the Fe^{2+}/Fe^{3+} ratio on the yield of the coprecipitation reaction and the diameter and polydispersity of the nanoparticles. When all of these parameters are modulated, it is possible to obtain particles with a size ranging from 16.6 to 4.2 nm.[51] Other studies have demonstrated that the modulation of acidity and ionic strength enables the tailoring of the particle size in the range of 2−15 nm. The shape variation is related to the variation of the electrostatic surface density of the nanoparticles.[52–54] The particles can be dispersed in either aqueous media or nonpolar liquids, such as oil or organic solvents, allowing for the preparation of magnetic emulsion, capsules, and vesicles.[55–57] The process engineered by Massart[58] for rapid synthesis of homogeneous γFe_2O_3 nanoparticles allowed for coating by a wide range of monomeric species, such as amino acids, α-hydroxyacids (citric, tartaric, and gluconic acids),[59] hydroxamate (arginine hydroxamate),[60] dimercaptosuccinic acid (DMSA),[61,62] or phosphoryl choline.[63] Conductimetric measurements and adsorption isotherm curves showed that DMSA is oxidized during the coating process in tetrameric polysulfide chains [DMSAox]$_4$, which are absorbed through the carboxylate moiety on the particles after alkalinization and neutralization to obtain stable particles at pH 7.[61,62]

Adding increasing amounts of citrate ions in the Massart process allows for a decrease in the diameter of citrate-coated nanoparticles from 8 to 3 nm. The effect of citrate can be rationalized by two processes: the chelation of citrate with iron ions prevents nucleation, and the adsorption of citrate on the nuclei produces hydrolysis, inhibiting the growth of the nuclei.[64]

Size selection is a process where an electrolyte solution or a nonsolvent is added to a stable colloid solution to disrupt it, causing larger particles to precipitate and leaving smaller and nearly monodisperse particles in the supernatant. Through such a process of size selection using NaCl as an extra electrolyte, the size distribution of the 7 nm citrate nanoparticles obtained by the Massart process can be reduced.[65,66] This size-sorting process was also reported on cationic Massart nanoparticles using nitric acid as an electrolyte and allowed to fractionate the particle size distribution with a very good yield.[67] Jolivet et al.[68] have studied the influence of the Fe^{2+}/Fe^{3+} ratio on the composition, size, morphology, and magnetic properties of coprecipitated nanoscale particles. Small values of the $x = Fe^{2+}/Fe^{3+}$ ratio are known to lead to goethite formation. For $x = 0.3$, two distinct phases are coexisting: one that it is likely to be an oxyhydroxide and is made of 4 nm sized particles with a low Fe^{2+} content (Fe^{2+}/Fe^{3+} about 0.07) and the other that is a nonstochiometric magnetite and consists of larger particles having a variable size and a composition Fe^{2+}/Fe^{3+} around 0.33. For $x = 0.35$, the latter phase is the only constituent and its Fe^{2+}/Fe^{3+} ratio is equal to x. For $x = 0.5$ corresponding to

magnetite stochiometry, particles are found to be homogeneous in size and composition.[69]

Babes et al.[9] have also studied the influence of different parameters, including the iron media and the iron concentration. In their setup, the most important factor is the Fe^{2+}/Fe^{3+} molar ratio. The mean size increased with the Fe^{2+}/Fe^{3+} ratio, whereas the preparation yield decreased. These results are corroborated by literature data.[51,69,70] Only particles synthesized with ratios between 0.4 and 0.6 are effective enough to be used as contrast agents.

The second most important factor influencing the synthesis is the iron concentration. The evolution of this factor is similar to that of the Fe^{2+}/Fe^{3+} ratio, with an optimum between 39 and 78 mM.

The particle mean size of magnetite is strongly dependent upon the acidity and the ionic strength of the precipitation medium.[71–73] The higher the pH and ionic strength, the smaller the particle size and size distribution width will be, because these parameters determine the chemical composition of the crystal surface and consequently the electrostatic surface charge of the particles.[17]

Qiu et al. investigated the dependence of the ionic strength of the reaction solution on the formation of magnetite.[74] The magnetite prepared with the addition of 1 M NaCl aqueous solution created iron oxide nanoparticles 1.5 nm smaller than those formed without its presence. In addition, these smaller nanoparticles formed in the higher ionic strength solutions display lower saturation magnetization (63 emu/g) than those prepared in NaCl-free solutions (71 emu/g). The lower magnetization was attributed to the decrease in size of the particle when prepared in the higher ionic strength media.

Some other factors have an influence on the size of the nanoparticles. For example, an increase of the mixing rate tends to decrease the particle size. In the same way, a decrease of the size as well as the polydispersity is observed when the base is added to the reactives as compared to the opposite process.[51] On the contrary, injection flux rates dot not seem to have a preponderant influence on the nanoparticle synthesis.[9]

Several researchers report the use of an elevated reaction temperature and suggest its significance in optimal crystal formation.[75] The different studies show that the formation of magnetite particles decreases with an increase in the temperature.[40,9] The investigations support the theory of nucleation and growth of the particles.

Bubbling nitrogen gas through the solution not only protects against critical oxidation of the magnetite but also reduces the particle size when compared to methods without oxygen removal.[76,77]

Magnetite nanoparticles, prepared by coprecipitation of Fe^{2+} and Fe^{3+} with NH_4OH, can be stabilized with silica to form well-dispersed magnetic silica nanospheres. An advantage of silica coating is the established surface chemistry for silica surface modification. The hydroxyl surface groups can be chemically modified to afford different bioconjugation groups, such as amine and carboxylate. The size of the particles can be controlled by changing the SiO_2/Fe_3O_4 ratio. Aminosilane has been covalently coupled to the surface of the magnetic silica nanoparticles and activated by glutaraldehyde to immobilize BSA.[78,79]

2.2. Reactions in Constrained Environments

Given that the particles obtained with the coprecipitation method have a broad size distribution, numerous other methods are currently being developed to produce nanoparticles with more uniform dimensions. Several attempts to form iron oxide nanoparticles of well-defined size using synthetic and biological nanoreactors have been reported. The constrained environments include amphoteric surfactants to create water-swollen reversed micellar structures in nonpolar solvents,[80–86] apoferritin protein cages,[87–90] dendrimers,[91] cyclodextrins,[92,93] and phospholipid membranes that form vesicles with iron oxide nanoparticles serving as solid supports.[94,95]

Carboxylated PAMAM dendrimers (generation 4.5) have been used as a stabilizing iron oxide coating.[91,96] Oxidation of Fe^{II} at a slightly elevated pH and temperature has resulted in the formation of water-soluble magnetodendrimers (nanocomposite of iron oxide and dendrimer), with an overall TEM diameter of 8 nm and a hydrodynamic diameter of 20–30 nm. The basic hydrolysis of Fe^{2+} ions in the presence of the water-soluble γ cyclodextrin allows for the acquisition of nanoparticles with a small diameter of 1.8 nm.[92] Ferritin can be demineralized affording apoferritin with an 8 nm internal cavity, which is used as a nanoreactor to slowly oxidize ferrous salts with air to provide spherical magnetoferritin encapsulating iron oxide nanoparticles of 6 nm in diameter.[87]

Surfactant molecules may spontaneously form nanodroplets of different sizes, micelles (1–10 nm) or water-in-oil emulsions (10–100 nm).[97] In these nanodroplet technologies, aqueous iron salt solutions are encapsulated by a surfactant coating that separates them from a surrounding organic solution. Consequently, this system can impose kinetic and thermodynamic constraints on particle formation, such as a nanoreactor. The surfactant-stabilized nanoreactor provides a confinement that limits particle nucleation and growth. The main advantage of the reverse micelle or emulsion technology is the diversity of nanoparticles that can be obtained by varying the nature and amount of surfactant and cosurfactant, the oil phase, or the reacting conditions.

The first magnetic nanoparticles formed in micelles were produced by oxidation of Fe^{2+} salts in γFe_2O_3 and Fe_3O_4.[98] The size of the magnetite particle can be controlled by the temperature and the surfactant concentration. Variations in the temperature and concentration of iron dodecyl sulfate $Fe(DS)_2$ micelles allow for the acquisition of particles of diameters ranging from 3.7 to 116 nm.[99] The inexpensive large-scale synthesis of uniform and highly crystalline magnetite nanoparticles using the reverse micelles technology at high temperature has been recently described by Lee.[100] In this work, the particle size could be adjusted from 2 to 10 nm by varying the relative proportion of the iron salts, the surfactant, and the solvent.

The water-in-oil emulsions are currently being used to synthesize superparamagnetic iron oxide nanoparticles[76,101–103] with a narrow size range and uniform physical properties because of the ability to control the size and shape of the nanoparticles.[104] This system is formed by well-defined nanodroplets of the aqueous phase, dispersed by the assembly of surfactant molecules in a continuous hydrocarbon phase.[105] The main advantage of using this type of emulsion system is that the size of the nanoparticles can be controlled by modulating the size of the aqueous droplets core.[106] Indeed, using variable reaction temperatures results in magnetites with diameters of 3–12 nm. The metal and base concentrations can also be used to vary the nanoparticle size.[107]

Salazar-Alvarez[108] has reported the synthesis of iron oxide nanoparticles by the use of reverse emulsions. The nanoemulsion system consisted of AOT-BuOH/cHex/H$_2$O, with a surfactant/water molar ratio of 2.85 and a surfactant/cosurfactant molar ratio of 1. A sequential synthetic procedure was used to prepare the nanoparticles. One nanoemulsion containing the iron source and another containing a solution of sodium hydroxide were mixed to form the magnetite nanoparticles. The nanoemulsion was lysed with acetone to remove the particles from the surfactant and washed several times with ethanol. The colloidal nanoparticles exhibit superparamagnetic behavior with high magnetization values.

The oil and water phases often contain several dissolved components, and therefore, the selection of the surfactant (and cosurfactant) depends upon the physicochemical characteristics of the system. Several types of surfactants, such as cationic, anionic, or non-ionic, can be used. The literature often reports the use of sodium bis(2-ethylhexylsulfosuccinate) (AOT),[80–82,85,86] cetyltrimethylammonium bromide (CTAB),[81] or sodium dodecylsulfate (SDS)[109] as ionic surfactants. Unfortunately, the ionic surfactants functional group in the hydrated core seems to limit the capability of forming highly crystalline magnetite nanoparticles.[110,111] The use of non-ionic surfactants, such as polyethoxylates[112] (Triton X-100, Igepal CO-520, and Brij-97), avoids the complication of the presence of a complexing functional species and offers great future potential.[83,84]

Vidal-Vidal et al. present a one-pot emulsion method to produce both coated and uncoated monodisperse magnetic nanoparticles.[113] A water-in-oil emulsion (cyclohexane/Brij-97/aqueous phase)[114] was chosen because it is stable at moderated temperatures and uses a non-ionic surfactant. The nanoparticles are formed by the coprecipitation reaction of ferrous and ferric salts with two organic bases, cyclohexylamine and oleylamine, into a water-in-oil emulsion. The results show that oleylamine acts as a precipitating and capping agent. However, cyclohexylamine acts only as a precipitating agent and does not avoid particle aggregation. The spherical-shaped particles, capped with a monolayer coating of oleylamine, show a narrow size distribution of 3.5 ± 0.6 nm, are well-crystallized, and have high saturation magnetization values.

Recently, Jia et al.[115] proposed a new method to prepare *in situ* magnetic chitosan/Fe$_3$O$_4$ composite nanoparticles in microreactors of tiny water pools of water-in-oil emulsion. When the basic solution of NaOH was added into the emulsion containing chitosan and ferrous salt, the magnetic Fe$_3$O$_4$ and chitosan nanoparticles were precipitated from the system. The magnetic iron oxide nanoparticles were surrounded by the chitosan nanoparticles. The size of the magnetic chitosan nanoparticles ranged from 10 to 80 nm with a different molecular weight of chitosan. The saturated magnetization of composite nanoparticles could reach 11.15 emu/g. The magnetization of composite particles can be adjusted by changing the weight ratio of chitosan and Fe$_3$O$_4$.

Another coating approach that has been proposed consists of encapsulating iron oxide nanoparticles in liposomes to obtain magnetoliposomes. Two kinds of magnetoliposomes are described in the literature: small liposomes consisting of nanoparticles stabilized by a phospholipidic bilayer without internal aqueous component (lipoparticles) or phospholipidic vesicles encapsulating iron oxide in an aqueous compartment (magnetovesicles). Different processes have been proposed to obtain lipoparticles. De Cuyper et al. developed a process to synthesize magnetoliposomes containing 1−6 crystals per vesicle[116,117] by dialysis of single unilamelar vesicles (SUVs) in the presence of a nanoparticle coated by lauric acid. In this process, the surfactant molecules (lauric acid) are exchanged with the phospholipid molecules and, consequently, the rate of dialysis is crucial. These magnetoliposomes were pegylated to prolong their blood half-life.[118] Variants of this process have been described using another surfactant (oleic acid) or a different phospholipid composition.[119–123] Magnetovesicles can be obtained by lipidic film hydration followed by extrusion[124] or sonication,[125] inverse phase evaporation,[126] congelation/decongelation,[127] or nanoreactor synthesis. Magnetoliposomes (25 nm in TEM diameter) were prepared directly using the phospholipid vesicle encapsulating Fe^{II} ions as nanoreactors. The slow diffusion of hydroxide ions inside the vesicles causes the formation of magnetic nanoparticles. The magnetoliposomes are separated from free liposomes by application of a high magnetic field gradient.[128] A similar process was also used by Mann.[129] Three purification methods can be employed: centrifugation, magnetic sorting, or gel-exclusion chromatography (GEC). Lesieur et al. have recently described an efficient GEC purification of monodisperse magnetovesicles (195 nm) that avoids dilution of the dispersion and ensures high magnetoliposome purity.[130]

Superparamagnetic iron oxides were introduced in solid lipid nanoparticles (SLNs) obtained from warm oil-in-water emulsions dispersed in cold water.[131] According to the process used for incorporation, magnetic SLNs of 233 or 159 nm were obtained with different loading in iron.

In 1998, a novel kind of microcontainer was introduced.[132] The particles were synthesized in a polyelectrolyte capsule with a wall made of polyelectrolyte multilayers of poly(styrene sulfonate) and poly(allylamine hydrochloride). The presence of polycations in the capsules maintains a pH gradient across the capsule wall. Fe^{III} ions in solution go through the capsule walls and precipitate inside, forming iron oxide nanoparticles.[133–135]

Complexing agents are also frequently used, but they mostly act on the morphology of the particles.[136]

A new source of magnetic nanoparticles is provided by biomineralization. Bacterial magnetic magnetosomes were obtained from cells of the magnetic bacterium *Magnetospirillum grysphiswaldense*. Bacteria were cultured in a medium containing 50 μM ferric citrate, and cells were disrupted in a French press to obtain magnetoliposomes with a narrow size distribution (mean diameter of 42 ± 9 nm).[137]

2.3. Hydrothermal and High-Temperature Reactions

Hydrothermal syntheses of Fe$_3$O$_4$ nanoparticles and Ultrafine powders have been reported in the literature.[138–145] These reactions are performed in aqueous media in reactors or autoclaves where the pressure can be higher than 2000 psi and the temperature can be above 200 °C.

There are two main routes for the formation of ferrites via hydrothermal conditions: hydrolysis and oxidation or neutralization of mixed metal hydroxides. These two reactions are very similar, except that ferrous salts are used in the first method.[16]

In this process, the reaction conditions, such as solvent, temperature, and time, usually have important effects on the products.[146] Indeed, it was observed that the particle size of

Fe_3O_4 powders increased with a prolonged reaction time and that higher water content resulted in the precipitation of larger Fe_3O_4 particles. In the hydrothermal process, the particle size in crystallization is controlled mainly through the rate processes of nucleation and grain growth, which compete for the species. Their rates depend upon the reaction temperature, with other conditions held constant.[146] Nucleation might be faster than grain growth at higher temperatures and results in a decrease in particle size. On the other hand, prolonging the reaction time would favor grain growth. Ferromagnetic Fe_3O_4 nanoparticles with a diameter of 27 nm have been prepared by a hydrothermal route in the presence of a surfactant, sodium bis(2-ethylhexyl)sulfosuccinate (AOT).[147]

Nanoparticles with a high level of monodispersity and size control can be obtained by high-temperature decomposition of iron organic precursors, such as $Fe(Cup)_3$, $Fe(CO)_5$, or $Fe(acac)_3$, using organic solvents and surfactants. For example, iron oleate can be formed from decomposition of iron carbonyl in the presence of octyl ether and oleic acid at 100 °C. Cooled to room temperature, $(CH_3)_3NO$ is added and the solution is refluxed.[138] Highly crystalline and monodisperse maghemite crystals were obtained at 100 °C by thermal decomposition of iron pentacarbonyl in the presence of oleic acid and then aging at 300 °C the iron oleic complex. This two-step process allowed for the production of selected particles sizes from 4 to 16 nm.[145] The reviews of Tartaj and Sata present in detail this chemistry.[17,148] The size and morphology of the nanoparticles can be controlled by controlling the reaction times and the temperature but also the concentration and ratios of the reactants, nature of the solvent, precursors, complexing strength, and addition of seeds. The adsorption of a surfactant onto the surface of the iron nanoparticle stabilizes the colloid solution. However, this type of process must be improved to be suitable for industrial preparation, especially in terms of safety of the reactant and the high temperature required.

Hydrophobic magnetite particles with a narrow size distribution have been prepared by thermal decomposition of $Fe(CO)_5$ in octyl ether solution of oleic acid and consecutive aeration. The nanoparticles were converted into a magnetite core/silica shell with hydrophilic and processible aminopropyl groups on their surfaces.[149]

Sun et al. have described a high-temperature reaction of iron(III) acetylacetonate with 1,2-hexadecanediol in the presence of oleic acid and oleylamine to obtain monodisperse magnetite nanoparticles. The particle diameter can be tuned from 4 to 20 nm, and the hydrophobic particles can be transformed into hydrophilic ones by adding a bipolar surfactant.[150]

The thermal decomposition of iron pentacarbonyl and iron oleate at different temperatures affords monodisperse nanoparticles ranging from 4 to 11 nm, dispersible in organic solvent.[151]

The use of nontoxic iron chloride salts as a precursor has been proposed by different groups.[152,153] The nanoparticles obtained are dispersible in different organic solvents (hexane and toluene) but probably not in water, and sophisticated postpreparative methods are required to make these nanocrystals water-soluble. Work is ongoing to overcome the required suspension in organic solvents. Li et al. have recently described a synthesis of water-dispersible magnetite in acidic or basic media by thermal decomposition of $Fe(acac)_3$[154–157] or inexpensive $FeCl_3$[156] in refluxing 2-pyr-

rolidone. 2-Pyrrolidone is a high boiling solvent but also a stabilizer because of its coordination capacity with metal ions. Moreover, the thermal decomposition of 2-pyrrolidone generates CO and azetidine. It is postulated that azetidine probably catalyzes the hydrolysis of $FeCl_3$ in ferric hydroxide FeOOH. FeOOH is then reduced by CO issued from the decomposition of 2-pyrrolidone. According to the reflux time, the size can be controlled to obtain nanoparticles with diameters of 4, 12, and 60 nm.[156] Interestingly, the nanoparticles change their shape from spherical to cubic with an increasing reflux time. With the same experimental procedure but with monocarboxyl-terminated poly(ethylene glycol)[158] or α,ω-dicarboxyl-terminated poly(ethylene glycol)[159] as a surface-capping agent, water-soluble PEG-coated nanoparticles were obtained. Recently, magnetite nanocrystals synthesized from thermal decomposition of $Fe(acac)_3$ in high boiling organic solvent with a controlled size of 4, 6, 9, and 12 nm and high monodispersity were coated by 2,3-dimercaptosuccinic acid (DMSA) in a procedure of ligand exchange to disperse the colloid in water. The obtained DMSA nanocrystals are fairly stable in water and phosphate-buffered saline without aggregation.[160]

2.4. Sol–Gel Reactions

The sol–gel process is a suitable wet route to the synthesis of nanostructured metal oxides.[161–163] This process is based on the hydroxylation and condensation of molecular precursors in solution, originating a "sol" of nanometric particles. Further condensation and inorganic polymerization lead to a three-dimensional metal oxide network denominated wet gel. Because these reactions are performed at room temperature, further heat treatments are needed to acquire the final crystalline state.[164,165] From the literature, it is clear that the properties of a gel are very dependent upon the structure created during the sol stage of the sol–gel process.

The main parameters that influence the kinetics, growth reactions, hydrolysis, condensation reactions, and consequently, the structure and properties of the gel are solvent, temperature, nature, concentration of the salt precursors employed, pH, and agitation.[166–169]

For example, it has been reported that γFe_2O_3 nanoparticles in a size range between 6 and 15 nm can be obtained after a direct heat treatment of the gels at a temperature of 400 °C.[170] This method offers some advantages, such as[171] (i) the possibility to obtain materials with a predetermined structure according to experimental conditions, (ii) the possibility to obtain pure amorphous phases, monodispersity, and good control of the particle size, (iii) the control of the microstructure and the homogeneity of the reaction products, and (iv) the possibility to embed molecules, which maintain their stability and properties within the sol–gel matrix. From the sol–gel method, γFe_2O_3 nanoparticles can be embedded in an inert, inorganic, transparent, and temperature-resistant silica matrix.[172–174]

Solinas et al.[175] have formed Fe_2O_3–SiO_2 nanocomposites with a Fe/Si molar concentration ranging between 0.25 and 0.57 by the sol–gel route. In this work, the influence of two factors on the gelation process was investigated: the surface of evaporation/volume (S/V) ratio of the sol and the temperature. This study shows that the gelation process determines the size and the phase of the nanoparticles formed in the silica matrix. First, when a high S/V ratio is adopted in the gelation process, very small particles of iron oxide are formed in the nanocomposite because of the microporos-

ity of the silica process. On the contrary, the sols gelated with a lower S/V ratio give rise to large iron oxide particles. Second, low S/V values and high temperatures in the gelation process favor the occurrence of γFe_2O_3, while high S/V values and low temperatures give rise to the formation of αFe_2O_3.

Raileanu et al.[176] have prepared sol−gel nanocomposite materials (Fe_xO_y−SiO_2) using alkoxide and aqueous routes. Different precursors of silica (tetramethoxysilane, methyl-triethoxysilane, colloidal silica solution, etc.) were used to compare the structure and properties of obtained nanoparticles. The structural and morphological results obtained by XRD, IR spectroscopy, and TEM were correlated with the magnetic interactions investigated versus the temperature by Mossbauer spectroscopy.

2.5. Polyol Methods

The polyol process,[177] which can also be understood as a sol−gel method, is a versatile chemical approach for the synthesis of nano- and microparticles with well-defined shapes and controlled sizes.[178–211]

The solvents as polyols (for example, polyethyleneglycol) offer interesting properties: owing to their high dielectric constants, they act as solvents able to dissolve inorganic compounds, and owing to their relatively high boiling points, they offer a wide operating-temperature range (from 25 °C to boiling point) for preparing inorganic compounds.[212] Polyols also serve as reducing agents as well as stabilizers to control particle growth and prevent interparticle aggregation.

In this process, a precursor compound is suspended in a liquid polyol. The suspension is stirred and heated to a given temperature that can reach the boiling point of the polyol. During this reaction, the metal precursor becomes solubilized in the diol, forms an intermediate, and is then reduced to form metal nuclei that will then nucleate and form metal particles. Submicrometer-sized particles can be synthesized by increasing the reaction temperature or inducing heterogeneous nucleation via adding foreign nuclei or forming foreign nuclei *in situ*.[213] The latter method is more convenient because the increase of the temperature leads to a more important thermal degradation of the polyol. Furthermore, heterogeneous nucleation allows, to some extent, for control of the particle size in the submicrometer range.[104]

Recently, Cai and Wan[214] developed an easy method to directly produce non-aggregated magnetite nanoparticles using a modified polyol process. Four types of polyols, including ethylene glycol (EG), diethyleneglycol (DEG), triethylene glycol (TREG), and tetraethylene glycol (TEG), were directly reacted with Fe(acac)$_3$ at an elevated temperature. Only the reaction with TREG yielded non-agglomerated magnetite particles with uniform shape and narrow size distribution. This result is correlated with the appropriate number of coordinating groups available on the polyol solvent molecules[215] and the suitable reaction temperature. The presence of polyol ligands on the surface of the magnetite nanoparticles is confirmed by TGA measurement and FTIR analysis.

Joseyphus et al.[216] have studied the influence of the nature of the polyol on the production and the morphological characteristics of Fe particles. Several factors governing the production yield of Fe particles were evaluated: type of polyols, ferrous salts, ferrous ion concentration, hydroxyl ion concentration, and reaction temperature. The yield and size

of Fe particles varied depending upon the reduction potential of the polyols.

In comparison to the aqueous method, this approach presents several advantages.[217] First, the surface of the prepared magnetite nanoparticles is coated by hydrophilic polyol ligands *in situ*; therefore, the nanoparticles can be easily dispersed in aqueous media and other polar solvents. Second, the relatively higher reaction temperature of this system favors particles with a higher crystallinity and therefore a higher magnetization. Finally, the size distribution of the nanoparticles is much narrower than those particles produced by traditional methods.

2.6. Flow Injection Syntheses

Reaction zone confinement in different "matrixes", such as emulsions, etc., has been used to produce particles with narrow size distributions and, in some cases, to tailor the particle morphology. However, a specific design of the reactor can serve as an alternative to the "matrix" confinement.

Alvarez et al.[23] have developed a novel synthesis of magnetite nanoparticles based on a flow injection synthesis (FIS) technique. The technique consisted of continuous or segmented mixing of reagents under laminar flow regime in a capillary reactor.

The FIS technique has some advantages, such as a high reproducibility because of the plug-flow and laminar conditions, a high mixing homogeneity, and an opportunity for a precise external control of the process. The influence of chemical parameters and conditions on the properties of the material was investigated. The obtained magnetite nanoparticles had a narrow size distribution in the range of 2−7 nm.

2.7. Electrochemical Methods

On the basis of an electrochemical method developed by Reetz,[218] Pascal et al.[219] have prepared 3−8 nm maghemite particles from an iron electrode in an aqueous solution of DMF and cationic surfactants. Adjustment of the current density controls the particle size. Electrochemical deposition under oxidizing conditions has been used to prepare nanoparticles of Fe_2O_3 and Fe_3O_4.[220]

2.8. Aerosol/Vapor Methods

Aerosol technologies, such as spray and laser pyrolysis, are attractive because these technologies are continuous chemical processes allowing for high rate production. In spray pyrolysis, a solution of ferric salts and a reducing agent in organic solvent is sprayed into a series of reactors, where the aerosol solute condenses and the solvent evaporates.[221] The resulting dried residue consists of particles whose size depends upon the initial size of the original droplets. Maghemite particles with size ranging from 5 to 60 nm with different shapes have been obtained using different iron precursor salts in alcoholic solution.[222]

Laser pyrolysis can be used to reduce the reaction volume. Laser heats a gaseous mixture of iron precursor and a flowing mixture of gas producing small, narrow size, and non-aggregated nanoparticles. When the pyrolysis experimental conditions are adjusted, the crystal size of maghemite nanoparticles is varied in the range from 2 to 7 nm with a very narrow size distribution. Laser pyrolysis as a tool for the gas-phase synthesis of nanoparticles is illustrated with recent results obtained in the preparation of iron-based

nanostructures, where sensitized iron-pentacarbonyl-based mixtures and ethylene as an energy-transfer agent are employed with air as an oxidant.[223–226]

The relationship between the main process conditions and the product characteristics is stressed. Iron−carbon core−shell nanoparticles with low mean size (about 4−5 nm) and modified morphologies are obtained by an increase of ethylene flow. In the case of γ-iron oxide nanopowder synthesis, low carbon contamination by ethylene depletion at an increased system pressure is observed.

Julian-Lopez et al. have reported the synthesis and characterization of hybrid silica-spinel iron oxide composite microspheres built with superparamagnetic nanoparticles for MRI, hyperthermia, and a hybrid mesoporous matrix, enabling the transport of bioactive molecules. These multi-fonctional platforms can be obtained by spray drying a sol of tunable composition, allowing for the control of the size and amount of magnetic particles embedded in the matrix.[227]

2.9. Sonolysis

Iron oxide can be prepared by the decomposition (by thermolysis or sonolysis) of organometallic precursors. Polymers, organic capping agents, or structural hosts are used to limit the nanoparticle growth.[228–239] The very high temperature hot spot generated by the rapid collapse of sonically generated cavities allows for the conversion of ferrous salts into magnetic nanoparticles. The sonolysis of an aqueous solution of $Fe(CO)_5$ in the presence of sodium dodecyl sulfate leads to the formation of a stable hydrosol of amorphous Fe_3O_4 nanoparticles.[240]

Superparamagnetic iron oxide nanoparticles (SPIO) having high magnetization and crystallinity have been synthesized using a sonochemical method.[241] Ferrofluids from these nanoparticles coated with oleic acid as a surfactant were prepared. The coated SPIO could be easily dispersed in chitosan. The hydrodynamic diameter of the coated SPIO in the chitosan solution was estimated to be 65 nm, and they had a good stability.

Nanostructured particles have been produced by sonochemical treatment of volatile organometallic precursors.[242–260] If stabilizers or polymers are added during sonication or postsonication, metal colloids are produced. Gedanken et al. have used sonochemical ways to prepare nanoparticles of Fe, Fe_3O_4, and Fe_2O_3.[247,248,255] Oxide formation was also observed if the sonication was performed in aqueous solution and with noncarbonyl precursors.[256–259]

3. Stabilization of Magnetic Particles

The stabilization of the iron oxide particles is crucial to obtain magnetic colloidal ferrofluids that are stable against aggregation in both a biological medium and a magnetic field. The stability of a magnetic colloidal suspension results from the equilibrium between attractive and repulsive forces. Theoretically, four kinds of forces can contribute to the interparticle potential in the system. van der Waals forces induce strong short-range isotropic attractions. The electrostatic repulsive forces can be partially screened by adding salt to the suspension. The theoretical description of these two forces is known as the Derjaguin−Landau−Verwey−Overbeek (DLVO) theory.[260,261] For magnetic suspensions, magnetic dipolar forces between two particles must be added. These forces induce anisotropic interactions, which are found to
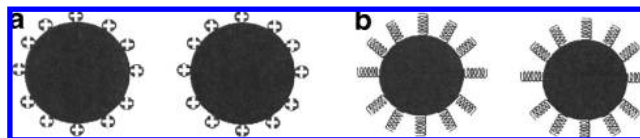

Figure 1. (a) Particles stabilized by the electrostatic layer. (b) Particles stabilized by steric repulsion.

be globally attractive if the anisotropic interparticle potential is integrated over all directions. Finally, steric repulsion forces have to be taken into account for non-naked particles.[262]

Stabilization of magnetic particles can be achieved by playing on one or both of the two repulsive forces: electrostatic and steric repulsion[39] (Figure 1).

Controlling the strength of these forces is a key parameter to elaborate particles with good stability. The steric force is difficult to predict and quantify. It is quite well-described theoretically for polymers. It depends, among other parameters, upon the molecular weight of the polymer and its density.[263,264] The electrostatic repulsion can be followed through the knowledge of the diffusion potential that may be very close to the zeta potential (ζ)[265,266] and the Debye−Huckel length that mainly depends upon the ionic strength and pH of the solution.

A way to test electrostatic stability is to follow the aggregation kinetics of colloidal suspensions by varying the salt concentration. This can be achieved through the stability factor (W) that measures the effectiveness of the potential barrier in preventing the particles from aggregation. W is defined as the ratio of the number of collisions between particles and the number of collisions resulting in aggregation. It can therefore be expressed as $W = k_{fast}/k$, where k_{fast} is the rate constant describing rapid aggregation (every collision leads to an aggregation) and k is the aggregation rate constant at the salt concentration used. This stability factor can be achieved through light scattering (static or dynamic) or turbidimetric measurements.[267–273] The stability factor as a function of added salt gives access to the critical concentration of coagulation. At this concentration, the double electrostatic layer is entirely suppressed and $k = k_{fast}$ becomes independent of the salt concentration.

In iron oxide, the surface iron atoms act as Lewis acids and coordinate with molecules that donate lone-pair electrons. Therefore, in aqueous solutions, the Fe atoms coordinate with water, which dissociates readily to leave the iron oxide surface hydroxyl functionalized. These hydroxyl groups are amphoteric and may react with acids or bases.[274] Dependent upon the pH of the solution, the surface of the magnetite will be positive or negative. The isoelectric point is observed at pH 6.8.[275] Around this point [point of zero charge (PZC)], the surface charge density (Σ) is too small and the particles are no longer stable in water and flocculate. Playing on both electrostatic and steric stabilization is then necessary to obtain stable iron oxide nanoparticles.

3.1. Monomeric Stabilizers

Functional groups, including carboxylates, phosphates, and sulfates, are known to bind to the surface of magnetites.[276,277] Furthermore, this stabilization can be tailored for dispersibility into oil/hydrocarbon carrier fluids or aqueous media.

3.1.1. Carboxylates

The surface of magnetite nanoparticles can be stabilized in an aqueous dispersion by the adsorption of citric acid.[278] This acid may be adsorbed on the surface of the magnetite nanoparticles by coordinating via one or two of the carboxylate functionalities, depending upon steric necessity and the curvature of the surface. This leaves at least one carboxylic acid group exposed to the solvent, which should be responsible for making the surface negatively charged and hydrophilic.

VSOP C184 is an iron oxide particle under clinical investigation stabilized by monomeric coating (citric acid). Optimization of the coprecipitation process in the presence of excess of citrate ions leading to VSOP C184 has led to a particle characterized by an iron core diameter of 4 nm and a hydrodynamic diameter of 8.6 nm.[279,280] Carboxylates have important effects on the growth of iron oxide nanoparticles and their magnetic properties. Bee et al. have investigated the effect of the concentration of citrate ions on the size of maghemite particles.[64] Krishnamurti and Huang have studied the influence of citrate on the kinetics of Fe^{2+} oxidation and the resulting hydrolytic products of Fe^{3+}.[111] Huang and Wang have shown that the rate constant governing the oxidation of Fe^{2+} in the presence of inorganic ligands decreases as perchlorate > fluoride > nitrate > chloride > carbonate > sulfate > silicate > phosphate.[281]

Liu and Huang have studied the effect of the presence of citric acid during iron oxide synthesis.[282] Increasing concentrations of citric acid caused significant decreases in the crystallinity of the iron oxides formed. Moreover, the presence of citrate led to changes in the surface geometry. Other studies on the influence of carboxylate ions show similar results.[60,283–285] Other coating molecules, such as gluconic acid,[59] dimercaptosuccinic acid,[61] and phosphorylcholine[286,287] can be used for the stabilization of iron oxide in aqueous medium. The stability range is strongly dependent upon pH and the concentration of adsorbed acids or phosphonates.

Cousin et al.,[288–290] Cabuil,[291] and Dubois et al.[292] report on the existence of phase diagrams (osmotic pressure as a function of the particle volume fraction) in citrate-coated particle suspensions. The behavior of these particles is explored by varying the ionic strength, volume fraction, or osmotic pressure. The structure of the colloidal suspension is determined from small-angle neutron scattering (SANS) measurements. They demonstrate that the nature of the phase diagram is controlled by the ratio of attractive/repulsive interactions, as predicted for colloidal suspensions. If the repulsion dominates, only fluid−solid phases exist. If the attraction dominates, a phase diagram with gas, liquid, and solid phases as in atomic systems is obtained. The same type of experiments has been performed under a magnetic field.[293]

3.1.2. Phosphates

Several researchers have studied the possibility of using alkanesulphonic and alkanephosphonic acid surfactants as efficient binding ligands on the surface of Fe_2O_3 nanoparticles and as stabilizers for particle dispersion in organic solvents.[294–296] Yee et al.[297] proposed two possible bonding schemes for the phosphonate ions on Fe^{3+}, i.e., one O or two O atoms of the phosphonate group binding onto the surface. Zeta potential and absorption measurements as well as IR spectroscopy[298,299] have suggested that the phosphate ions

form bidentate complexes with adjacent sites on the iron oxide surface. Sahoo et al.[277] have reported the surface derivatization of magnetite by oleic acid, lauric acid, dodecylphosphonic acid, hexadecylphosphonic acid, and dihexadecyl phosphate. This study showed that alkyl phosphonates and phosphates could be used for obtaining thermodynamically stable dispersions of magnetic ferrite nanoparticles. The ligands seem to form a quasi-bilayer structure, with the primary layer strongly bound to the surface of the nanoparticles as shown from the temperature and enthalpy of desorption.

Recently, superparamagnetic nanosized magnetite particles have been prepared by controlled coprecipitation of Fe^{2+} and Fe^{3+} in the presence of highly hydrophilic poly(vinylalcohol phosphate) (PVAP). The impact of the polymer concentration on the particle size, size distribution, colloidal stability, and magnetic property has been studied. The aqueous suspension of magnetite, prepared using 1% PVAP solution, is stable for 4 weeks at pH 5−8. Transmission electron microscopy confirmed well-dispersed cubic magnetite particles with a size of about 5.8 nm. A dynamic light scattering measurement showed a narrow distribution of hydrodynamic size. Infrared spectra of samples showed a strong Fe−O−P bond on the oxide surface.[300]

The acceptable biocompatibility[301] of phosphonate and phosphate ligands may advance toward the use of encapsulated magnetic nanoparticles in medical applications, such as magnetic resonance imaging, and other biophysical purposes.

3.2. Inorganic Materials

Iron oxide nanoparticles can be coated with silica,[302–306] gold,[307–309] or gadolinium(III).[310–312] These coatings not only provide stability to the nanoparticles in solution but also help in binding various biological ligands to the nanoparticle surface. These nanoparticles have an inner iron oxide core with an outer metallic shell of inorganic materials.

3.2.1. Silica

Silica has been exploited as a coating material for magnetic nanoparticles.[313–319] Usually, an inert silica coating on the surface of magnetite nanoparticles prevents their aggregation in liquid, improves their chemical stability, and provides better protection against toxicity.[320] This coating stabilizes the magnetite nanoparticles in two different ways.[321] One is by shielding the magnetic dipole interaction with the silica shell. On the other hand, the silica nanoparticles are negatively charged. Therefore, the silica coating enhances the coulomb repulsion of the magnetic nanoparticles.

Ferumoxsil (AMI-121), has been tested in clinical trials by oral administration at 600−900 mL.[322–324] This product is composed of iron oxide particles coated with a layer of inert silicon ([3-(2-amino-ethylamino)propyl]trimethoxysilane) and a diameter of 300 nm. After oral administration, it significantly improves the definition of organ boundaries, such as the uterus and lymph nodes.

Three different approaches have been explored to generate magnetic silica nanospheres. The first method relies on the well-known Stöber process, in which silica was formed *in situ* through the hydrolysis and condensation of a sol−gel precursor, such as tetraethyl orthosilicate (TEOS).[325–330] For example, Im et al.[330] have prepared silica colloids loaded with superparamagnetic iron oxide nanoparticles using this

process. This study showed that the final size of silica colloids depends upon the concentration of iron oxide nanoparticles and the type of solvent because the size of silica is closely related to the number of seeds (emulsion drops). Larger colloids were obtained at lower concentrations of iron oxide nanoparticles and in alcohols with higher molecular weights.

The second method is based on the deposition of silica from silicic acid solution.[331,78] Different studies have proven that the silicic acid method appears to be more efficient in covering a higher proportion of the magnetite surface than the TEOS method.[332] This approach is very easy to perform, and the particle size can be controlled from tens to several hundred nanometers by changing the ratio of SiO_2/Fe_3O_4 or repeating the coating procedure.[108]

The third method is an emulsion method, in which micelles or inverse micelles are used to confine and control the silica coating. This method might require a greater effort to separate the core−shell nanoparticles from the large amount of surfactants associated with the emulsion system.[326,333−335] For example, Yang et al.[336] have used the emulsion method for the preparation of monodisperse silica-coated iron oxide superparamagnetic nanoparticles and the further entrapment of biological macromolecules in the pore of the nanoparticles.

Recently, Tartaj et al. have prepared submicronic silica-coated magnetic sphere aerosol by the pyrolysis method.[304,305]

One of the advantages of having a surface enriched in silica is the presence of surface silanol groups that can easily react with various coupling agents to covalently attach specific ligands to these magnetic particles.[337,338] For example, amine groups have been introduced on the surface of silica-coated magnetite nanoparticles by hydrolysis and condensation of an organosilane, such as aminopropyltriethoxysilane, on the surface of magnetite nanoparticles.[339−341] This is known as the silanization method.[342]

3.2.2. Gold

Gold is another inorganic coating highly adequate to implement functionality to magnetic nanoparticles as well as to improve their stability in aqueous dispersions. Some protocols exist in the literature to obtain magnetic nanoparticles coated with gold. For example, Lin et al.[308] have synthesized core−shell-structured Fe/Au nanoparticles by a reverse-micelle approach. The Au shell was expected to protect the Fe core and provide further organic functionalization. Water-soluble Au-coated magnetite nanoparticles with diameters of about 60 nm were synthesized by the reduction of Au^{III} onto the surface via iterative hydroxylamine seeding.[343]

Magnetic gold nanoshells have been described recently. Magnetite nanoparticules stabilized by oleic acid and 2-bromo-2-propionic acid and gold seed nanoparticules were covalently attached to amino-modified silica particles, and then, the growth of a complete gold shell provided superparamagnetic gold nanoshells.[344]

3.3. Polymer Stabilizers

Several approaches have been developed to coat iron oxide nanoparticles, including *in situ* coatings and post-synthesis coatings. In the first approach, nanoparticles are coated during the synthesis. For example, Josephson et al. have developed a coprecipitation process in the presence of dextran.[345] The post-synthesis coating method consists of grafting the

polymer on the magnetic particles once synthesized[346−348] (polymeric surfactants). In the literature, the most common coatings are dextran, carboxymethylated dextran, carboxydextran, starch, arabinogalactan, glycosaminoglycan, sulfonated styrene−divinylbenzene, polyethylene glycol (PEG), polyvinyl alcohol (PVA), poloxamers, and polyoxamines.[349,350]

3.3.1. Dextran

Dextran is a polysaccharide polymer composed exclusively of α-D-glucopyranosyl units with varying degrees of chain length and branching. Dextran has been used often as a polymer coating mostly because of its biocompatibility.[351−355] Molday and Mackenzie were the first who reported the formation of magnetite in the presence of dextran 40 000.[356] In this study, the dextran was functionalized after iron oxide stabilization by oxidation with periodate to create more hydroxyl groups to allow for the binding of the amino groups of proteins. Ferumoxtran-10 and ferumoxides are prepared by the Molday coprecipitation method with *in situ* coating by dextran. The same process is used for ferucarbotran and ferumoxytol with *in situ* coating by carboxydextran and carboxymethyl dextran, respectively. Ferumoxtran-10, which has a small hydrodynamic diameter (15−30 nm), and ferumoxytol (hydrodynamic diameter of 30 nm) show a prolonged blood residence time, which allows those USPIO to access macrophages located in deep and pathologic tissues (such as lymph nodes, kidney, brain, osteoarticular tissues, etc.).

The effect of reducing the terminal glucose of dextran upon the formation and stability of dextran-coated ultrasmall superparamagnetic iron oxides (USPIO) has demonstrated to be of significance for particle size, coating stability, and magnetic properties. For low-molecular-weight dextrans (MW < 10 kDa), reduction resulted in a 10-fold or greater decrease in the carbohydrate/iron ratio necessary during particle formation to produce the desired particle size (<20 nm) in the coprecipitation process. Particles prepared with reduced dextran yielded a more stable coating as evidenced by stability upon autoclaving.[357]

Pardoe et al. offered detailed magnetic and structural properties on iron oxide formed in the presence of dextran (40 000 g/mol).[358] The results of the analysis suggested that the presence of the polymer limits the particle size compared to particles prepared without the polymer.

An important factor in the choice of dextran appears to be the favorable size of dextran chains, which enables optimum polar interactions (mainly chelation and hydrogen bonding) with iron oxide surfaces. Although single hydrogen bonds are relatively weak, the total bonding energy of hydrogen bonds over the length of a polysaccharide molecule can be very high because of the large number of hydroxyl groups per molecule.[17] Jung[359] has considered a model for polymer adsorption in which the interactions take place at different segments of the polymer. However, the dextran molecules can be desorbed from the iron oxide surface by heating at 120 °C[291] or dilution.[360] The usual way to avoid desorption of dextran is to use epichlorhydrin, that is, agents with cross-linking capacities.[271,361]

Recently, Bautista et al.[360] described dextran surface modification of pure superparamagnetic iron oxide nanoparticles prepared by laser pyrolysis and the coprecipitation method. Physical characterization techniques were used to delineate the nature and the mechanism of dextran particulate adsorption. The favored mechanism of adsorption of dextran

on the surface of maghemite nanoparticles prepared by laser pyrolysis seems to be the collective hydrogen bonding between dextran hydroxyl groups and the iron oxide particle surface.

Duguet et al. have used silane derivatives to functionalize iron oxide nanoparticles.[339,362,363] These authors developed an original synthetic route to obtain versatile ultrasmall superparamagnetic iron oxide (VUSPIO) in a multistep procedure consisting of colloidal maghemite synthesis, surface modification by silanation of the iron core with aminopropylsylane groups and conjugation with partially oxidized dextran, and subsequent reduction of the Schiff base.

3.3.2. Polyethylene Glycol (PEG)

PEG is a hydrophilic, water-soluble, biocompatible polymer. Several investigations have reported the use of PEG[364–371] to increase the biocompatibility of the iron oxide dispersions and blood circulation times.[357,372,373]

Feruglose (Clariscan) can be regarded as true "stealth nanoparticles", because of the pegylation of the coating starch, that are hardly recognized by the macrophage−monocytic system and probably not suitable for macrophage imaging.[474–478]

Recently, novel superparamagnetic iron oxide nanoparticles coated with polymerized polyethylene glycolylated bilayers were prepared.[479] Various methods of coating were developed to prepare small (60−100 nm) and ultrasmall (20−35 nm) particles without size-separation processes. Kumagai et al.[480] have reported a simple route to synthesize PEG-coated iron oxide nanoparticles by hydrolysis of $FeCl_3 \cdot 6H_2O$ in water and the subsequent treatment with poly(ethylene glycol)−poly(aspartic acid) block copolymer. The PEG-coated nanoparticles revealed excellent solubility and stability in aqueous solution as well as in physiological saline. The FTIR experimental results proved that PEG−PAsp molecules are multivalently bound on the surface of the iron oxide nanoparticles via the coordination between the carboxylic acids in the PAsp segment of the block copolymer and Fe on the surface of the iron oxide nanoparticles.

3.3.3. Polyvinyl Alcohol (PVA)

PVA is a hydrophilic, biocompatible polymer. PVA coating onto the particle surface prevents their agglomeration, giving rise to monodisperse particles.[381–384] For example, Lee et al.[385] have modified the surface of nanoparticles with PVA by precipitation of iron salts in PVA aqueous solution to form stable dispersion. These investigators suggest that PVA irreversibly binds to the surface of magnetite using FTIR absorbance shifts.

Recently, Chastellain et al.[386] have synthesized PVA-coated iron oxide nanoparticles according to a well-know method.[64] The colloidal stability of the final polymer-coated product as well as the resulting particle size distribution were determined for different iron/polymer ratios. All results showed a very different behavior for iron/polymer mass ratios smaller and larger than 2. From these results, a model for the stabilization mechanism was proposed. Interestingly, this recurring iron/polymer mass ratio $r = 2$ also plays a major role in cell tests. In a different study, the cytotoxicity and uptake of PVA-coated iron oxide nanoparticles by human melanoma cells in culture were determined for various iron/polymer mass ratios, confirming again the importance of this critical ratio $r = 2$.[387]

As is known, PVA is a unique synthetic polymer that can transform into a polymer gel[387] that is a class of macromolecular network with unique properties. Albornoz et al.[388] have reported the synthesis of an aqueous ferrofluid and the preparation of a magnetic gel with PVA and glutaraldehyde (GTA). They reported a good stability of its properties versus time. The magnetic gel was dried to generate a biocompatible film.

3.3.4. Alginate

Alginate is an electrolytic polysaccharide with many carboxyl groups. Researchers have thus speculated that the COO^- of alginate and iron ion would interact and that the electrostatic repulsion may make the superparamagnetic iron oxide nanoparticles (SPIONs)−alginate stable. Recently, several investigations dealing with the preparation of iron oxide nanoparticles with alginate have been developed.[389–392]

The standard chemical synthesis consists of three steps: (a) gelation of alginate and ferrous ions, (b) *in situ* precipitation of ferrous hydroxide by the alkaline treatment of alginate, and (c) oxidation of ferrous hydroxide with an oxidizing agent, such as O_2 or H_2O_2. This method is complex. Ma et al.[393] have developed a new modified two-step coprecipitation method. The results revealed that typical iron oxide nanoparticles were Fe_3O_4 with a core diameter of 5−10 nm and that SPIONs−alginate had a hydrodynamic diameter of 193.8−483.2 nm.

Morales et al.[394] have also described a new method to synthesize magnetic iron oxide nanoparticles into alginate beads with controlled size and magnetic properties for drug delivery applications. The results strongly suggested that the use of a polymer in the material synthesis limits the particle size. The iron oxide particle mean sizes were between 4.3 and 9.5 nm.

3.3.5. Chitosan

Chitosan is an alkaline, nontoxic, hydrophilic, biocompatible, and biodegradable polymer. Nowadays, the preparations of magnetic nanoparticles encapsulated in chitosan are of great interest.[395–398]

Kim et al.[399] have synthesized SPIO by a sonochemical method. From these particles, they synthesized ferrofluids for use as MRI contrast agents by coating them with oleic acid as a surfactant and then dispersing them in the chitosan, which is a suitable carrier for bioapplications. These spherical particles of about 15 nm in diameter showed superparamagnetic behavior.

Microspheres composed of superparamagnetic iron oxide nanoparticles and chitosan were developed as a novel MRI-detectable embolic material. Lee et al.[400] have prepared spherical SPIO nanoparticles about 15 nm in radius by sonochemistry and embedded them in chitosan to synthesize a ferrofluid. The SPIO−chitosan microspheres showed a strong enhancement of MR image contrast similar to the ferrofluid *in vitro*.

3.3.6. Other Polymers

Different polymers[98] that have been used also are polymethacrylic acid,[401] poly(ethyleneoxide)-*b*-poly(methacrylic acid),[402] polyvinylpyrrolidone (PVP),[403,404] poly(acrylic acid) (PAA),[405–409] polyalkylcyanoacrylate,[410] poly(lactic acid),[411] ethylcellulose,[412] poly(ε-caprolactone),[413,414] sulfonated

styrene−divinylbenzene,[415] or arabinogalactan. Arabinogalactan-coated iron oxide nanoparticles are recognized by asialoglycoprotein receptors present in normal hepatocytes.[416−420] PAA coatings increase the stability and biocompatibility of the particles and also help in bioadhesion.[421]

Superparamagnetic iron oxide nanoparticles can be coated with polyethylenimine (PEI).[390,391] PEI is known to form cationic complexes that interact nonspecifically with negatively charged species, such as DNA, and enter the cell via endocytosis.[276] PEI coating of iron oxide has led to colloidally stable beads even in high salt concentrations over a wide pH range.

Another study showed that maghemite could be stabilized with polymers in two layer-by-layer deposition steps. The first layer around the maghemite core is formed by PEI, and the second one is formed by poly(ethylene oxide)-block-poly(glutamic acid) (PEO−PGA).[183] The hydrodynamic diameter of the particles increases stepwise from $D(h) = 25$ nm (parent) via 35 nm (PEI) to 46 nm (PEI and PEO−PGA) because of stabilization. This is accompanied by a switching of their zeta potentials from moderately positive to highly positive and finally slightly negative. The coated maghemite nanoparticles were found to be stable in water and physiological salt solution. In contrast to novel methods for magnetic nanoparticle production, where organic solvents are necessary, this procedure can dispense with organic solvents. MRI experiments on living rats have indicated that the nanoparticles are useful as a MRI contrast agent.

Okassa et al.[348] have developed biodegradable and biocompatible submicrometer poly(lactide-co-glycolide) particles loaded with magnetite nanoparticles for intravenous drug targeting. Magnetite/PLGA particles were prepared by a modified double emulsion method (w/o/w) or an emulsion evaporation process (o/w).[348,422,423] To optimize the composite nanoparticles, experimental parameters were changed and the properties of the resulting nanosystems were determined. TEM showed SPIONs ranging in hydrodynamic diameter from 5 to 15 nm embedded inside the polymer and indicated that they were dispersed uniformly within the PLGA particles.

3.4. Other Strategies for Stabilization

Another method to synthesize polymeric core/shell magnetic nanoparticles is to use preformed synthetic polymers as a matrix to control the formation of magnetic cores.[424−429] We describe here some examples.

One synthetic method is offered by Underhill and Liu who report the preparation of an ABC triblock polymer nanosphere template for maghemite formation.[430] This structure was synthetically designed to act as a nanoreactor for the oxidation of Fe^{2+} solution and form water-dispersible iron oxide nanoparticles with controlled sizes. The triblock polymer is polyisoprene-block-poly(2-cinnamoylethyl methacrylate)-block-poly(tert-butyl acrylate).

Recent advances in the synthesis of magnetic nanoparticles in the presence of polymers are based on the use of polymer gels.[431] The advantages of using polymer gels are multiple, but the most important advantage is that the nucleation and growth of iron oxide can be controlled by the constrained architectures of the polymer gel.[432,433]

The gel serves as a nanoreactor where iron oxide nanoparticles are formed *in situ*. For example, Breulmann et al.[432] investigated the formation of magnetite inside the pore of an elastic polystyrene−polyacrylate copolymer gel template.

The synthetic parameters of the polymerization allow for the pore size and carboxylate functionality to be tailored. The authors report that the iron oxide content of the gels is ∼3.5−8% Fe_3O_4 with one reaction cycle and that the loading can increase up to 20% iron with successive swelling/reaction cycles. The particles are 16 nm in diameter and are bound to carboxylate functional groups of the polyacrylate component of the gel pore. These authors have also used the gel obtained by copolymerization of acrylic acid (AA), 2-hydroxyethylmethacrylate (HEMA), and ethyleneglycoldimethacrylate (EGDMA) monomer mixtures, but formation of magnetite in this gel structure was not possible.[434]

Gass et al. have reported the first deposition of magnetic nanocomposite poly(methylmethacrylate)/polypyrrole bilayers from solution using spin coating. Fe_3O_4 nanoparticles have been synthesized using a chemical coprecipitation route. Nanocomposites with uniform dispersion have been prepared using a combination of dissolving the polymer and mixing fatty acid surfactant-coated Fe_3O_4 nanoparticles.[435]

Finally, another method to prepare magnetic nanoparticles is to incorporate the iron oxide particles inside polymer particles by *in situ* polymerization.[436−440] Pich et al.[441] have prepared composite particles by a two-step method, in which, in the first step, the iron oxide nanoparticles were prepared and, during the second step, they were encapsulated into formed poly(styrene/acetoacetoxyethylmethacrylate) (PS−AAEM) particles directly during the polymerization process. It has been found that modifying the iron oxide nanoparticle surface with sodium oleate significantly improves the encapsulation during the polymerization process. Changing the monomer/iron oxide ratio gives the possibility to change the morphology of hybrid particles. However, the polydispersity of composite particles increases at higher contents of magnetic particles in the system. Modification of the AAEM concentration in the reaction mixture at constant iron oxide particles concentration gives the possibility to control the particle size of formed hybrid microspheres.

4. Methods of Vectorization of the Particles

Vectorized nanoparticles are used for intravenous administration. For molecular imaging, biovectors able to recognize a biological target must be grafted onto the surface of iron nanoparticles. Moreover, vectorized nanoparticles must be highly stable in aqueous ionic solutions at physiological pH. Particles must be nontoxic and remain in the circulation for a time long enough to reach their target.

Many biovectors are used in molecular imaging, such as antibodies[442] or their fragments, oligosaccharides, proteins, peptides, peptidomimetics, and small targeting ligands.[50] Various processes have been used to couple these biovectors (pharmacophore) onto different kinds of iron oxide nanoparticles (contrastophore).

The first strategy used to vectorize nanoparticles was electrostatic chimio-adsorption of antibody[443,444] or protein[445,446] onto the iron oxide surface. However, this noncovalent grafting does not seem to be versatile enough because it is difficult to control the reproducibility and scale-up of the process, the stability in biological media, and, according to the ionic strength, the coating and the amount of grafted pharmacophore. Another noncovalent strategy has used streptavidin-coated iron oxide particles or biotynilated iron oxide particles and streptavidin protein, which bind to biotynilated ligands.[447−450]
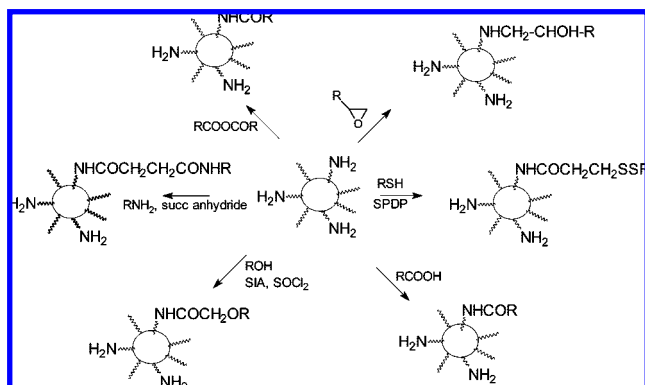
Figure 2. Synthesis of grafted particles using various heterofunctional linkers: SPDP, succinimidyl iodoacetate, activated suberic acid, succinic anhydride, EDCI, thionyl chloride, or epoxide.

Several covalent conjugation strategies using amine, carboxyl, aldehyde, or thiol groups exposed on the surface of nanoparticles have been developed.[451]

Oxidated antibodies have been coupled to amino PEG iron oxide through Schiff base formation.[452] Glutaraldehyde bioconjugation[453] or amide formation with EDI on carboxylated iron oxide nanoparticles has been reported for peptides[454–456] and protein[452,457,458] grafting.

Tiefenauer et al. have developed an original technology based on poly(glutamic–lysine–tyrosine) (PEKY)-coated iron oxide stabilized by cross-linking with ethylene glycol bis(succinimidyl succinate).[459,460] This iron oxide platform was functionalized with *N*-hydroxysulfosuccinic ester (sulfo-MBS) to allow for the coupling of thiolated antibody.

A commonly used process is based on an oxidative conjugation strategy, which produces aldehydes on a carbohydrate coating, such as dextran. This oxidative process using periodate oxidation followed by reduction of the Schiff base has been used to covalently couple different kinds of peptides,[461] protein, such as the C2 domain of synaptotagmin or transferrin,[462–464] different monoclonal antibodies,[465–469] or a wheat germ agglutinin lectin onto a dextran nanoparticle[470–473] or polymer[474] onto dextran derivative-coated iron oxide particles.

However, in the case of the transferrin biovector, a substantial loss of the biological activity of the protein was observed with the oxidative conjugation strategy.[475] These results suggest that the oxidative conjugation chemistry significantly interferes with the binding of the conjugates of the receptor. To minimize this type of detrimental effect, a new versatile nonoxidative technology has been developed allowing for the introduction of various chemical linkers. Hogemann et al. have linked the protein and the iron oxide particle via a linker molecule.[475] First, a dextran nanoparticle was cross-linked by epichlorohydrin and ammonia. The resulting amine-terminated cross-linked iron oxide nanoparticle (CLIO) is a powerful platform to conjugated biovectors with a wide range of heterobifunctional linkers.[476]

The target molecules (peptides, antibodies, proteins, and oligonucleotides) can be covalently linked through a three-step reaction sequence as described by Josephson et al.[477] A peptide or protein was attached to the amino group of a cross-linked dextran iron oxide (CLIO–NH₂) using different classical heterofunctional linkers, such as SPDP[475,478–489] (disulfide bound formation) (Figure 2), succinimidyl iodoacetate[474,475,484,486,489–495] (carbon–thiol formation), activated suberic acid[496–500] (amide formation), succinic anhydride[501] (amide formation), EDCI[484,501–503] (amide forma-

tion), thionyl chloride[484] (ether formation), epoxide[484] (carbon–nitrogen-bound formation).

This technology has recently been used to develop a nanoparticle library that recognizes apoptotic cells comprising 146 nanoparticles decorated with different synthetic small ligands.[501,503]

Recently, Sun et al. have developed "click chemistry" (azide–alkyne reaction) for vectorization of iron oxide nanoparticles with small molecules.[504] The easy preparation of stable particles bearing azido or alkyne groups capable of reaction with their corresponding counterpart functionalized small molecules has been showed (Figure 3).

Other research groups have used dextran nanoparticles cross-linked by epichlorohydrin and direct substitution by terminal amino groups of a pharmacophore.[7,8,505] Although this CLIO technology has provided interesting targeted USPIO, which have been used to reach proof of principle in molecular imaging, its industrialization raises a major problem because the cross-linking agent, epichlorohydrin, is classified as a carcinogenic, mutagenic, and reprotoxic substance.

The grafting of vector molecules on the particles can also be performed with 2,3-dimercaptosuccinic acid (DMSA) and *N*-succinimidyl 3-(2-pyridyldithio)propionate (SPDP).[506] In this case, the nanoparticular system is constituted by two subunits, the particle coated with the chelating agent DMSA and the vector linked to SPDP through a peptide bond. These subunits are joined by a S–S bridge between DMSA and SPDP (Figure 4). The synthesis of nanoparticles–DMSA sol has been carried out in three steps:[61] flocculation of the cationic ferrofluid by an aqueous solution of DMSA, peptization of the DMSA-complexed nanoparticles in an alkaline medium, and neutralization of the iron oxide suspension. The vector–SPDP was obtained by reacting SPDP with the amino function of the vector. Finally, the 2-pyridyl sulfide moiety of SPDP was substituted by the aliphatic SH group of the DMSA-complexed particles to form a S–S bridge between the particle and the vector. This technology has been used to couple antibodies and annexin V to DMSA nanoparticles.[507–513]

The DMSA technology, described previously, also allowed coupling of biovectors through C–S bonds using maleinido-benzoyl-*N*-hydroxysuccinimide ester (MBS) as a heterobifunctional linker, as demonstrated recently by coupling a maleimide-activated Herceptin antibody to manganese-doped spinel DMSA ferrite.[514]

Recently, magnetite nanoparticles coated with silica have been prepared.[515] This kind of process has been used to bioconjugate folic acid to a silane-coated iron oxide[516,517] and BSA.[79,363] After surface modification with an amino-silane-coupling agent, SG-Si900, amine has been covalently linked using glutaraldehyde as a cross-linker. Alternatively, vectors with carboxylic functions can be directly grafted on the silica-coated particles using EDC to activate the carboxyl groups.

The silane-coupling materials (such as 3-aminopropyltrimethoxysilane or *p*-aminophenyl trimethoxysilane)[518] are able to adsorptively or covalently bind to the metal oxide and are able to form covalent bonds with bioaffinity adsorbents through organofunctionalities. The mechanism of the silane-coupling agent reaction according to Arkles is depicted in Figure 5.[519]

The silane is deposited on the metal oxide core from acidic solution. The silanization reaction occurs in two steps: (i) the trimethoxysilane is placed in acidic water, phosphorous
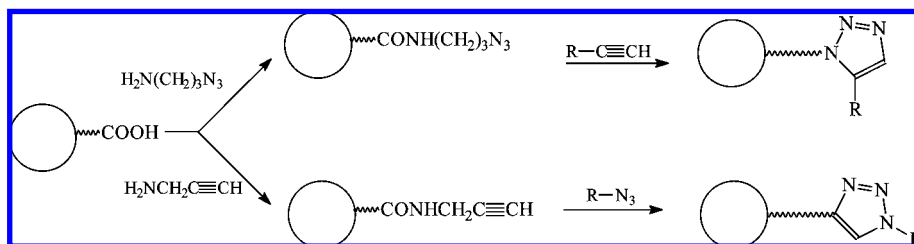
Figure 3. Synthesis via "click chemistry": reaction between an azide and an alkyne group to yield a triazole derivative.
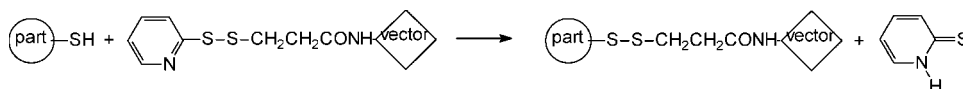

Figure 4. Particles with S−S bridge: the pyridyl sulfide moiety of SPDP grafted on the vector is substituted by the SH group on the nanoparticles.
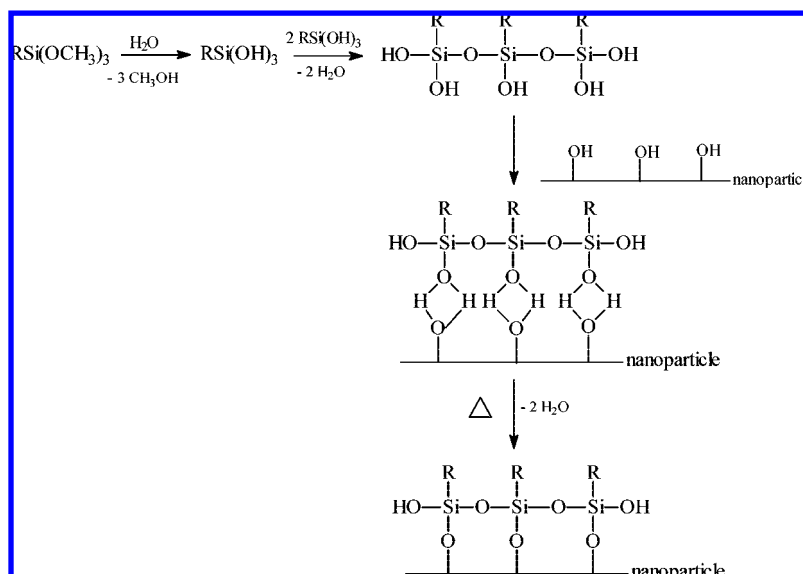

Figure 5. Chemical reactions of silane-coupling agents on magnetic particles.

acid, and glacial acetic acid and condenses to form silane polymers, and (ii) these polymers associate with the metal oxide by forming a covalent bond with surface OH groups through dehydration or adsorption of silane polymers to the metal oxide. Diazotation of aminophenyl-terminated silane or the use of glutaraldehyde on 3-aminopropyl-terminated silane can be used to couple antibodies or immunoglobulins. This second procedure consists of two basic steps: (i) activation of the particle by reaction with glutaraldehyde followed by removal of unreacted glutaraldehyde and (ii) reaction of the proteins with the activated particles followed by removal of the unreacted proteins. If the magnetic particles are coated by carboxy-terminated silanes, proteins can be coupled to them by treating the particles with 3-(3-dimethylaminopropyl)carbodiimide.

The surface chemistry involving reactions with alkyltrialkoxysilane or trichloroalkylsilane compounds is a good way for grafting biomolecules[520,521] (Figure 6). Nanoparticles with functional groups other than inorganic hydroxyls were prepared by the reaction with alkylsilane derivatives containing different functional groups [$SiR_3(CH_2)_nX$, where R = Cl, OCH_3, OC_2H_5, etc., $n = 3-17$, and X = CH_3, CN, CO_2CH_3, etc.] to form ether bonds. Particles with ω-hydroxyl or primary amine groups were prepared by reaction of the surface with alkylalkoxysilane compounds [$Si(OEt)_3(CH_2)_3$-

CO_2CH_3, $Si(OEt)_3(CH_2)_3NH_2$, etc.] or with trichloroalkylsilane derivatives [$SiCl_3(CH_2)_3CO_2CH_3$, $SiCl_3(CH_2)_3CN$, etc.] followed by diborane reduction. Particles with thiol functions were formed by thiourea reaction and hydrolysis of the ω-phenylchloromethyl.

In several studies, magnetoliposomes were used as a platform to incorporate antibodies or peptides in the lipidic membrane to biovectorize the nanoparticles.[522–527]

Recently, Nitin et al.[528] developed a PEG-modified phospholipid micelle coating for functionalization of superparamagnetic iron oxide nanoparticles. The PEG−phospholipid coating results in high water solubility, and the functional groups of modified PEG allow for bioconjugation of various moieties, including proteins, oligonucleotides, and delivery peptides. Multifunctional polymeric micelles incorporating 6 nm Fe_3O_4 nanoparticles and RGD peptides to target $\alpha_v\beta_3$ cancer cells have been recently described.[529]

5. Structural and Physicochemical Characterization

The magnetic properties of nanoparticles depend upon their physical structure: the size and the shape of the particles, their microstructure, and the chemical phases in which they are present. Moreover, the biological behavior of magnetic
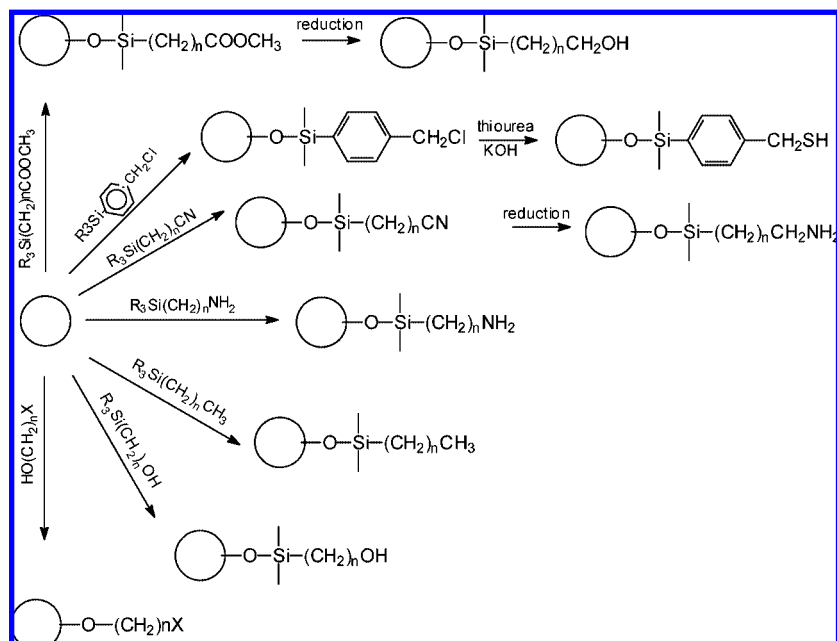
Figure 6. Chemistry of silane on the iron oxide particle surface (the detailed chemical reactions are shown in Figure 5).

nanoparticles also strongly depends upon their size and shape as well as their polydispersity, charge, and nature of the coating. Several physicochemical techniques are used to determine these parameters.

5.1. Size, Polydispersity, Shape, and Surface Characterization

Different methods can be used to determine the sizes characterizing nanoparticles. However, "size" is an ambiguous concept. First, it can define different parts of the nanoparticle: the crystalline part of the core, the whole iron core (crystalline and amorphous), the core, the shell, and the hydrated layer, or even a size with no geometrical meaning on the particle but just a physical meaning. Second, in almost all cases, nanoparticles are polydisperse. This heterogeneity of sizes gives rise to different values (even if characterizing the same size) depending upon whether the technique gives access to a number, volume, or even intensity (volume to the power of two)-weighted mean size. In the case of volume and, even more, of intensity weighted, the mean size is boosted toward high values even in the case of very small quantities of the biggest nanoparticles.

The size of the particle core can be determined by TEM images.[530–533] This technique reports the total particle size of the core (crystalline and amorphous parts) and gives access to a number-weighted mean value (Figure 7). Furthermore, it provides details on the size distribution and the shape. However, this technique needs an analysis by image treatment, and it has to be performed on a statistically significant number of particles. Moreover, the sample preparation can induce aggregation of the colloids, and the TEM measurements may consequently not reflect the size and the distribution in solution. Aggregates of smaller particles can be discerned.[534–541]

High-resolution transmission electron microscopy (HR-TEM) gives access to the atomic arrangement. It can be used to study local microstructures (such as lattice vacancies and defects, lattice fringe, glide plane, or screw axes) and surface atomic arrangement of crystalline nanoparticles.[542–544]
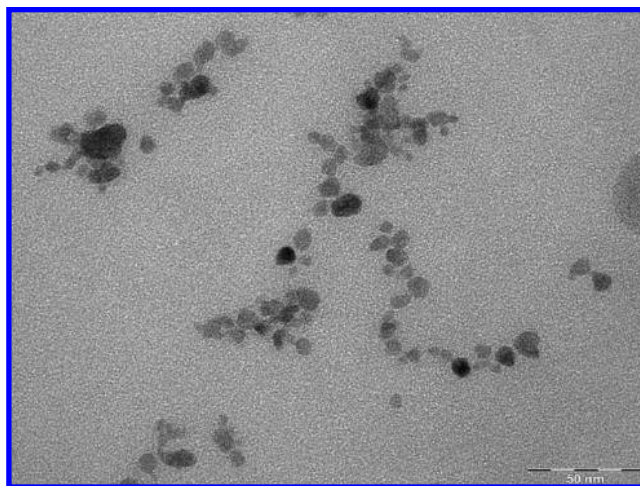

Figure 7. TEM of iron oxide nanoparticles.

XRD can be performed to obtain the crystalline structure of the particles. In a diffraction pattern, the intensity can be used to quantify the proportion of iron oxide formed in a mixture by comparing experimental peak and reference peak intensities.[545] The crystal size can be calculated also from the line broadening from the XRD pattern using the Scherrer formula.[546,547] Extended X-ray absorption fine structure (EXAFS) gives information on the particle size, especially for small sizes.[548,549] Energy dispersive X-ray diffraction (EDXD) provides the advantage of being carried out on the suspension and is used to improve the knowledge of fine structural details. For example, Di Marco et al.[550] studied the structure of maghemite nanoparticles by both classical angular-dependent XRD and EDXD. They found that, although the apparent size of the particles, as determined from both XRD and TEM, is of the order of 7.5 nm, the best correlation with a spherical model used for EDXD gives a far smaller diameter of 4.2 nm only. These results are interpreted as demonstrating the existence of a part in the core with a size of 4.2 nm, characterized by a perfect crystalline coherency and a more disordered surface layer.

SANS is a powerful technique to obtain information on the size, polydispersity, shape (form factor), and even the structure of nanoparticles.[551] The singularity of neutrons is that they interact with the nuclei of the atoms present in the sample. The technique of contrast variation (or contrast matching) relies on the differential scatter of hydrogen versus deuterium. Using certain ratios of H_2O/D_2O, it is possible to achieve the scatter from a part of the particle (typically the core or the shell) as equal to that of the solvent and thus be eliminated when the scatter from the solvent is subtracted from the data. This can be used to study independently the size of the core and the shell of the nanoparticles.

Photon correlation spectroscopy (PCS), also called dynamic light scattering (DLS) or quasi-elastic light scattering (QELS), is a common technique to obtain a nanoparticle size. The determination of the diffusion coefficient of the nanoparticles in solution gives access to the hydrodynamic radius of a corresponding sphere and the polydispersity of the colloidal solution.[552] This radius is an intensity-weighted mean value. A correct conversion to a number or volume-weighted mean value requires the knowledge of the complex refractive index. Unfortunately, the imaginary part is rarely available. Static light scattering at different angles can be used to reach the gyration radius, which is defined as the root-mean-square of mass-weighted distances of all subvolumes in a particle from the center of mass. This technique is also classically used for the determination of form factors. Finally, birefringence measurements can also be used to obtain the hydrodynamic radius. Indeed, magnetic nanoparticles are magnetically and optically uniaxial. Such particles in solution will align along a strong enough magnetic field. As they align, they impart an optical birefringence to the whole medium. If the field is suppressed, the magnetic nanoparticles randomly disorientate and the magneto-optical birefringence relaxes with a characteristic time related to the rotational diffusion time of the particles, giving access to the hydrodynamic radius. Additionally, magnetometry and relaxivity profiles recorded over a wide range of magnetic fields can be used to determine the mean crystal size, among numerous other parameters.

Other physicochemical techniques, such as atomic and chemical force microscopy (AFM and CFM), thermogravimetric analysis (TGA), differential scanning calorimetry (DSC), X-ray photoelectron spectroscopy, thermally programmed desorption, infrared spectroscopy (IR), Fourier transform infrared spectroscopy (FTIR), secondary ion mass spectra (SSIMS and TOF−SIMS), conductimetry, potentiometry, and solid-state NMR, have been used to investigate the surface properties of coated iron oxide nanoparticles. These techniques have been reviewed very recently.[550] It is worth noting that all of these techniques are used to describe the nature and strength of the bonding between the iron oxide surface and the coating but are also used to understand the influence of the coating on the magnetic properties of the nanoparticles.[550]

5.2. Structure of Ferro- or Ferrimagnetic Nanoparticles

5.2.1. Ferro- and Ferrimagnetic Nanoparticles

To be able to form a colloid suspension, the size of the ferromagnetic particle should be much smaller than 1 μm. The usual diameter of the magnetic crystals ranges between 4 and 18 nm, either in isolated crystals or in agglomerated
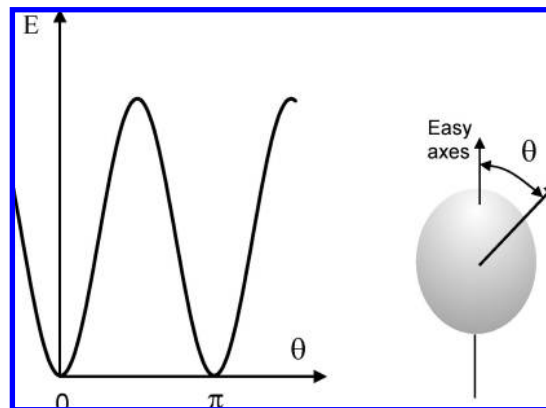

Figure 8. Evolution of the magnetic energy with the tilt angle between the easy axis.
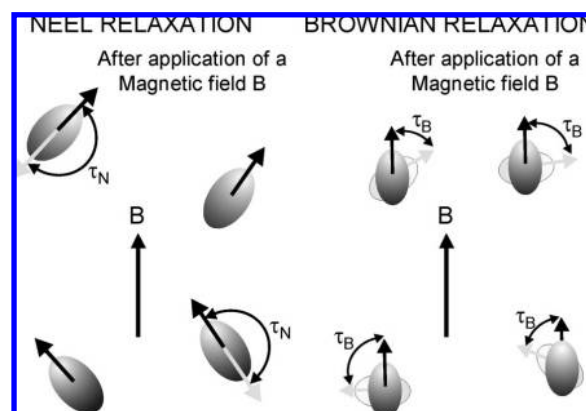

Figure 9. Illustration of the two components of the magnetic relaxation of a magnetic fluid.

crystals forming larger particles. Because each crystal of ferro- or ferrimagnetic material present in the colloid is much smaller than the size of one domain, it is completely magnetized. It constitutes then a nanomagnet made of single domains fully magnetized. It is interesting to note that, at present, the only ferro-fluid used for biomedical applications is based on suspensions of ferrimagnetic ferrite material. In fact, a suspension of small crystals of iron, as magnetite, for example, should be a better material than a ferrite because its magnetization is about 5 times higher than for Fe_3O_4. However, pure iron nanoparticles are very unstable and very quickly oxidized into iron oxide in aqueous media. The development of ferromagnetic nanoparticles useful for biomedical applications will need, therefore, a coating protecting them from oxidation.

In addition to the value of its magnetization, the single monodomain is also characterized by another important property: its anisotropy energy.

As illustrated in Figure 8, the magnetic energy of a nanomagnet depends upon the direction of its magnetization vector (with respect to the crystallographic directions). The directions that minimize this magnetic energy are called anisotropy directions or easy axes. The magnetic energy increases with the tilt angle between the magnetization vector and the easy directions.[553] The variation amplitude of this curve, called anisotropy energy, is given by the product of the crystal volume times a constant, the anisotropy constant.[554] The anisotropy energy proportional to the crystal volume increases thus very rapidly as the crystal radius increases (eq 3).

$$E_a = K_a V \qquad (3)$$

where K_a is the anisotropy constant and V the volume of the crystal.

There are four contributions to the anisotropy field, which may be influenced by the extent of crystal agglomeration: (1) The first one is the bulk magnetocrystalline anisotropy field, which depends upon the chemical composition and the crystallographic structure of the material. (2) The second one is the demagnetising field, which is determined by the shape of the crystal. This component of the anisotropy is equal to zero for a sphere and increases with the elongation of the shape. (3) The third one is the anisotropy constant, which also depends upon the surface structure of the crystal. (4) Finally, for agglomerated structures, there is the dipolar interaction between two neighboring crystals, which increases when the intercrystal distance decreases.

It is usual to consider that the anisotropy has a uniaxial symmetry. Although rather crude if applied to ferrite crystals, this assumption is reasonable for systems of higher symmetry based on cubic models. More complicated symmetries would be more time-consuming for calculation without producing a complete solution because anisotropy is influenced by several contributions. For example, in the case of ferrite, only the bulk magnetocrystalline anisotropy has a cubic symmetry but the shape and intercrystal anisotropy have a uniaxial symmetry.

The anisotropy energy determines also the Néel relaxation time, which constitutes another important parameter of the magnetic behavior of a single nanodomain particle. For dry powder of monodomain particles, the Néel relaxation time is characterized by the time constant of the return to equilibrium of the magnetization after a perturbation. In high anisotropy conditions, the crystal magnetization is locked in the easy axes because of the Boltzman law, which favors the direction of less magnetic energy. The Néel relaxation defines then the fluctuations that arise from the jumps of the magnetic moment between different easy directions.

The function that gives the evolution of the Néel relaxation time τ_N with the anisotropy energy E_a is the product of two factors. One of these is an exponential function of the anisotropy; indeed, to flip from one easy direction to other one, the nanodomain magnetization has to jump over an anisotropy energy hump. This process is similar to a chemical reaction, which needs an energy equal to or larger than an activation energy to occur. The kinetics of the phenomenon is given, therefore, by the Arrhenius law (eq 4).[555]

$$\tau_N = \tau_o(E_a) e^{\frac{E_a}{kT}} \qquad (4)$$

where E_a is the total anisotropy energy, k is the Boltzman constant, and T is the absolute temperature. $\tau_o(E_a)$ is the pre-exponential factor of the Néel relaxation time expression. This factor is also an expression of the anisotropy energy[556,557] given by eq 5

$$\tau_o(E_a) = \frac{\sqrt{\pi}}{4} \frac{(M_s(0)V)}{E_a \gamma_e} \left[\frac{1}{\eta_f} + \eta_f \left(\frac{M_s(T)}{M_s(0)} \right)^2 \right] \sqrt{\frac{kT}{E_a}} \left(1 + \frac{kT}{E_a} \right) \qquad (5)$$

where V is the crystal volume, $M_s(0)$ is the specific magnetization of the crystal extrapolated at 0 K, $M_s(T)$ is the specific magnetization at the laboratory temperature, γ_e is the gyromagnetic ratio of the electron, η_f is a dimensionless
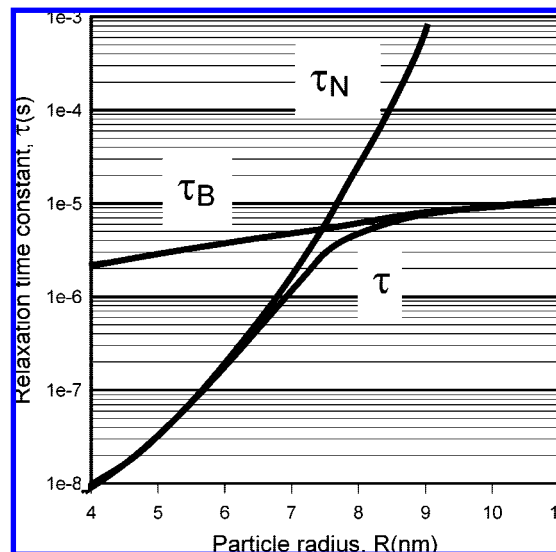

Figure 10. Evolution of the two components of magnetic relaxation with magnetite crystal radius (according to Rosensweig[662]).

constant, and $\eta_f = \eta \gamma_e M_s(0)$, with η being the damping constant.

Contrary to the exponential factor, $\tau_o(E_a)$ decreases as the value of the anisotropy energy increases. For small values of the anisotropy energy and at high temperatures, the following condition is fulfilled: $E_a \ll kT$, and therefore, the exponential factor tends to 1. The Néel relaxation time is determined then by the pre-exponential term, which decreases as the anisotropy energy increases. These conditions of low anisotropy are fulfilled, for example, at ambient temperature for USPIO magnetite particles, which have a radius lower than 4 nm. On the contrary, for the highest anisotropy energy, when $E_a \gg kT$, the evolution of the Néel relaxation time is mainly determined by the exponential factor, which predicts a very fast increase with an increasing E_a.

The magnetization curve of a dry powder of single monodomain ferri- or ferromagnetic particles could have two different behaviors as described below.

5.2.2.1. Frozen Single-Domain Particles. If the Néel relaxation time is longer than the measurement time, the curve is irreversible and presents one hysteresis loop.[558] When the magnetization of the particle is completely frozen, its reversal needs a Zeeman coupling, with the external magnetic field sufficiently strong to overcome the anisotropy energy hump. For example, for very high anisotropy conditions, the Néel relaxation time should be longer than several centuries and the material can be used in the production of computer hard disks. The researches in this field tend to maximize the anisotropy constant K_a of the material with the purpose of storing a given amount of information in as less as possible magnetic material.

5.2.2.2. Superparamagnetism. More often, the condition of frozen magnetization is not fulfilled for the particles used in biomedical applications; this means that the Néel relaxation time is much faster than the measurement time. In addition, in the case of a magnetic fluid, the ferromagnetic crystals are dispersed in a liquid media to form a colloid. In these conditions, the return of the magnetization to equilibrium is determined by two different processes. The first one is the Néel relaxation, and the second one is the Brownian relaxation, which characterizes the viscous rotation of the entire particle (Figures 9 and 10). The global magnetic

relaxation rate of the colloid is therefore the sum of the Néel relaxation rate and the Brownian relaxation rate (eq 6).[559]

$$\frac{1}{\tau} = \frac{1}{\tau_N} + \frac{1}{\tau_B} \qquad (6)$$

where τ is the global magnetic relaxation time and τ_B is the Brownian relaxation time (eq 7).

$$\tau_B = \frac{3V\eta}{kT} \qquad (7)$$

For large particles, τ_B is shorter than τ_N because the Brownian component of the magnetic relaxation is proportional to the crystal volume and the Néel relaxation is an exponential function of the volume. Thus, the viscous rotation of the particle becomes the dominant process determining the global relaxation, which becomes then much faster than for dry powders. In these conditions, the magnetization curve is perfectly reversible because the fast magnetic relaxation allows the system to be always at thermodynamic equilibrium. This behavior has been named "superparamagnetism" by Bean and Livingston.[560]

When these equilibrium conditions are completely fulfilled, the material is superparamagnetic and the magnetization evolution with the external magnetic field is proportional to the Langevin function that takes into account a Boltzman distribution of the energy level corresponding to all of the possible orientations of the particle magnetization moment (eq 8)

$$m_a(B_o) = m_a(\infty)L(x) \qquad (8)$$

where $m_a(B_o)$ is the magnetization of the suspension at a field B_o, $m_a(\infty)$ is the magnetization at saturation, and $L(x)$ is the Langevin function (eq 9)

$$L(x) = [\coth(x) - 1/x] \qquad (9)$$

$$\text{with } x = \frac{M_s(T)VB_o}{kT}$$

The fitting of the experimental magnetization curve (Figure 11) of a magnetic fluid by eqs 8 and 9 allows for the determination of the size of the crystal and its specific
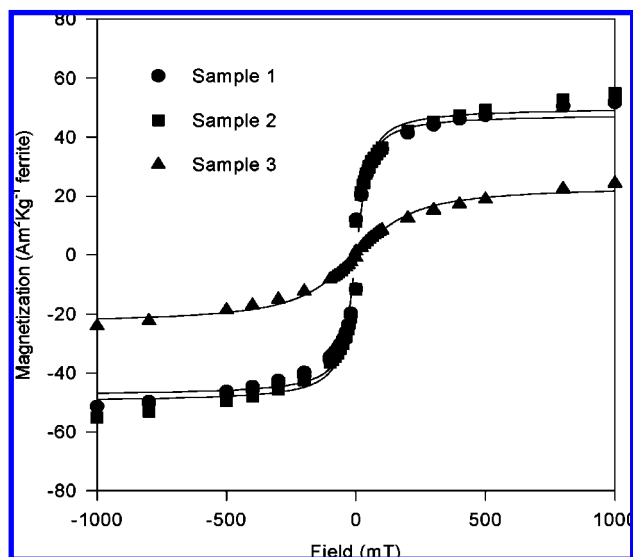

Figure 11. Magnetometric curves for different iron oxide nanoparticles (sample 1 with $r = 5.59$ nm, sample 2 with $r = 5.67$ nm, and sample 3 with $r = 4.84$ nm).

magnetization.[561] The determination of the anisotropy energy is a much more difficult task. Numerous attempts are based on the blocking temperature determination, which characterizes the temperature where the magnetic relaxation time is roughly equal to the measurement time. Considering the magnetization curves, for example, it is the temperature below which a hysteresis can be observed. A more useful and fast measurement method consists of comparing the evolution of the magnetization as the temperature increases when the sample has been cooled, with and without a saturation magnetic field. The two curves diverge below the blocking temperature.[562]

The blocking temperature can also be determined by the Mossbauer spectra evolution. It is determined by the temperature for which the sextuplet lines of iron collapse into a quadrupolar doublet because the Néel relaxation time becomes shorter than the precession period of the iron magnetic moment.[563]

A number of methods can be used to determine the Néel relaxation time. The most common one consists of determining the abscissa of the maximum point ν_{max} in the curve that gives the frequency dependence of the susceptibility of the complex in alternative current units. This frequency allows for the determination of the magnetic relaxation time[564] (eq 10)

$$\tau = 1/2\nu_{max} \qquad (10)$$

For long magnetic relaxation times, one method consists of measuring the rate at which the magnetization of the sample decreases after release from the external magnetization field. For shorter ones, as shown later, fitting of relaxometric data can be used.

In conclusion, the magnetic properties of the colloid are mainly determined by the diameter of the crystal, its saturation magnetization, and its Néel relaxation time, which depends upon the anisotropy constant. The stage of aggregation of a particle should also have a strong effect on the Néel relaxation because of the dipolar intercrystal coupling aspect of the anisotropy.

5.3. Use of Nanoparticles as Contrast Agents for MRI

Because of their very high transverse relaxivity,[565] colloidal suspensions of superparamagnetic nanocrystals are very good candidates for the development of new smart contrast agents, allowing for an early detection of several pathologies. The optimization of the efficiency of these "smart" contrast agents requires a good knowledge of the relationship between proton relaxation and physical and morphological properties of the particle.[566]

The nuclear magnetic relaxation properties of a compound are ideally obtained by the study of its nuclear magnetic resonance dispersion (NMRD) profile. These curves give the relaxivity evolution versus the external magnetic field. The relaxivity is defined as the increase of the relaxation rate of the solvent (water) induced by 1 mmol/L of the active ion. For example, in the case of magnetite, the relaxivity is the relaxation rate enhancement observed for an aqueous solution containing 1 mmol of iron/L (eq 11)

$$R_{i(obs)} = \frac{1}{T_{i(obs)}} = \frac{1}{T_{i(diam)}} + r_iC; \quad i = 1 \text{ or } 2 \qquad (11)$$

where $R_{i(obs)}$ is the global relaxation rate of the aqueous system (s^{-1}), $T_{i(diam)}$ is the relaxation time of the system

before the addition of the contrast agent, C is the concentration of the paramagnetic center (mmol L^{-1}), and r_i is the relaxivity (s^{-1} $mmol^{-1}$ L).

Paramagnetic Relaxation

The USPIO relaxation mechanism is built on the original theory developed for paramagnetic systems. There are two contributions to proton relaxation in paramagnetic systems: the inner- and outersphere relaxations. Innersphere relaxation deals with the direct exchange of energy between protons and electrons located in the first hydratation sphere of the paramagnetic ion and is dominated by dipolar and scalar coupling of the spins. The dipolar coupling is modulated by the rotation of the paramagnetic center characterized by τ_R, the residence time of water molecules in the first hydratation sphere τ_M, and the electron relaxation of the electronic spin associated with the paramagnetic ion τ_{S1} and τ_{S2}. The correlation terms τ_{C1} and τ_{C2} are used to define the modulation of the dipolar couplings and are defined by eq 12.

$$\frac{1}{\tau_{Ci}} = \frac{1}{\tau_R} + \frac{1}{\tau_M} + \frac{1}{\tau_{Si}} \quad (12)$$

The contribution of the innersphere relaxation on the total relaxation rate of water protons may be predicted using the Solomon–Bloembergen equation

$$\frac{1}{\tau_{1M}} = \frac{2}{15}\left(\frac{\mu_o}{4\pi}\right)^2 \gamma_I^2 \gamma_S^2 \bar{h}^2 S(S+1)\frac{1}{r^6}\left[\frac{7\tau_{C2}}{1+(\omega_S\tau_{C2})^2} + \frac{3\tau_{C1}}{1+(\omega_I\tau_{C1})^2}\right] \quad (13)$$

$$\frac{1}{\tau_{S1}} = \frac{1}{5\tau_{SO}}\left[\frac{1}{1+\omega_S^2\tau_V^2} + \frac{4}{1+4\omega_S^2\tau_V^2}\right] \quad (14)$$

$$\frac{1}{\tau_{S2}} = \frac{1}{10\tau_{SO}}\left[3 + \frac{5}{1+\omega_S^2\tau_V^2} + \frac{2}{1+4\omega_S^2\tau_V^2}\right] \quad (15)$$

where γ_S and γ_I are the gyromagnetic ratios of the electron (S) and the proton (H), respectively, ω_S and ω_I are the angular frequencies of the electron and the proton, r is the distance between coordinated water protons and the unpaired electron spin, and τ_{C2} and τ_{C2} are the correlation times modulating the interaction, defined by eq 12. τ_{S1} and τ_{S2} are the longitudinal and transverse relaxation times of the electron. These latter parameters are field-dependent (eqs 14 and 15). τ_{SO} is the value of τ_{S1} and τ_{S2} at zero field, and τ_V is the correlation time characteristic of the electronic relaxation times.

For superparamagnetic particles, the innersphere contribution to the relaxation is minor and more often completely negligible as compared to the dominant outersphere contribution. This relaxation is due to the movement of the water protons near the local magnetic field gradients generated by the paramagnetic ion. The interaction between proton spins and the magnetic moment is also a dipolar interaction. This intermolecular mechanism is modulated by the translational correlation time (τ_D) that takes into account the relative diffusion constant (D) of the paramagnetic center and the solvent molecule, as well as their distance of closest approach (d). The outersphere model has been described by Freed,[567]

and for paramagnetic ions, the outersphere contribution is given by eq 16.

$$R_1^{OS} = \frac{6400\pi}{81}\left(\frac{\mu_0}{4\pi}\right)^2 \gamma_I^2 \gamma_S^2 \bar{h}^2 S(S+1)N_A\frac{[C]}{dD}[7j(\omega_S\tau_D) + 3j(\omega_I\tau_D)] \quad (16)$$

with

$$j(\omega\tau_D) = \mathrm{Re}\left[\frac{1+\frac{1}{4}(i\omega\tau_D + \tau_D/\tau_{S1})^{1/2}}{1+(i\omega\tau_D + \tau_D/\tau_{S1})^{1/2} + \frac{4}{9}(i\omega\tau_D + \tau_D/\tau_{S1}) + \frac{1}{9}(i\omega\tau_D + \tau_D/\tau_{S1})^{3/2}}\right] \quad (17)$$

where [C] is the molar concentration of the paramagnetic ion, and $\tau_D = d^2/D$ is the translational correlation time, and N_A is the Avogadro number.

Superparamagnetic Relaxation

Superparamagnetic relaxation is generally governed by Freed's equations when τ_{S1} is the Néel relaxation time.[568] When the translational diffusion correlation time is much shorter than the Néel relaxation time, Freed's equations reduce to the earlier equations of Ayant.[569]

The ability of a fluctuation to relax the proton spins depends upon whether its correlation time is longer or shorter than the precession period of the spins within the external magnetic field B_o: if the global correlation time τ_C ($\tau_C^{-1} = \tau_D^{-1} + \tau_N^{-1}$) is longer than this period, the fluctuation is averaged by the precession and it is inefficient, while it is efficient in the opposite situation.

Furthermore, electron polarization may or may not itself be relaxed by the same fluctuation, depending upon how its correlation time is situated (longer or shorter) regarding the electron spin precession period. Equation 18 thus defines the boundary separating domains, where the fluctuation characterized by a correlation time τ_C induces relaxation ($\omega_I\tau_C < 1$) and where it does not ($\omega_I\tau_C > 1$), with ω_I being the angular frequency of the proton precession.

$$\omega_I\tau_C = 1 \quad (18)$$

The indirect influence of the magnetic moment precession of the crystal is also visible through the dispersion centered around $\omega_S\tau_C = 1$, where ω_S is the electron spin angular frequency. Because ω_S is 658 times faster than ω_I, the center of the dispersion points of the electron appear at a much lower field than the center of the dispersion of the proton.[570] The relaxation induced by superparamagnetic crystals is moreover complicated by another feature: the influence of the electron magnetic moment is modulated by the Néel relaxation, which depends upon the crystal anisotropy.

For large superparamagnetic crystals or crystals with a very high anisotropy constant,[571] the anisotropy energy is larger than the thermal energy, which maintains the direction of the crystal magnetic moment very close to that of the anisotropy axes. This feature validates a simplified model, where the precession of the electron magnetization is forbidden.

On the contrary, in small crystals, the anisotropy energy is comparable to the thermal energy, so that the probability of the magnetic moment pointing toward a direction far from
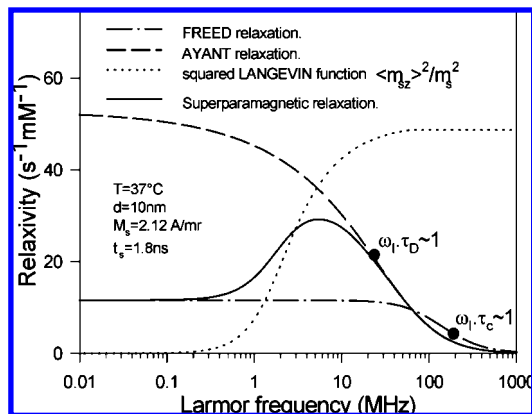
Figure 12. Different contributions to proton relaxation in the simplified model for crystals with large anisotropy.

the easy axis is no longer negligible, which allows at least for some electron precession.

Explaining the field dependence of the longitudinal relaxation rate (NMRD profile) is in any case based on the so-called Curie relaxation,[572] which arises from considering separately two contributions to relaxation: first, diffusion into the inhomogeneous nonfluctuating magnetic field created by the mean crystal moment, aligned onto B_o (strictly speaking, this contribution is precisely termed the Curie relaxation), and second, the fluctuations of the electronic magnetic moment or the Néel relaxation. The Curie relaxation accounts essentially for the high field part of the NMRD profiles (B_o > 0.02 T), namely, by considering that the mean magnetization is an increasing function of B_o, given by the Langevin function.

5.3.1. High Anisotropy Model

When the anisotropy energy is large enough it prevents any precession of the magnetic moment of superparamagnetic crystals. The magnetic fluctuations then arise from the jumps of the moment between different easy directions.

At low field, the proton longitudinal relaxation rate is obtained by introducing into the Freed equations the precession prohibition mentioned above: the electron Larmor precession frequency is set to zero.[573] The spectral density function determining this component of the relaxation is characterized by a global correlation time depending upon

τ_N and τ_D (eqs 19 and 20). Figure 12 shows the dispersion of this density spectral function, called Freed function, centered around $\omega_I = 1/\tau_C$.

$$1/T_1 = 10c\mu^2 J_F(\omega_I, \tau_D, \tau_N) \quad (19)$$

$$1/T_2 = c\mu^2\{8J_F(\omega_I, \tau_D, \tau_N) + 2J_F(0, \tau_D, \tau_N)\} \quad (20)$$

$$\text{where } c = (32\pi/40\,5000)\gamma^2 N_A[M]/r^3$$

In eqs 19 and 20, r is the particle radius, N_A is the Avogadro number, μ is the magnetic moment of the particle, and γ is the proton gyromagnetic ratio.

Freed's spectral density function, J_F, is defined according to eq 21.

$$J_F(\omega_I, \tau_D, \tau_N) = \text{Re}\left(\frac{1 + \frac{1}{4}\Omega^{1/2}}{1 + \Omega^{1/2} + \frac{4}{9}\Omega + \frac{1}{9}\Omega^{3/2}}\right) \quad (21)$$

$$\text{where } \Omega = i\omega_I\tau_D + \tau_D/\tau_N$$

At high field, the magnetic vector is locked along the B_o direction and the Curie relaxation dominates. The corresponding relaxation rates are given by Ayant's model,[569] assuming a stationary magnetization component in the B_o direction

$$R_2 = c\mu^2\{4.5J_A(\sqrt{2\omega_I\tau_D}) + 6J_A(0)\} \quad (22)$$

$$1/T_1 = c\mu^2\{9L^2(x)J_A(\sqrt{2\omega_I\tau_D})\} \quad (23)$$

where J_A, Ayant's density spectral function, is

$$J_A(z) = \frac{1 + \frac{5z}{8} + \frac{z^2}{8}}{1 + z + \frac{z^2}{2} + \frac{z^3}{6} + \frac{4z^4}{81} + \frac{z^5}{81} + \frac{z^6}{648}} \quad (24)$$

The dispersion of this spectral density occurs for $\omega_I\tau_D \sim 1$.

At intermediate field, the proton relaxation rates (R_1 and R_2) are combinations of the high- and low-field contributions, weighed by factors depending upon the Langevin function[574] (Figure 12).
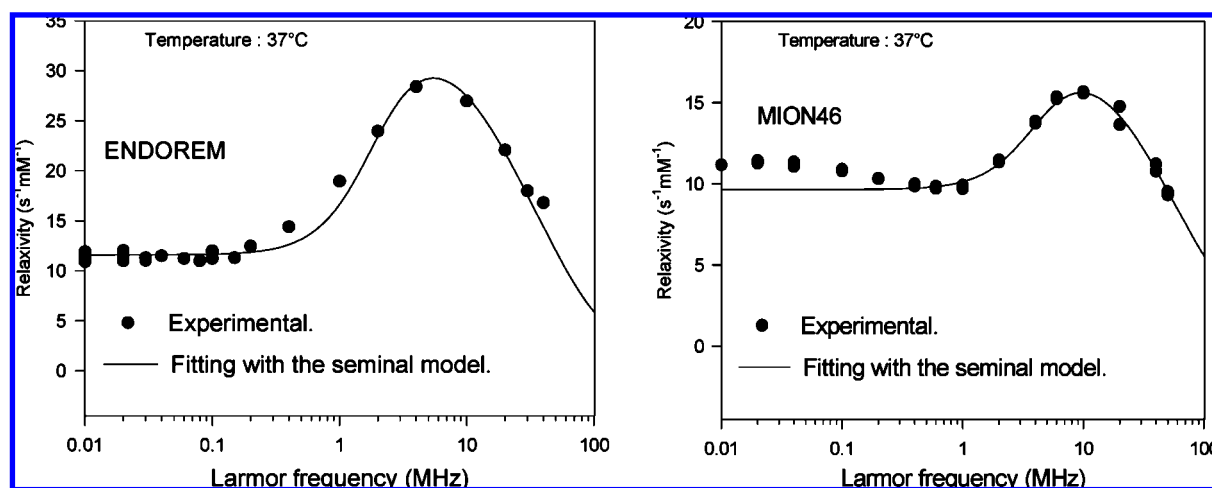

Figure 13. Fitting with the simplified model of the NMRD profile of an endorem solution (a typical SPIO sample) and a MION46 solution (USPIO sample).

$$1/T_1 = c\mu^2\{(L(x)/x)21J_F(\omega_I, \tau_D, \tau_N) + 9[1 - L^2(x) -$$
$$2(L(x)/x)]J_F(\omega_I, \tau_D, \tau_N) + 9L^2(x)J_A(\sqrt{2\omega_I}, \tau_D)\} \quad (25)$$

$$1/T_2 = c\mu^2\{(L(x)/x)[19.5J_F(\omega_I, \tau_D, \tau_N)] + [1 - L^2(x) -$$
$$2(L(x)/x)]4.5[J_F(\omega_I, \tau_D, \tau_N) + 6J_F(0, \tau_D, \tau_N)] +$$
$$L^2(x)[4.5J_A(\sqrt{2\omega_I}, \tau_D) + 6J_A(0)]\} \quad (26)$$

where $L(x)$ is the Langevin function.

This model matches the experimental relaxation results for large particles containing more than one crystal by coating flake (SPIO particles) but fails to describe the low-field part of the NMRD curves of USPIO containing only one magnetic crystal by particle (Figure 13).

5.3.2. Small Crystal and Low Anisotropy Energy Limit

Equations 25 and 26 arise from an assumption of rigorous locking of the magnetization along the easy axes, assuming infinite anisotropy energy. This assumption becomes less and less valid when the particle size and, consequently, the anisotropy energy decrease. Accounting for such a reduced coupling with the anisotropy field requires a new theory[575] aimed at introducing anisotropy energy as a quantitative parameter of the problem, going beyond the two limits considered so far (eqs 25 and 26), where anisotropy energy has been assumed to be infinite and the classical outer sphere theory, adapted to high susceptibility paramagnetic material,[576–578] is neglected.

However, from a practical point of view, considering calculation time constraints, it seems hopeless to fit experimental NMRD curves with an alternative heuristic model, which reproduces the gradual vanishing of the low field dispersion through a linear combination of the rate for infinite and zero anisotropy energy (eqs 27 and 28).

$$1/T_1 = c\mu^2\{(L(x)/x)[21PJ_F(\omega_S, \tau_D, \tau_N) + 21(1 -$$
$$P)J_F(\omega_I, \tau_D, \tau_N)] + 9[1 - L^2(x) -$$
$$2(L(x)/x)]J_F(\omega_I, \tau_D, \tau_N) + 9L^2(x)J_A(\sqrt{2\omega_I}, \tau_D)\} \quad (27)$$

$$1/T_2 = c\mu^2\{(L(x)/x)[10.5PJ_F(\omega_S, \tau_D, \tau_N) +$$
$$9PJ_F(\omega_I, \tau_D, \tau_N)] + 19.5(1 - P)J_F(\omega_I, \tau_D, \tau_N)] + [1 -$$
$$L^2(x) - 2(L(x)/x)][4.5J_F(\omega_I, \tau_D, \tau_N) + 6J_F(0, \tau_D, \tau_N)] +$$
$$L^2(x)[4.5J_A(\sqrt{2\omega_I}, \tau_D) + 6J_A(0)]\} \quad (28)$$

The theory predicts a clear difference between the low field relaxation profiles observed for small particles (weak dispersion) and those for larger particles (no dispersion). These predictions are confirmed by the difference between the NMRD profiles of SPIO and USPIO particles. Further experimental confirmation of this theoretical approach was provided by the NMRD curves of suspensions of colloidal magnetite doped with cobalt, an element which considerably enhances the energy of anisotropy.[574] For these small particles, a weak low field dispersion is apparent at very low cobalt content but disappears if the crystals are doped more heavily.

5.3.3. Practical Interests of Magnetic Nuclear Relaxation for the Characterization of Superparamagnetic Colloid

The study of the nuclear magnetic relaxation presents two main interests. The first step in the characterization of a new
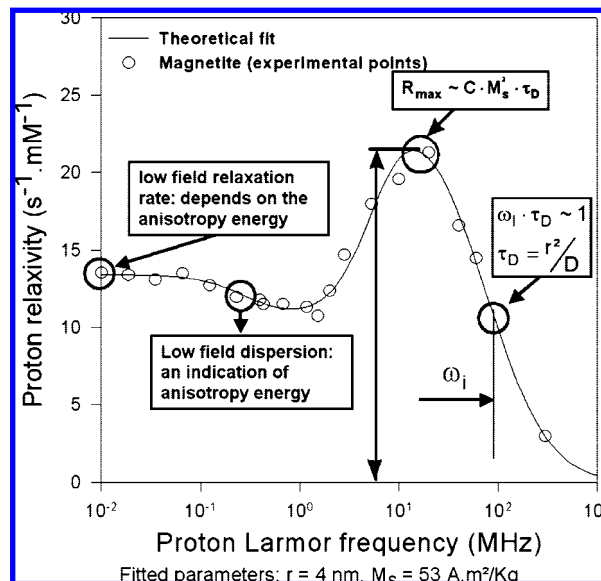

Figure 14. NMRD profile of magnetite particles in colloidal solution.

superparamagnetic colloid is obviously the evaluation of its relaxometric properties, which determine its potential efficiency for MRI.[579] Relating these valuable relaxometric data to the morphological and physical properties of the particles may be performed thanks to the above proton relaxivity theory.

Furthermore, the analysis of the NMRD profiles constitutes an interesting tool to control the reproducibility and optimize the parameters of nanomagnet synthesis.[580] The fitting of the NMRD profiles by adequate theories provides information about the nanomagnet crystals, namely, their average radius r, their specific magnetization M_s, their anisotropy energy E_a, and their Néel relaxation time τ_N.[581]

(1) Average Radius (r). At high magnetic fields, the relaxation rate only depends upon τ_D and the inflection point corresponds to the condition $\omega_I\tau_D \sim 1$ (Figure 14). Because $\tau_D = r^2/D$, the determination of τ_D gives the crystal size r.

(2) Specific Magnetization (M_s). At high fields, M_s can be obtained from the equation $M_s \sim (R_{max}/C\tau_D)^{1/2}$, where C is a constant and R_{max} is the maximal relaxation rate.

(3) Crystal Anisotropy Energy (E_a). The absence or presence of a dispersion at low fields provides information about the magnitude of the anisotropy energy. For crystals characterized by a high E_a value as compared to the thermal agitation, the low field dispersion disappears. This has been confirmed in a previous work with cobalt ferrites,[575] which are known to have high anisotropy energy.

(4) Néel Relaxation Time (τ_N). The relaxation rate at very low fields R_0 is governed by a "zero magnetic field" correlation time τ_{C0}, which is equal to τ_N if $\tau_N \ll \tau_D$. Often, however, this situation is not met; therefore, τ_N is often reported as qualitative information in addition to the crystal size and the specific magnetization.

5.3.4. Relaxation of Agglomerated Systems

The aggregation of nanomagnets has two different types of consequences on the proton relaxation properties: on the one hand, those related to the global structure of the cluster and to the magnetic field distribution around them and, on the other hand, those limited to the inner part of the

aggregate.[582] While the global effect dominantly affects R_2, the inner one influences less R_2 and affects mainly R_1.

Let us focus on the first effect that allows for control of the aggregation stage of the ferrofluid.

The cluster itself may be considered as a large magnetized sphere where the total magnetic moment increases according to Langevin's law. The global magnetization of the agglomerate is always aligned with the external field. It is characterized by a long correlation time, because of its large size, so that it mainly affects the secular term of the relaxation rate. This contribution is given by the outersphere diffusion theory, provided that the motional averaging condition is fulfilled: $\Delta\omega\tau_D < 1$, where $\Delta\omega$ is the difference in angular frequencies between the local field experienced by a proton at the equatorial line of the cluster surface and in the bulk ($\Delta\omega = \mu_o M\gamma/3$, where μ_o is the vacuum magnetic permeability, M is the particle magnetization, and γ is the proton gyromagnetic ratio) and τ_D is the translational diffusion time around the cluster ($\tau_D = R_a^2/D$, with R_a being the cluster radius and D being the water diffusion coefficient)

$$1/T_2 = 16f_a\Delta\omega^2\tau_D/45 \quad (29)$$

with f_a being the volumic fraction occupied by the clusters. This secular contribution explains the increase of $1/T_2$ at high fields.[583,584] Equation 29 can be rewritten to make the cluster magnetic moment appear (eq 30)

$$1/T_2 = (64\pi/135)[\mu_o\gamma\,\mu_{sp}N_gL(x)/(4\pi)]^2N_AC_a/(R_aD) \quad (30)$$

where μ_{sp} is the magnetic moment of an elementary crystal, N_g is the crystal number in an agglomerated particle, N_A is the Avogadro number, C_a is the agglomerate concentration in mmol/L, and $x = \mu_{sp}N_gB_o/(kT)$, with B_o being the static field, k being the Boltzmann constant, and T being the temperature. The Langevin function $L(x)$ is defined in eq 9.

For an aggregate with a radius of 100 nm, $\tau_D = 3\ \mu s$, which is much shorter than usual echo times ($\tau_{CP} = TE/2$); refocusing pulses are thus inefficient, and there is no difference between T_2 and T_2^*. When the motional averaging condition breaks down, T_2^* has been shown to be given by the static dephasing regime, which refers to the dephasing of motionless magnetic moments in a nonuniform field created by randomly distributed dipoles[585,586]

$$1/T_2^* = 2\pi\sqrt{3}f_a\Delta\omega/9 \quad (31)$$

It applies to spheres with a radius large enough to fulfill the condition $\tau_D > \tau_{SDR}$,[587] where

$$\pi_{SDR} = \pi\sqrt{3}/(2\Delta\omega) \quad (32)$$

T_2 remains equal to T_2^* as long as the refocusing pulses are not efficient. This only occurs for larger spheres, for diffusion times larger than τ_L, where

$$\tau_L = (1.49/\Delta\omega)x^{1/3}(1.52 + f_ax)^{5/3} \quad (33)$$

$$\text{with } x = \Delta\omega\tau_{CP}$$

For $\tau_D > \tau_L$, the relaxation rate decreases with the radius[587] (Figure 15)

$$1/T_2 = 1.8f_ax^{1/3}(1.52 + f_ax)^{5/3}/\tau_D \quad (34)$$

while T_2^* remains, given by eq 31.

In conclusion, the aggregation of superparamagnetic crystals affects mainly the transverse relaxation and can be detected by a modification of the r_1/r_2 ratio.

Typical Superparamagnetic MR Contrast Agents. Particulate magnetic contrast agents include ultrasmall particles [ultra small particles of iron oxide (USPIO), diameter between 10 and 40 nm], small particles [small particles of iron oxide (SPIO), diameter between 60 and 150 nm], and oral (large) particles (diameter between 300 nm and 3.5 μm). Two subcategories of USPIO are called monocrystalline iron oxide nanoparticles (MION, diameter between 10 and 30 nm,[588,589] and CLIO, diameter between 10 and 30 nm,[590] a form of MION with cross-linked dextran coating).

Some particles have been approved for clinical application or are being clinically tested (Table 1).[591] Particles with submicrometer size can be used for intravenous administration.

6. Applications

6.1. MRI: Cellular Labeling, Molecular Imaging (Inflammation, Apoptose, etc.)

Molecular imaging is of course one of the most promising applications of targeted iron oxide nanoparticles. Various applications using targeted iron oxide nanoparticles have been evaluated *in vitro* and in animal experiments.

Different antibodies or fragments directed to several types of receptors (HER2/Neu, LHRH, EGFR, myosine, lymphocyte, selectin, V-CAM1, etc.) have been coupled to iron oxide nanoparticles and have been tested either *in vitro* or *in vivo*. *In vivo*, specific binding to the tumor has been assessed by comparison to the lack of binding of naked nanoparticles. While various "proof of concept" studies have been performed, transposition into human applications is not yet available.

A modified cellular enzyme-linked immunosorbent assay (ELISA), named cellular magnetic-linked immunosorbent assay (C-MALISA), has been developed as an application of MRI for *in vitro* clinical diagnosis.[7] To validate the method, three contrast agents targeted to integrins were synthesized by grafting to USPIO: (a) the CS1 (connecting
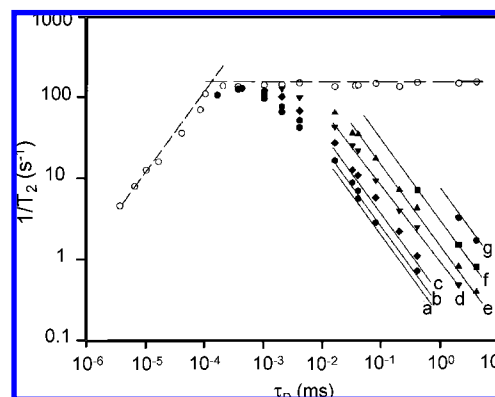
Figure 15. Computer-generated data for spheres with $v = 5 \times 10^{-6}$ and $\Delta\omega_r = 2.36 \times 10^7$ rad/s, plotted versus τ_D. The open symbols represent the $1/T_2^*$ value, while the filled symbols represent rates obtained, respectively, with $\tau_{CP} = 0.1$ ms (● and line a), 0.2 ms (● and line b), 0.5 ms (◆ and line c), 2 ms (▼ and line d), 5 ms (▲ and line e), 10 ms (■ and line f), 20 ms (● and line g). The short dashed line is the rate predicted by the outer sphere theory (eq 30), and the long dashed line is the static dephasing relaxation model given in ref 584. Lines a–g are the rates given by eq 34.

Table 1. Characteristics of USPIO and SPIO Agents: Commercial or under Clinical Investigation

names	company	applications	relaxometric properties × 1.5 T mM^{-1} s^{-1}	coating agent	hydrodynamic size (nm)
ferumoxides AMI-25 (ref 592) Endorem/Feridex	Guerbet, Advanced Magnetics	liver imaging cellular labeling	$r_1 = 10.1$ $r_2 = 120$	dextran T10	120−180
ferumoxtran-10 AMI-227 (ref 593) BMS-180549 Sinerem/Combidex	Guerbet, Advanced Magnetics	metastatic lymph node imaging macrophage imaging blood pool agent cellular labeling	$r_1 = 9.9$ $r_2 = 65$	dextran T10, T1	15−30
ferumoxytol Code 7228 (ref 592)	Advanced Magnetics	macrophage imaging blood pool agent cellular labeling	$r_1 = 15$ $r_2 = 89$	carboxylmethyl-dextran	30
ferumoxsil AMI-121 (ref 359) Lumirem/Gastromark	Guerbet, Advanced Magnetics	oral GI imaging	na	silicon	300
ferucarbotran SHU-555A (ref 594) Resovist	Schering	liver imaging cellular labeling	$r_1 = 9.7$ $r_2 = 189$	carboxydextran	60
SHU-555C (ref 595) Supravist	Schering	blood pool agent cellular labeling	$r_1 = 10.7$ $r_2 = 38$	carboxydextran	21
feruglose NC100150 (refs 377 and 407) Clariscan	GE-Healthcare (abandoned)	blood pool agent	na	pegylated starch	20
ferristene Abdoscan	GE-Healthcare	oral GI imaging	na	sulphonated styrene− divinylbenzene copolymer	3500
VSOP-C184 (ref 280)	Ferropharm	blood pool agent cellular labeling	$r_1 = 14$ $r_2 = 33.4$	citrate	7

segment-1) fragment of fibronectin (FN) (USPIO-g-FN), (b) the peptide GRGD (USPIO-g-GRGD), and (c) a nonpeptidic RGD mimetic. After cell fixation on ELISA plates, incubation of Jurkat cells and rat mononuclear cells stimulated to activate their integrins with the contrast agents, rinsing, and digestion, the samples were analyzed by MRI. The apparent dissociation constants (K_d^*) of the three contrast agents were estimated on the basis of the MRI measurement.

Small pharmacophores, such as peptides or small organic ligands, are promising approaches. Biologically active molecules can be selected by phage display from large populations of randomly generated peptide sequences to target different pathologies, such as apoptosis.[596] The selected peptides are synthesized and conjugated to a reporter molecule for subsequent detection by MRI for diagnostic imaging. This approach opens up a wide range of targeting possibilities, but the difficulty will be to select the most promising pharmacophore for clinical imaging, taking into account the sensitivity of MRI that limits the selection of biological targets, which are present in small quantities.

Two examples are detailed below to illustrate the interest of iron oxide particles in MR molecular imaging.

Targeting of the endothelial inflammatory adhesion molecule E-selectin by MRI was successfully performed with a superparamagnetic contrast agent in the context of *in vitro* and *in vivo* models of inflammation.[8] The specific contrast agent was obtained by grafting a synthetic mimetic of sialyl Lewis^x (sLe^x), a natural ligand of E-selectin expressed in leukocytes, on the dextran coating of ultrasmall particles of iron oxide (USPIO). This new contrast agent, USPIO-g-sLe^x, was tested *in vitro* on cultured human umbilical vein endothelial cells (HUVECs) stimulated to express inflammatory adhesion molecules and *in vivo* on a mouse model of hepatitis. Both *in vitro* and *in vivo* results indicated that USPIO-g-sLe^x recognizes endothelial E-selectin. USPIO-g-sLe^x is thus well-suited for the MRI diagnosis of inflammation and the *in vitro* evaluation of endothelial cell activation. Nanoparticles 10−100 nm in size can deliver large payloads

to molecular targets but undergo slow diffusion and/or slow transport through delivery barriers. To examine the feasibility of nanoparticles targeting a marker expressed in tumor cells, Montet et al. used the binding of cyclic arginine−glycine−aspartic acid (RGD) nanoparticle targeting integrins on BT-20 tumor as a model system using the CLIO technology.[497,499,597] The results suggest that nanoparticles could be targeted to the cell-surface markers expressed in tumor cells, at least in the case wherein the nanoparticles and the tumor model have characteristics similar to those of the BT-20 tumor.

Another successful application of iron oxide nanoparticles in MRI is specific cell tracking. The ability to load enough magnetic particles (micromolar Fe concentration) in cell culture via cell-permeable peptide or transfection agents in combination with the negatively charged surface of magnetic particles has provided a useful technique to label and track cells *in vivo* by MRI.[96,598]

The first cellular imaging studies were performed with unfunctionalized iron oxide nanoparticles for labeling leukocytes, lymphocytes, etc.[599–602] If a cell can be sufficiently loaded with magnetic particles, MRI allows for cell tracking with a resolution approaching the size of the cell.[6] To increase the cellular uptake of magnetic iron oxide particles, particles have been vectorized with various peptides, fragments of proteins[603–606] or coated with dendrimers.[91] Folic acid has been grafted on magnetic particles for targeting folate receptors.[607,608]

Bulte has used MRI to provide information on the location and migration of cells after transplantation or transfusion. This approach requires magnetic prelabeling of the cells. With the currently available magnetic labeling methods, it is anticipated that cellular MRI will find applications in biology and medicine.[609]

A magnetic nanoparticle conjugate has been developed that can potentially serve both as a contrast agent in MRI and as a drug carrier in controlled drug delivery, targeted at cancer diagnostics and therapeutics. The conjugate is made of iron oxide nanoparticles covalently bound with methotrexate

(MTX), a chemotherapeutic drug that can target many cancer cells overexpressing folate receptors on their surface. The nanoparticles were first surface-modified with (3-aminopropyl)trimethoxysilane to form a self-assembled monolayer and were subsequently conjugated with MTX through amidation between the carboxylic acid end groups on MTX and the amine groups on the surface of the particle. Drug-release experiments demonstrated that MTX was cleaved from the nanoparticles under low pH conditions mimicking the intracellular conditions in the lysosome. Cellular viability studies in human breast cancer cells (MCF-7) and human cervical cancer cells (HeLa) further demonstrated the effectiveness of such chemical cleavage of MTX inside the target cells through the action of intracellular enzymes. The intracellular trafficking model proposed was supported through nanoparticle-uptake studies, which demonstrated that cells expressing the human folate receptor internalized a higher level of nanoparticles.[610]

SPIONs functionalized by PVAs to enhance detection of neurodegenerative diseases are under clinical evaluation. A major improvement would be to link therapeutic drugs to the SPIONs to achieve targeted drug delivery, either at the cell surface or intracellularly, together with active disease detection, without inducing cell reaction. The objectives are to define the characteristics of SPIONs able to achieve cell-specific interaction with brain-derived structures. The cellular uptake, cytotoxicity, and interaction of these various nanoparticles with brain-derived endothelial cells, microglial cells, and differentiating three-dimensional aggregates have been investigated. Amino-PVA−SPIONs were taken up by isolated brain-derived endothelial and microglial cells at a much higher level than other SPIONs, and no inflammatory activation of these cells was observed. Amino-PVA−SPIONs did not invade brain cell aggregates lower than the first cell layer and did not induce inflammatory reaction in the aggregates. Fluorescent amino-PVA-SPIONs derivatized with a fluorescent reporter molecule and confocal microscopy has demonstrated intracellular uptake by microglial cells. The functionalized amino-PVA-SPIONs represent potential biocompatible vector systems for drug delivery to the brain that may be combined with MRI detection of active lesions in neurodegenerative diseases.[611]

A biocompatible surface-functionalized nanoparticle has been designed to sense phosphatidylserine exposed on apoptotic cells. Quinti et al. conjugated synthetic phosphatidylserine-binding ligands in a multivalent fashion onto magnetofluorescent nanoparticles.[612] Their results showed that the synthetic nanoparticles bind to apoptotic cells, that there is an excellent correlation with annexin V staining by microscopy, and that FACS analysis with nanoparticles allows for the measurement of therapeutic apoptosis induction. The described nanomaterials should be useful for a variety of biomedical applications including *in vivo* imaging of apoptosis.

Recently, magnetic nanoparticles have been converted into sensing superparamagnetic agents.[613] These nanosensors have been designed to detect molecular interactions in biological media after grafting of biomolecules to their surface.[614,615] In the presence of a biological target, the surfacic biomolecules induce either aggregation or dispersion of the nanosensors. These cooperative processes of either assembly or disassembly cause changes in the spin−spin relaxation times, T_2, of water molecules that can be detected by magnetic relaxation measurements or MRI.[613] These

mechanisms have been used to detect biomolecules in homogeneous assays without the need of protein purification or signal amplification. Experiments can be conducted in turbid media and whole cell lysates, and the assay does not require immobilization of the target. Applications have included the detection of oligonucleotide sequences,[615,616] proteins (GFP protein), enzyme activity (myeloperoxidase, endonuclease, protease, caspase, and telomerase),[617–621] pathogens (herpes simplex viruses and adenovirus 5),[618] ions (calcium),[622] analyte (glucose),[623] and enantiomeric impurities[624] with a fentomolar sensitivity.

Table 2 summarizes the different targeted iron oxide nanoparticles for molecular and cellular imaging.

6.2. *In Vitro* Bioseparation

Another important kind of application of iron oxide nanoparticles is the functionalization for *in vitro* protein or cell separation.[631] Magnetic separation techniques have several advantages in comparison to traditional separation procedures. This process is very simple, and all steps of the purification can take place in one test tube without expensive liquid chromatography systems.[632]

Fan et al.[633] have developed magnetic nanoparticles coated with charged bipyridinium carboxylic acids and biotin. Such functionalized particles have been used for affinity isolation of fluorescein-labeled protein avidin. The same strategy using dopamine has been reported by Xu.[634] Dopamine was anchored on magnetic nanoparticles via interactions between the bidentate functional group and the iron oxide surface. Nitriloacetic acid was linked via a linker to dopamine. Upon chelation to Ni ions, dopamine magnetic particles separated histidine-tagged proteins from a cell lysate with efficiency and high capacity. Other −OH, −SH, or −NH$_2$ functional groups have been used for their interaction with metal oxides as capping agents of magnetic cores. For example, the amino groups of vancomycin have been used for immobilizing the antibiotic to the surface of magnetic particles. This system could capture and detect vancomycin-resistant enterococci or Gram-positive bacteria at low concentrations.[635] These −OH, −SH, or −NH$_2$ functional groups can be introduced also through a surface exchange reaction on iron oxide particles coated with a different functional group[636–641] or by coprecipitation of ferrous/ferric salts in the presence of organic capping groups.[642] For example, particles stabilized by oleate can be transferred from the organic to the aqueous phase by surface modification with cyclodextrin.[643]

Organosilane groups have a strong interaction with metal oxide and can also be used for grafting bioactive molecules on magnetic particles.[644–646] Two strategies are known to give a silica coating: (i) silica is formed *in situ* through the hydrolysis and condensation of a sol−gel precursor (Stöber process),[647,648] and (ii) micelles are used to confine the coating of silica on the crystal core.[649]

Magnetoliposomes, magnetic iron oxide nanoparticles coated with phospholipids, have also been useful for separation of proteins from the mixture.[650]

6.3. Drug Delivery

Internalization of iron oxide particles strongly depends upon the size of the particles. After administration, larger particles with a diameter higher than 200 nm are easily sequestered by the spleen and eventually removed by the cells of the phagocyte system, resulting in decreased blood

Table 2. Targeted Iron Oxide Nanoparticles for Molecular and Cellular Imaging

targeted contrast media	physicochemical characteristics	contrastophore	pharmacophore	coupling conditions	biological target	reference
MION–wheat germ agglutinin	D_h = 60 nm	2 WGA per MION dextran-coated MION	fluorescent (rhodamine) labeled polylysine and wheat germ agglutinin	(1) sodium periodate (2) fluorescent (rhodamine) labeled polylysine (3) sodium borohydride (4) SPDP (5) WGA purification by Sephadex chromatography	axon terminals	470–473
MION–mAb(L6)	ND	dextran-coated MION	monoclonal antibody IgG2a mAb(L6) 12 mAb/MION	(1) sodium periodate (2) antibody (3) sodium borohydride purification by biogel chromatography	surface antigen on human carcinoma	468
USPIO–transferrin protein	D_h = 35 nm r_1 = 24 mM^{-1} s^{-1} r_2 = 52 mM^{-1} s^{-1}	carboxy-dextran T2000-coated USPIO	tranferrin protein 280 μg/mg transferrin per iron	(1) sodium periodate (2) protein (3) sodium borohydride purification by Sephadex chromatography and ultrafiltration	transferrin receptors	464
MION–mAb(antimyosin)	ND	dextran-coated MION	antimyosin monoclonal antibody	electrostatic binding of antibody purification by Sephadex chromatography	myocardial infarction	442
MION–Aβ1–40	ND	dextran-coated MION	Aβ1–40 peptide 17 peptides per particle	electrostatic binding	Aβ-amyloid plaque	445
Tf–MION	r_1 = 20 mM^{-1} s^{-1} r_2 = 62 mM^{-1} s^{-1} 0.47 T D_h = 39.6 ± 1.3 nm	dextran-coated MION	transferrin 0.6 tranferrin per particle	(1) sodium periodate (2) transferrin (3) sodium borohydride purification by magnetic separation	transferrin receptors	475, 625–627

Table 2. Continued

targeted contrast media	physicochemical characteristics	contrastophore	pharmacophore	coupling conditions	biological target	reference
Tf–CLIO	$r_1 = 26$ mM^{-1} s^{-1} $r_2 = 114$ mM^{-1} s^{-1} 0.47 T	epiclorohydrin cross-linked dextran-coated CLIO	transferrin 1.2 tranferrin per particle	(1) sodium periodate (2) transferrin (3) sodium borohydride purification by magnetic separation	transferrin receptors	475
MION–Ab(anti-Her2/neu)	$D = 8.3$ nm (TEM) $r_2 = 24$–29 mM^{-1} s^{-1} 1.5 T	dextran-coated MION	monoclonal antibodies anti-Her2 neu 1.8–2.1 antibody per particle	(1) sodium periodate (2) antibody (3) sodium borohydride purification by magnetic separation	Her2/neu receptor on tumor cells	469
MION–succinylated polylysine	ND	dextran-coated MION	succinylated poly-L-lysine	(1) potassium periodate (2) succinylated polylysine (3) sodium borohydride	lymph nodes	474
MION–IgG	$r_2 = 23.4$ mM^{-1} s^{-1} 0.47 T 37 °C	dextran-coated MION	human nonspecific polyclonal IgG 36 μg/mg IgG per iron	electrostatic binding of antibody purification by chromatography	inflammation	465
MION–IgG	$r_2 = 23.4$ mM^{-1} s^{-1} 0.47 T 37 °C	dextran-coated MION	human nonspecific polyclonal IgG 36 μg/mg IgG per iron	(1) potassium periodate (2) antibody (3) sodium borohydride purification by chromatography	inflammation	465
SPIO–mAb(A7)	ND	ferumoxide (dextran-coated)	monoclonal antibodies Mab A7	(1) sodium periodate (2) antibody (3) sodium borohydride purification dialysis and centrifugation	colorectal tumor antigen	466
USPIO–antibody	ND	dextran T40-coated USPIO	monoclonal antihuman mammary cancer antibodies	(1) sodium periodate (2) antibody (3) sodium borohydride purification Sephacryl chromatography	mammary cancer	467
USPIO–RGD	ND	carbohydrate-coated USPIO	cyclic-RGD peptide	(1) sodium periodate (2) peptide O-alkyloxime	$\alpha_{IIb}\beta3$, thrombus imaging	461

Table 2. Continued

targeted contrast media	physicochemical characteristics	contrastophore	pharmacophore	coupling conditions	biological target	reference
SPIO–C2	$D_h = 37$ nm $\pm$ 3 nm $r_2 = 61$ mM^{-1}s^{-1} 9.4 T 37 °C	carboxydextran USPIO	C2 domain of synaptotagmin I	(1) periodate (2) protein (3) sodium borohydride purification Sephadex chromatography and ultrafiltration	phosphatidylserine of apoptotic cells	464
SPIO–C2	ND	streptavidin SPIO	biotinylated C2A domain of synaptotagmin –GST fusion protein	(1) streptavidin SPIO (2) biotinylated protein	apoptotic cells	447
USPIO–antibody	ND	amino-polymer-coated USPIO	monoclonal antibodies	(1) glutaraldehyde (2) antibody	neuroblastoma cancer	453
USPIO–PEG–antibody	$D_h = 237$ nm	carboxy-PEG-coated USPIO	human antibody E-907 492 μg/mg antibody per iron	(1) EDCI (2) antibody purification: magnetic separation	human colon carcinoma	452
USPIO–PEG–antibody	$D_h = 237$ nm	carboxy-PEG-coated USPIO	human antibody E-907 107 μg/mg antibody per Iron	(1) EDCI (2) NHS (3) antibody purification: magnetic separation	human colon carcinoma	452
USPIO–PEG–antibody	$D_h = 237$ nm	amino-PEG-coated USPIO	antibody oxidized with sodium periodate 110 μg/mg antibody per iron	formation of Schiff base with oxidized antibody purification: magnetic separation	human colon carcinoma	452
MION–20 CKK	ND	MION 20	CCK protein	electrostatic binding of protein by sonication	pancreatic cholecystokinin receptor	446
USPIO–mAb-610	ND	uncoated USPIO	monoclonal antibodies mAb-610	electrostatic binding of antibody by sonication purification by centrifugation	surface antigen on colon carcinoma cell line	628
USPIO–mAb(antiEGFR)	$D = 8.7 \pm 0.8$ nm (TEM) $D_h = 13.2 \pm 1.9$ nm	lignosite FML	monoclonal antibodies 1.5 mg of antibody per 30 mg of Fe nanoparticle	electrostatic binding of antibody by sonication purification by centrifugation	epidermal growth factor receptor (EGFR) in esophageal squamous cell carcinoma	444

Table 2. Continued

targeted contrast media	physicochemical characteristics	contrastophore	pharmacophore	coupling conditions	biological target	reference
USPIO–PEG–anti-CEA	ND	USPIO-coated with HOOC–PEG2000–COOH	monoclonal antibodies anti-CEA 3 antibodies per particle	(1) USPIO PEG2000–COOH (2) EDCI and sulfo-NHS (3) antibody	carcino embryonic antigen	158
SPION–LHRH	D = 20 nm (TEM)	amine-coated USPIO (SPION)	luteinizing hormone releasing hormone (LHRH)	(1) EDCI/ sonication (2) LHRH protein	breast tumor expressing LHRH receptors	454,455
BSA–USPIO	D = 10 nm (TEM)	uncoated USPIO	bovine serum albumin	(1) EDCI/ sonication (2) BSA protein purification: magnetic separation	ND	455
BSA–USPIO	ND	hydroxide-uncoated USPIO	bovine serum albumin	(1) EDCI/ sonication (2) BSA protein in PBS purification: magnetic separation	ND	458
USPIO–$\alpha\nu\beta3$	D = 10 nm (TEM) r_1 = 1 mM^{-1} s^{-1} r_2 = 134 mM^{-1} s^{-1} 1.5 T	APTMS-coated USPIO APTMS = 3-aminopropyltrimethoxysilane	cyclo(Arg-Gly-Asp-D-Tyr-Glu)	(1) EDCI/NHS (2) peptide in buffer purification: magnetic separation	tumoral angiogenesis	456
USPIO–PEKY–anti-CEA	D = 9.6 ± 0.8 nm (TEM) D_h = 30–50 nm r_2 = 305 mM^{-1} s^{-1} 4.7 T	poly(glutamic–lysine–tyrosine)- coated USPIO stabilized by cross-linking with ethylene glycol bis(succinimidyl succinate)	monoclonal antibodies anti-CEA	(1) USPIO PEKY (2) sulfo-MBS (3) dithiothreitol reduced antibody purification gel chromatography	carcino embryonic antigen	459
USPIO–PEKY–anti-CEA	D_h = 30–50 nm	PEKY = poly(glutamic–lysine–tyrosine)-coated USPIO stabilized by cross-linking with ethylene glycol bis(succinimidyl succinate)	monoclonal antibodies anti-CEA	(1) USPIO PEKY (2) N-acetyl neuraminic NHS ester or glucuronic NHS ester (3) sulfo-MBS (4) dithiothreitol-reduced antibody	carcino embryonic antigen	460

Table 2. Continued

targeted contrast media	physicochemical characteristics	contrastophore	pharmacophore	coupling conditions	biological target	reference
USPIO−PEKY−anti-CEA	D_h = 30−50 nm	PEKY = poly(glutamic−lysine−tyrosine)-coated USPIO stabilized by cross-linking with ethylene glycol bis(succinimidyl succinate) PEK = poly(glutamic−lysine)-coated USPIO stabilized by cross-linking with ethylene glycol bis(succinimidyl succinate) PK = poly(lysine)- coated USPIO stabilized by cross-linking with ethylene glycol bis(succinimidyl succinate)	monoclonal antibodies anti-CEA	(1) USPIO PEKY or PEK or PK (2) sulfo-MBS (3) dithiothreitol-reduced antibody (4) PEG-cysteamine or thiolated glycophorin b or thiolated mucin (5) mercaptoethanol	carcino embryonic antigen	460
IgG magnetoliposome	ND	magnetoliposome PC/PE (3:1)	IgG 94 μg/mL liposome	(1) succinic anhydride (2) CMC carbodiimide (3) IgG	ND	522
IgG magnetoliposome	ND	magnetoliposome PC/PE (2/1)	human antibody E-907 90−180 antibodies per magnetoliposome	(1) magnetoliposome (2) incorporation of hydrazide cholesteryl-pullulan (3) oxidized (periodate) antibody purification gel chromatography	human colonic cancer cells	523
anti-CD34− magnetoliposome	D_h = 445 ± 25 nm	magnetoliposome (citrate USPIO) PC/Chol/PEG−PE/PDP−PEG−PE (12:6:0.8:0.2) PDP = pyridyldithioproprionate	100 mAb/ liposome anti-CD34 antibody My10mAb thiolated with SPDP	(1) thiolated magnetoliposome (2) thiolated antibody (3) DTT (4) incubation 24 h purification by centrifugation	haematopoietic CD44+ cells	524
anti-Her2 Neu− magnetoliposome	D_h = 138 ± 7.6 nm	magnetoliposome PC/PE (2:1) containing N-(6-maleimido-caproyloxy)-dipalmitoyl PE	anti-Her2 Neu antibody (herceptin) thiolated with SPDP 55.6 μg of antibody/mg of magnetite	(1) magnetoliposome (2) thiolated antibody (3) DTT (4) incubation for 20 h	SKBr3 breast cancer cells	525

Table 2. Continued

targeted contrast media	physicochemical characteristics	contrastophore	pharmacophore	coupling conditions	biological target	reference
RGD–magnetoliposome	$D_h = 243 \pm 63.2$ nm	magnetoliposome TMAG, DLPC, PDP–DOPE (1:2:1) PDP = pyridyldithioproprionate	RGDC peptide 0.226 mg of peptide/mg of magnetite	(1) thioated magnetoliposome (2) RGDC peptide (3) incubation for 3.5 h	NIH/3T3 fibroblasts	526
biotin–magnetoliposome	ND	magnetoliposome DC$_{140}$ PG/ PE–PEG–biotin (9:1)	biotine	lauric-acid-coated USPIO dialysed in the presence of preformed sonicated phospholipid vesicles	streptavidine	527
USPIO–strept-mAb(antiHer2/Neu)	ND	MACS streptavidin microbeads SPIO	biotinylated herceptin	(1) streptavidin SPIO (2) biotinylated herceptin	Her2/neu receptor on tumor cells	448
USPIO–mAb(anti-lymphocyte)	ND	biotinylated dextran-coated USPIO	biotinylated anti-lymphocyte antibody (moab anti-L)	(1) biotinylated SPIO (2) fluorescein–streptavidin (3) biotinylated antibody	lymphocyte	449, 450
Tf–SS–CLIO	$r_1 = 32$ mM^{-1} s^{-1} $r_2 = 146$ mM^{-1} s^{-1} 0.47 T	CLIO–NH$_2$	transferrin 4 transferrins per particle	(1) CLIO–NH$_2$ (2) SPDP (3) transferrin purification: magnetic separation	transferrin receptors	475, 478
Tf–SC–CLIO	$r_1 = 32$ mM^{-1} s^{-1} $r_2 = 144$ mM^{-1} s^{-1} 0.47 T	CLIO–NH$_2$	transferrin 1–2 transferrin per particle	(1) CLIO–NH$_2$ (2) SIA (succinimyl iodoacetate) (3) transferrin purification: magnetic separation	transferrin receptors	475
CLIO–Tat	$r_1 = 22$ mM^{-1} s^{-1} $r_2 = 72$ mM^{-1} s^{-1} 0.47 T $D_h = 42$ nm	CLIO–NH$_2$	Tat peptide 6–13 peptides per particle	(1) CLIO–NH$_2$ (2) SPDP (3) Tat peptide purification gel chromatography	lymphocytes uptake	477, 487, 488
CLIO–Tat	$r_1 = 22$ mM^{-1} s^{-1} $r_2 = 72$ mM^{-1} s^{-1} 0.47 T $D_h = 42$nm	CLIO–NH$_2$	Tat peptide 9.6–21 peptides per particle	(1) CLIO–NH$_2$ (2) SIA (succinimyl iodoacetate) (3) Tat peptide purification gel chromatography	T cells and CaCo-2 monolayers uptake	489, 490

Table 2. Continued

targeted contrast media	physicochemical characteristics	contrastophore	pharmacophore	coupling conditions	biological target	reference
CLIO−F(ab')2 (anti-E-selectin)	D_h = 40 nm	CLIO−NH$_2$	thioacetyl−anti-human E-selectin antibody fragment 0.1−0.2 F(ab')2 per particle	(1) CLIO−NH$_2$ (2) SPDP (3) thioacetylared F(ab')2 purification: magnetic separation	endothelial cells	479
CLIO−annexin V−Cy5.5	r_1 = 21 mM^{-1} s^{-1} r_2 = 45 mM^{-1} s^{-1} 0.47 T D_h = 53 ± 1 nm	CLIO−NH$_2$	thiolated snnexin V 2.7 annexin V per particle	(1) CLIO−NH$_2$ (2) SPDP (3) thiolated annexin V purification: filtration	apoptotic cells	480−482
CLIO−small molecule−FITC	ND	CLIO−NH$_2$	small thiol molecule library	(1) CLIO−NH$_2$ (2) FITC (3) SPDP (4) thiol small molecules purification: gel chromatography	apoptotic cells	483
CLIO−Cy5.5− mAb(anti-VCAM-1)	ND	CLIO−NH$_2$	anti-mouse anti VCAM-1 antibody 0.87 mg of antibody/ mg of Fe 10 Cy5.5 per particle	(1) CLIO−NH$_2$ (2) Cy5.5 NHS ester (3) NHS suberic acid (4) EDC1 (5) antibody purification: magnetic separation	vascular cell adhesion molecule 1 VCAM-1	496
CLIO−Cy5.5−bombesin	D_h = 35 nm	CLIO−NH$_2$	bombesin peptide 50 peptides per particles	(1) CLIO−NH$_2$ (2) Cy5.5 NHS ester (3) succinimidyl iodoacetic acid (4) bombesin peptide	pancreatic ductal adenocarci-noma	497
CLIO−small molecule	ND	CLIO−azido	small alkyne molecule library for click chemistry	(1) CLIO−azido (2) Cu^1 catalyst (3) alkyne molecule purification: gel chromatography	macrophage uptake	504
CLIO−small molecule	ND	CLIO−alkyne	small azido molecule library for click chemistry	(1) CLIO-azido (2) Cu^1 catalyst (3) azido molecule purification: gel chromatography	macrophage uptake	504
CLIO−F(ab')2 (anti-E-selectin)	D_h = 40 nm	CLIO−NH$_2$	mouse−anti-human E-selectin antibody fragment 0.1−0.2 F(ab')2 per particle	(1) CLIO−NH$_2$ (2) SPDP (3) DTT (4) F(ab')2 purification: magnetic separation	inflammation	485

Table 2. Continued

targeted contrast media	physicochemical characteristics	contrastophore	pharmacophore	coupling conditions	biological target	reference
CLIO−Cy5.5− VINP$_{28}$	ND	CLIO−Cy5.5−NH$_2$	V-CAM-1-binding peptide (VIN$_{28}$) 12 VINP$_{28}$ peptide per particle	(1) CLIO− Cy5.5−NH$_2$ (2) succinimidyl iodo acetate (3) VINP$_{28}$ purification: gel chromatography	vascular cellular adhesion molecule-1 (VCAM-1)	629
CLIO−Cy5.5− E-selectin-binding peptide	ND	CLIO−Cy5.5−NH$_2$	E-selectin-binding peptide (ESBP) 30 ESBP peptides per particle	(1) CLIO− Cy5.5−NH$_2$ (2) succinimidyl iodo acetate (3) ESBP	E-selectin	491
CLIO−Cy5.5-cRGD	D_h = 29−39 nm	CLIO−Cy5.5−NH$_2$	cyclic RGD peptide functionalized with NHS suberic acid 4−52 RGD peptides per particle 7.2 Cy5.5 per particle	(1) CLIO− Cy5.5−NH$_2$ (2) activated cRGD peptide purification: gel chromatography	$\alpha v\beta 3$ integrin	498, 499
CLIO−Cy5.5	D_h = 32 nm	CLIO−NH$_2$	Cy5.5 1 Cy5.5 per particle	(1) CLIO−NH$_2$ (2) Cy5.5	delineation of brain tumor	502
CLIO−small molecule	ND	CLIO−NH$_2$	small carboxylic molecule library	(1) CLIO−NH$_2$ (2) EDCI (3) small carboxylic molecule purification: gel chromatography	macrophage uptake	505
CLIO−small molecule	ND	CLIO−NH$_2$	small amine molecule library	(1) CLIO−NH$_2$ (2) succinic anhydride (3) EDCI (4) small amine molecule purification: gel chromatography	macrophage uptake	503
CLIO−small molecule	ND	CLIO−NH$_2$	small thiol molecule library	(1) CLIO−NH$_2$ (2) SPDP (3) small thiol molecule purification: gel chromatography	macrophage uptake	503
CLIO−small molecule	ND	CLIO−NH$_2$	small hydroxyl molecule library	(1) CLIO−NH$_2$ (2) succinimidyl iodo acetate (3) hydrolysis pH 7.4 (4) SOCl$_2$ small alcohol molecule purification: gel chromatography	macrophage uptake	503

Table 2. Continued

targeted contrast media	physicochemical characteristics	contrastophore	pharmacophore	coupling conditions	biological target	reference
CLIO–small molecule	ND	CLIO–NH$_2$	small epoxide molecule library	(1) CLIO–NH$_2$ (2) small epoxide molecule purification: gel chromatography	macrophage uptake	503
CLIO–SC–R4Cy5.5	$r_1 = 29.9$ mM^{-1} s^{-1} 92.5 mM^{-1} s^{-1} $r_2 = 0.47$ T $D_h = 62 \pm 7$ nm	CLIO–NH$_2$	RRRRGC peptide and Cy5.5 1.8 Cy5.5 per particle 15.5 peptide per particle	(1) CLIO–NH$_2$ (2) succinimidyl iodoacetate (3) RRRRGC peptide (4) Cy5.5–NHS ester purification: gel chromatography	cathepsin B	486, 493
CLIO–SS–R4Cy5.5	$r_1 = 27.8$ mM^{-1} s^{-1} 91.2 mM^{-1} s^{-1} $r_2 = 0.47$ T $D_h = 68 \pm 13$ nm	CLIO–NH$_2$	RRRRGC peptide and Cy5.5 1.19 Cy5.5 per particle 11.9 peptide per particle	(1) CLIO–NH$_2$ (2) SPDP (3) RRRRGC peptide (4) Cy5.5–NHS ester purification: gel chromatography	cathepsin B	486, 493
CLIO–Cy5.5–Cy7	$r_1 = 16$ mM^{-1} s^{-1} $r_2 = 45$ mM^{-1} s^{-1} 0.47 T $D_h = 28$ nm	CLIO–Cy7–NH$_2$	RRRRGC peptide and Cy5.5 2.3 Cy5.5 per particle 2.5 Cy7 per particle	(1) CLIO–Cy7–NH$_2$ (2) succinimidyl iodoacetate (3) RRRRGC peptide (4) Cy5.5–NHS ester purification: gel chromatography	protease	493
CLIO–EPPT1	$r_1 = 26.4$ mM^{-1} s^{-1} 53.4 mM^{-1} s^{-1} $r_2 = 0.47$ T $D_h = 35.8$ nm	CLIO–Cy5.5–NH$_2$	EPPT1 peptide 5 Cy5.5 per particle 14 peptides per particle	(1) CLIO–Cy5.5–NH$_2$ (2) succinimidyl iodoacetate (3) peptide	underglycosy-lated mucin 1 tumor antigen (uMUC-1)	494
CLIO–small molecule	ND	CLIO–NH$_2$	small thiol molecule library	(1) CLIO–NH$_2$ (2) SPDP (3) small thiol molecules purification: gel chromatography	macrophage, endothelial cells, pancreatic cancer cells	501
CLIO–small molecule	ND	CLIO–NH$_2$	small carboxylic molecule library	(1) CLIO–NH$_2$ (2) EDCI (3) small carboxylic molecule purification: gel chromatography	macrophage, endothelial cells, pancreatic cancer cells	501

Table 2. Continued

targeted contrast media	physicochemical characteristics	contrastophore	pharmacophore	coupling conditions	biological target	reference
CLIO–small molecule	ND	CLIO–NH$_2$	small amine molecule library	(1) CLIO–NH$_2$ (2) succinic anhydride (3) EDCI (4) small amine molecule purification: gel chromatography	macrophage, endothelial cells, pancreatic cancer cells	501
CLIO–peptides	ND	CLIO–NH$_2$	cysteine peptide library	(1) CLIO–NH$_2$ (2) succinimidyl iodoacetate (3) cysteine-peptides purification: gel chromatography	cell uptake	495
USPIO–peptide (VCAM-1)	ND	CLIO–Cy5.5–NH$_2$	peptide targeting VCAM-1 (VPN)	(1) CLIO–Cy5.5–NH$_2$ (2) NHS suberic acid (3) peptide purification: gel chromatography	vascular cellular adhesion molecule-1 VCAM-1	500
USPIO–nonpeptidic RGD mimetic	$r_1 = 10.1$ mM^{-1} s^{-1} $r_2 = 68.4$ mM^{-1} s^{-1} 1.5 T	dextran-coated USPIO	nonpeptidic RGD mimetic 2.8–4 peptidic mimetics per particle	(1) dextran-coated USPIO (2) epichlorhydrin (3) peptide mimetic	integrin	7
USPIO– GRGD peptide	$r_1 = 11.2$ mM^{-1} s^{-1} $r_2 = 84.9$ mM^{-1} s^{-1} 1.5 T	dextran-coated USPIO	GRGD peptide 2.8–4 peptides per particle	(1) dextran-coated USPIO (2) epichlorhydrin (3) peptide	integrin	7
USPIO–fibronectin fragment	$r_1 = 11.3$ mM^{-1} s^{-1} $r_2 = 76.0$ mM^{-1} s^{-1} 1.5 T	dextran-coated USPIO	fibronectin fragment 2.8–4 fragments per particle	(1) dextran-coated USPIO (2) epichlorhydrin (3) fibronectin fragment	integrin	7
anti-Her2 Neu–WSIO	$D = 9$ nm (TEM)	2,3-dimercaptosuccinic acid-coated WSIO	Anti-Her2 Neu-antibody herceptin	(1) DMSA WSIO (2) sulfo-SMCC–herceptin purification: gel chromatography	Her2/neu receptors on tumor cells	507, 508
USPIO–folate USPIO–PEG–folate	$D = 10$ nm (TEM)	(3-aminopropyl)-trimethoxysilane-coated USPIO	folic acid polyethylene glycolylated folic acid	(1) folic acid (2) EDCI (3) USPIO purification sonication and centrifugation	folate receptor (FR)	516, 517

Table 2. Continued

targeted contrast media	physicochemical characteristics	contrastophore	pharmacophore	coupling conditions	biological target	reference
USPIO–folate	D = 5–10 nm (TEM) D_h = 10–20 nm	oxidated dextran versatile USPIO	amino-PEG–folic acid	(1) versatile USPIO (2) amino-PEG–folic acid (3) sodium borohydride purification: tangential ultrafiltration	folate receptor (FR)	630
USPIO–folate	D = 9–11 nm (TEM)	silane–PEG–trifluoroethyl ester-coated USPIO	folic acid	(1) silane–PEG–trifluoroethyl(FR) ester-coated USPIO (2) ethylenediamine (3) DCC (4) folic acid purification: washing	folate receptor	484
USPIO annexin V	D = 9 nm (TEM)	dimercaptosuccinic acid (DMSA)-coated USPIO	SPDP-activated annexin V	(1) DMSA-coated USPIO (2) SPDP-bound annexin V purification: washing	apoptotic red blood cells	509–513
USPIO herceptin	D = 12 nm (TEM)	dimercaptosuccinic acid (DMSA)-coated MnFe$_2$O$_4$ (Mn MEIO)	SMCC-activated herceptin	(1) DMSA-coated MnMEIO (2) SMCC-activated herceptin purification: gel filtration	Her2neu positive cancer cells	514
polymeric RGD–USPIO micelles	D_h = 46 ± 4 nm	6 nm USPIO incorporated in polymeric maleimide micelles	cRGD–SH peptide	(1) maleimide micelles (2) cRGD–SH peptide purification: centrifugal filtration	integrin $\alpha v\beta 3$	423
USPIO–mimetic sLe^x	r_1 = 21 mM^{-1} s^{-1} r_2 = 75.5 mM^{-1} s^{-1} 0.47 T	dextran-coated USPIO	sialyl Lewis x mimetic	(1) dextran-coated USPIO (2) epichlorhydrin (3) sialyl Lewis x mimetic	E-selectin	8

circulation times. Small particles with diameters less than 10 nm are rapidly removed through extravasations and renal clearance. Particles with a diameter ranging from 10 to 100 nm are optimal for intravenous injection and have the most prolonged blood circulation times. These particles are small enough to evade the RES of the body as well as to penetrate small capillaries of the tissues and offer the most effective distribution in targeted tissues.

Magnetic drug targeting employing nanoparticles as carriers is a promising cancer treatment avoiding the side effects of conventional chemotherapy. Iron oxide nanoparticles covered by starch derivatives with phosphate groups, which bound mitoxantrone, have been used as chemotherapy. Alexiou et al. have shown that a strong magnetic field gradient at the tumor location induces accumulation of the nanoparticles.[651] Electron microscope investigations show that the ferrofluids can be enriched in tumor tissue and tumor cells.

Kohler et al.[652] have reported the development of a biostable methotrexate-immobilized iron oxide nanoparticle drug carrier that may potentially be used for real-time monitoring of drug delivery through magnetic resonance imaging. Methotrexate (MTX) was immobilized on the surface of the nanoparticle via a poly(ethylene glycol) self-assembled monolayer (PEG−SAM). Cellular uptake experiments showed that the uptake of NP−PEG−MTX conjugates by glioma cells was considerably higher than that of control nanoparticles. Magnetic resonance imaging in 9 L cells cultured with NP−PEG−MTX of various concentrations showed significant contrast enhancement. Leucovorin, a MTX antidote, was used to rescue the cells that had been exposed to NP−PEG−MTX or free MTX, and the experiment verified the biocompatibility of NP−PEG−MTX conjugates and the MTX on NP−PEG−MTX conjugates to be the true source of the cytotoxicity to the target cells. TEM results showed that NP−PEG−MTX conjugates were internalized into the 9 L cellular cytoplasm and retained their crystal structure therein for up to 144 h, as identified by electron diffraction.

Gallo et al.[653] have shown that, after administration of magnetic microspheres containing oxantrazole, the brain contained 100−400 times higher oxantrazole levels than those obtained after the solution dosage form, indicating the successfulness of drug delivery via magnetic particles.

6.4. Hyperthermia

Ferrofluids are not only a very powerful material for diagnosis by MRI, but they can be used also for therapeutic purposes. Their applications for hyperthermia treatment were first envisaged in the seminal work of Jordan et al. in 1993.[654] This study experimentally proves the high efficiency of a superparamagnetic crystal suspension to absorb the energy of an oscillating magnetic field and convert it into heat. This property can be used *in vivo* to increase the temperature of tumor tissue and to destroy the pathological cells by hyperthermia. Tumor cells are more sensitive to a temperature increase than healthy ones.[655,656] The more classical approach consists of submitting the patient to an electromagnetic wave of several 100 MHz frequency. The thermoablation of a tumor can be achieved by an electromagnetic wave emitted by a RF electrode implanted in the pathological area. A less invasive method consists of irradiating the pathological area with an array of external resonant microwave dipolar emitters.[657] Preclinical and clinical data show

that hyperthermia is feasible and effective in combination with radiation therapy. A study of 112 patients with glioblastoma multiformae has shown that survival is doubled when γ therapy is combined with hyperthermia as compared to γ therapy alone.[658]

In fact, the hyperthermia treatment allows an increase of perfusion in the tumor tissue and therefore a higher oxygen constant, which makes the γ radiation more powerful in destroying the pathological cells.[659] The main parameter determining the heating of the tissue is the specific absorption rate (SAR), defined as the rate at which electromagnetic energy is absorbed by a unit mass of a biological material. It is expressed in calories per kilogram and is proportional to the rate of the temperature increase ($\Delta T / \Delta t$) (eq 35)

$$\text{SAR} = 4.1868 \frac{P}{m_e} = C_e \frac{\Delta T}{\Delta t} \qquad (35)$$

where P is the electromagnetic wave power absorbed by the sample, m_e is the mass of the sample, and C_e is the specific heat capacity of the sample.

For classical high frequency irradiation by external antennas, the power deposition patterns lack selectivity. Another major difficulty in electromagnetic regional hyperthermia is the occurrence of local high temperatures (hot spots) because of the inhomogeneities of electrical permeability and conductivity of the tissue, which cause variation of the SAR.[660,661]

A better control of the energy is obtained for an irradiation of the tissue doped by a ferrofluid at a low-frequency magnetic wave (100−400 KHz). For a given superparamagnetic material, the SAR is very precisely determined by the volume ratio of these crystals in the tissue. Rosensweig theoretically proved a strong relationship between the SAR of this material and its magnetic relaxation[662] (eq 36)

$$\text{SAR} = 4.1868 \pi \mu_o^2 \frac{\varphi M_s^2 V}{1000 kT} H_o^2 \nu \frac{2\pi\nu\tau}{1 + (2\pi\nu\tau)^2} \qquad (36)$$

where φ is the volume fraction of superparamagnetic material, ν is the frequency of the oscillating magnetic field, H_o is the magnetic field intensity (the other parameters have been defined before), and τ is the relaxation time.

The expression (eq 36) shows that if the irradiation magnetic field is uniform, the SAR only depends upon the nature and the volume fraction of the superparamagnetic particles. A very high spatial selectivity can therefore be achieved if the particles are only localized in the pathological area. The irradiation frequency should be sufficiently low to avoid an interaction of the electromagnetic field with the intracellular ions.

For small anisotropy and crystal size nanoparticles, the SAR is proportional to the relaxation time and is due to the dissipation caused by the magnetic viscosity. It is maximum if eq 37 is verified.

$$\tau = \frac{1}{2\pi\nu} \qquad (37)$$

For a τ longer than this optimal value, the SAR decreases very quickly because the magnetic relaxation is too slow to allow for the superparamagnetic crystal "to follow" the oscillating magnetic field. Considering the evolution of τ with the crystal volume given by eqs 3, 5, and 6, Rosensweig[662] has shown a very sharp maximum of the SAR for a diameter of about 14 nm in the case of magnetite. He has also proven that an increase of the size distribution caused a very fast

decrease of the SAR. In his calculation, Rosensweig only took into account the bulk magnetocrystalline component of the anisotropy, but an evolution of the stage of aggregation of the particle should also cause a modification of the SAR because of the effect of dipolar intercrystal coupling on Néel relaxation times.

The selective remote inactivation of cancer cells by an AC magnetic field has been demonstrated *in vitro*.[663] This new approach for localized thermotherapy induced by a magnetic fluid is already suitable for both hyperthermia and thermoablation. Evaluation of the feasibility and survival benefit of this new hyperthermia approach is in progress on animals, and first clinical trials have been started recently.[664,665]

Ideally, the superparamagnetic crystals should be encapsulated with a drug in a liposome. Its irradiation by an oscillating magnetic field wave could increase the temperature and allow the phase transition temperature of the liposome membrane to be reached. The drug should then massively and selectively be released in the area submitted to the magnetic field.[666]

In conclusion, superparamagnetic colloids can be seen as a very promising agent for hyperthermia therapy, but this new field of application requires an improvement of the reproducibility and the size control during the synthesis of particles.

7. Conclusions and Perspectives

The use of superparamagnetic nanoparticles in MRI has been a major development in the range of tools available to clinicians. The efficacy of these agents has led to their being proposed for GI tract and hepatic lesion imaging. The prospects for increased use in lymph node and functional imaging also seem very promising. New applications of iron oxides in molecular and cellular imaging are being thoroughly studied. Most of the recent research has concerned cellular imaging of *in vivo* macrophage activity, whereas stem cell migration and immune cell trafficking, as well as targeted iron oxide nanoparticles for molecular imaging studies, are at the stage of the proof of concept, mainly in animal models.[11]

However, numerous challenges have to be overcome to provide new efficient and specific iron oxides for cellular and molecular imaging.

The synthesis of magnetic nanoparticles, covering a wide range of compositions and tuneable sizes, has made substantial progress, especially over the past decade. Different kinds of monodisperse spherical nanocrystals with controllable particle sizes and compositions have been synthesized by a wide range of chemical synthetic procedures: coprecipitation, reactions in constrained environments, thermal decomposition of metal–surfactant complexes, sol–gel reactions, polyol processes, flow injection synthesis, sonolysis, and electrochemical and aerosol methods. However, synthesis of high-quality magnetic nanoparticles in a controlled manner resulting in a homodisperse population of magnetic grains of controllable size and detailed understanding of the synthetic mechanisms of nucleation and growth during particle formation are still challenges to be faced in the coming years. The large-scale synthesis of iron oxide crystalline nanoparticles characterized by a high degree of crystallinity and, consequently, a high magnetization at saturation requires a reproducible and industrial process without any laborious purification step to ensure cost-effective synthetic procedures. An unavoidable problem

associated with nanoparticles is their intrinsic instability over long periods of time. Such small particles tend to form agglomerates to reduce the energy associated with the high surface area/volume ratio of the nanosized particles. Consequently, it is crucial to develop coating strategies to chemically improve the stability of the magnetic nanoparticles. The nature of the coating has to be optimized to simplify the process and to effectively prevent any aggregation and sedimentation of the superparamagnetic nanoparticle to provide a stable injectable solution or a lyophilizate freeze-dried powder that is easy to reconstitute.

From a more fundamental point of view, the mechanism of surface anchoring of the poly- or monomeric coating must be investigated using new surface characterization techniques to be able to describe the nature and the force of the surface binding (hydrogen, pseudo-covalent, or ionic bonds) and also the influence of the coating layer on the structural and magnetic properties of iron oxides. Indeed, surface effects can lead to a decrease of the magnetization of small particles, for instance oxide nanoparticles, with respect to the bulk value. This reduction has been associated with different mechanisms, such as the existence of a magnetically dead layer on the surface of the particle, the existence of canted spins, or the existence of a spin-glass-like behavior of the surface spins, that modify the anisotropy and magnetic moment of surfacic atoms. However, the magnetic modification of the superparamagnetic system because of the coating is rather complex, and no correlation between the chemical nature of the coating and the magnetic properties has been firmly established at present. Understanding surface anchoring of the coating will be very useful to predict the stability toward agglomeration of the coating in various media (aqueous, saline, cell culture, and biological) either by electrostatic, steric, or electrosteric repulsion. It will be of great help to develop a surfacic model of the interaction between the coating and the iron oxide surface to improve the rational design of new stable coatings. For that purpose, new physicochemical methods need to be improved to describe the fundamental characteristics of the superparamagnetic particle surface, such as surfacic composition, surfacic charge, hydrophilicity, and hydrophobicity.

A key point in superparamagnetic research is probably to establish robust structure–pharmacokinetic relationships. The nature of the surface coating as well as the geometric arrangement of the coating on the iron oxide surface will not only determine the size of the colloid but also play a significant role in the pharmacokinetic, metabolic, vascular clearance, and biodistribution properties and will modulate the capture by the RES system or tissular diffusion in tumor tissue. Mathematical models have already been constructed to explain the protein-rejecting abilities of PEG coating, which depend upon the conformation (mushroom or brushes) and the surfacic density of the PEG polymer or the surface.[667] Further investigations should help to define rational models to optimize the physicochemical and biological properties of USPIO as proposed in a recent work,[668] where a relationship between the saturation magnetization, the size of the nanoparticles, and some simple electronic descriptors of the coating was established using a quantitative structure–property relationship analysis.

Concerning targeted iron oxides incorporating biovectors able to recognize a biological target, the surface modification techniques used to graft biovectors need to be improved to achieve high reproducibility and to allow for the accurate

introduction of a well-defined quantity of biovectors. This point seems crucial to optimize the avidity for biological targets of targeted superparamagnetic nanoparticles based on the concept of multivalency.[669] Indeed, when the surface density of the biovectors is varied, it is possible to increase the avidity of the targeted nanoparticles for its biological target and consequently to modulate the biological behavior. For this purpose, new accurate analytical tools able to quantify the number of biovectors onto the nanoparticle surface need to be developed. Great efforts have to be undertaken to understand the interactions of nanoparticles with the immune systems and to optimize the molecular interaction of particle-conjugated receptors or ligands *in vivo*. For example, the optimization of the targeting activity should be systematically investigated by modifying the flexibility and length of the linker between the surface and the biovectors to minimize a coating interference with the binding.

Future studies should also aim to address different challenges faced in nanomedicine application. Additional preclinical and clinical studies in relevant animal models and disease states should be performed to substantiate proof of concept using different controls especially in MRI molecular imaging. Finally, safety and biocompatibility studies, in particular long-term toxicity studies, should be carried out beyond proof-of-concept studies.

8. Acknowledgments

9. References

(1) Sun, S.; Murray, C. B.; Weller, D.; Folks, L.; Moser, A. *Science* **2000**, *287*, 1989.
(2) Miller, M. M.; Prinz, G. A.; Cheng, S. F.; Bounnak, S. *Appl. Phys. Lett.* **2002**, *81*, 2211.
(3) Jain, T. K.; Morales, M. A.; Sahoo, S. K.; Leslie-Pelecky, D. L.; Labhasetwar, V. *Mol. Pharm.* **2005**, *2* (3), 194.
(4) Chourpa, I.; Douziech-Eyrolles, L.; Ngaboni-Okassa, L.; Fouquenet, J. F.; Cohen-Jonathan, S.; Souce, M.; Marchais, H.; Dubois, P. *Analyst* **2005**, *130* (10), 1395.
(5) Bulté, J. W. *Methods Mol. Med.* **2006**, *124*, 419.
(6) Modo, M.; Bulté, J. W. *Mol. Imaging* **2005**, *4* (3), 143.
(7) Burtea, C.; Laurent, S.; Roch, A.; Vander Elst, L.; Muller, R. N. *J. Inorg. Biochem.* **2005**, *99* (5), 1135.
(8) Boutry, S.; Laurent, S.; Vander Elst, L.; Muller, R. N. *Contrast Med. Mol. Imaging* **2006**, *1* (1), 15.
(9) Babes, L.; Denizot, B.; Tanguy, G.; Le Jeune, J. J.; Jallet, P. *J. Colloid Interface Sci.* **1999**, *212* (2), 474.
(10) Sonvico, F.; Dubernet, C.; Colombo, P.; Couvreur, P. *Curr. Pharm. Des.* **2005**, *11*, 2091.
(11) Corot, C.; Robert, P.; Idee, J. M.; Port, M. *Adv. Drug Delivery Rev.* **2006**, *58* (14), 1471.
(12) Modo, M. M. J.; Bulté, J. W. M. *Molecular and Cellular MR Imaging*; CRC Press: Boca Raton, FL, 2007.
(13) Charles, S. W.; Popplewell, J. *Endeavour* **1982**, *6*, 153.
(14) Gupta, A. K.; Gupta, M. *Biomaterials* **2005**, *26* (18), 3995.
(15) Chastellain, M.; Petri, A.; Gupta, A.; Rao, K. V.; Hofmann, H. *Adv. Eng. Mater.* **2004**, *6* (4), 235.
(16) Willard, M. A.; Kurihara, L. K.; Carpenter, E. E.; Calvin, S.; Harris, V. G. *Encyclopedia of Nanoscience and Nanotechnology*; Nalwa, H. S., Ed.; American Scientific Publishers: Valencia, CA, 2004; Vol. 1, p 815.
(17) Tartaj, P.; Morales, M. P.; Veintemillas-Verdaguer, S.; Gonzalez-Carreno, T.; Serna, C. J. Synthesis, properties and biomedical applications of magnetic nanoparticles. *Handbook of Magnetic Materials*; Elsevier: Amsterdam, The Netherlands, 2006; p 403.
(18) Chin, A. B.; Yaacob, I. I. *J. Mater. Process. Technol.* **2007**, *191*, 235–237.
(19) Albornoz, C.; Jacobo, S. E. *J. Magn. Magn. Mater.* **2006**, *305*, 12.
(20) Kim, E. H.; Lee, H. S.; Kwak, B. K.; Kim, B. K. *J. Magn. Magn. Mater.* **2005**, *289*, 328.
(21) Wan, J.; Chen, X.; Wang, Z.; Yang, X.; Qian, Y. *J. Cryst. Growth* **2005**, *276*, 571.
(22) Kimata, M.; Nakagawa, D.; Hasegawa, M. *Powder Technol.* **2003**, *132*, 112.
(23) Alvarez, G. S.; Muhammed, M.; Zagorodni, A. A. *Chem. Eng. Sci.* **2006**, *61*, 4625.
(24) Basak, S.; Chen, D.-R.; Biswas, P. *Chem. Eng. Sci.* **2007**, *62*, 1263.
(25) Sjogren, C. E.; Johansson, C.; Naevestad, A.; Sontum, P. C.; Briley-Saebo, K.; Fahlvik, A. K. *Magn. Reson. Imaging* **1997**, *15*, 55.
(26) Nunes, A. C.; Yu, Z. C. *J. Magn. Magn. Mater.* **1987**, *65*, 265.
(27) Thurm, S.; Odenbach, S. *J. Magn. Magn. Mater.* **2002**, *252*, 247.
(28) Martinez-Mera, I.; Espinosa, M. E.; Perez-Hernandez, R.; Arenas-Alatorre, J. *Mater. Lett.* **2007**, *61*, 4447–4451.
(29) Morisson, S. A.; Cahill, C. L.; Carpenter, E.; Calvin, S.; Harris, V. G. *J. Nanosci. Nanotechnol.* **2005**, *5*, 1323.
(30) Sun, Y.-K.; Ma, M.; Zhang, Y.; Gu, N. *Colloids Surf., A* **2004**, *245*, 15.
(31) Qiu, J.; Yang, R.; Li, M.; Jiang, N. *Mater. Res. Bull.* **2005**, *40*, 1968.
(32) Lee, S.-J.; Jeong, J.-R.; Shin, S.-C.; Kim, J.-C.; Kim, J.-D. *J. Magn. Magn. Mater.* **2004**, *282*, 147.
(33) Jolivet, J. P.; Chaneac, C.; Tronc, E. *Chem. Commun.* **2004**, *5*, 481.
(34) Morales, M. P.; Veintemillas-Verdaguer, S.; Montero, M.; Serna, C. J.; Roig, A.; Casas, L.; Martınez, B.; Sadiumenge, F. *Chem. Mater.* **1999**, *11*, 3058.
(35) Cornell, R. M.; Schwertmann, U. *The Iron Oxides*; VCH Publishers: Weinheim, Germany, 1996.
(36) Boistelle, R.; Astier, J. P. *J. Cryst. Growth* **1988**, *90*, 14.
(37) Sugimoto, T. *Chem. Eng. Technol.* **2003**, *26*, 3.
(38) Schwarzer, H.-C.; Peukert, W. *Chem. Eng. Commun.* **2004**, *191*, 580.
(39) Cornell, R. M.; Schertmann, U. *Iron Oxides in the Laboratory: Preparation and Characterization*; VCH Publishers: Weinheim, Germany, 1991.
(40) Gribanow, N. M.; Bibik, E. E.; Buzunov, O. V.; Naumov, V. N. *J. Magn. Magn. Mater* **1990**, *85*, 7.
(41) LaMer, V. K.; Dinegar, R. H. *J. Am. Chem. Soc.* **1950**, *72*, 4847.
(42) Lefebure, S.; Franck, R.; Massart, R.; Perzynski, R. *Prog. Colloid Polym. Sci.* **1989**, *79*, 128.
(43) Tominaga, M.; Matsumoto, M.; Soejima, K.; Taniguchi, I. *J. Colloid Interface Sci.* **2006**, *299*, 761.
(44) Weissleder, R. U.S. Patent 5,492,814, 1996; *Chem. Abstr.* 1997, *124*, 283285.
(45) Sjorgren, C. E.; Briley-Saebo, K.; Hanson, M.; Johansson, C. *Magn. Reson. Med.* **1994**, *31*, 268.
(46) Itoh, H.; Sugimoto, T. *J. Colloid Interface Sci.* **2003**, *265*, 283.
(47) Thapa, D.; Palkar, V. R.; Kurup, M. B.; Malik, S. K. *Mater. Lett.* **2004**, *58*, 2692.
(48) Pardoe, H.; Chua-anusorn, W.; St. Pierre, T. G.; Dobson, J. *J. Magn. Magn. Mater* **2001**, *225*, 41.
(49) Khalafalla, S. E.; Reimers, G. W. *IEEE Trans. Magn.* **1980**, *16*, 178.
(50) Massart, R. *IEEE Trans. Magn.* **1981**, *17*, 1247.
(51) Massart, R.; Cabuil, V. *J. Chim. Phys.* **1987**, *84*, 7.
(52) Jolivet, J. P.; Froidefond, C.; Pottier, A.; Chaeneac, C.; Cassaignon, S.; Tronc, E.; Euzen, P. *J. Mater. Chem.* **2004**, *14* (21), 3281.
(53) Jolivet, J. P.; Vassiere, L.; Chaeneac, C.; Tronc, E. *Mat. Res. Symp. Proc.* **1997**, *432*, 145.
(54) Jolivet, J. P.; Chaeneac, C. Tronc. *Comp. Rend. Series* **2002**, *5*, 659.
(55) Bacri, J. C.; Perzynski, R.; Salin, D.; Cabuil, V.; Massart, R. *J. Magn. Magn. Mater.* **1990**, *85*, 27.
(56) Massart, R.; Roger, J.; Cabuil, V. *Braz. J. Phys.* **1995**, *2*, 135.
(57) Neveu-Prin, S.; Cabuil, V.; Massart, R.; Escaffre, P.; Dussaud, J. *J. Magn. Magn. Mater.* **1993**, *122*, 42.
(58) Massart, R.; Cabuil, V. *J. Chem. Phys.* **1987**, 967.
(59) Fauconnier, N.; Bee, A.; Roger, J.; Pons, J. N. *Prog. Colloid Polym. Sci.* **1996**, *100*, 212.
(60) Fauconnier, N.; Bee, A.; Roger, J.; Pons, J. N. *J. Mol. Liq.* **1999**, *83*, 233.
(61) Fauconnier, N.; Pons, J. N.; Roger, J.; Bee, A. *J. Colloid Interface Sci.* **1997**, *194*, 427.
(62) Roger, J.; Pons, J. N.; Massart, R.; Halbreich, A.; Bacri, J. C. *Eur. Phys. J. Appl. Phys.* **1999**, *5*, 321.
(63) Denizot, B.; Tanguy, G.; Hindre, F.; Rump, E.; Le Jeune, J. J.; Jallet, P. *J. Colloid Interface Sci.* **1999**, *209*, 66.
(64) Bee, A.; Massart, R.; Neveu, S. *J. Magn. Magn. Mater.* **1995**, *149*, 6.
(65) Massart, R.; Dubois, E.; Cabuil, V.; Hasmonay, E. *J. Magn. Magn. Mater.* **1995**, *149*, 1.

(66) Cabuil, V.; Dubois, E.; Neveau, S.; Bacri, J. C.; Hasmonay, E.; Perzynski, R. *Prog. Colloid Polym. Sci.* **1995**, *98*, 23.
(67) Lefebure, S.; Dubois, E.; Cabuil, V.; Neveu, S.; Massart, R. *J. Mater. Res.* **1998**, *13*, 2975.
(68) Jolivet, J. P. *De la Solution à l'Oxyde*; InterEditions et CNRS Editions: Paris, France, 1994.
(69) Jolivet, J. P.; Belleville, P.; Tronc, E.; Livage, J. *Clays Clay Miner.* **1992**, *40*, 531.
(70) Tronc, E.; Belleville, P.; Jolivet, J.-P.; Livage, J. *Langmuir* **1992**, *8*, 313.
(71) Vayssières, L.; Chanéac, C.; Tronc, E.; Jolivet, J.-P. *J. Colloid Interface Sci.* **1998**, *205*, 205.
(72) Jiang, W.; Yang, H.-C.; Yang, S. Y.; Horng, H. E.; Hung, J. C.; Chen, Y. C.; Hong, C.-Y. *J. Magn. Magn. Mater.* **2004**, *283*, 210.
(73) Jolivet, J. P. *Metal Oxide Chemistry and Synthesis. From Solution to Solid State*; Wiley: Chichester, U.K., 2000.
(74) Qui, X. *Chin. J. Chem.* **2000**, *18*, 834.
(75) Sun, S.; Zeng, H. *J. Am. Chem. Soc.* **2002**, *124*, 8204.
(76) Gupta, A. K.; Wells, S. *IEEE Trans. Nanobiosci.* **2004**, *3*, 66.
(77) Kim, D. K.; Zhang, Y.; Voit, W.; Rao, K. V.; Muhammed, M. *J. Magn. Magn. Mater.* **2001**, *30*, 225.
(78) Liu, X.; Ma, Z.; Xing, J.; Liu, H. *J. Magn. Magn. Mater.* **2004**, *270*, 1.
(79) Liu, X.; Xing, J.; Guan, Y.; Shan, G.; Liu, H. *Colloids Surf., A* **2004**, *238*, 127.
(80) Lee, K. M.; Sorensen, C. M.; Klabunde, K. J.; Hadjipanayis, G. C. *IEEE Trans. Magn.* **1992**, *28*, 3180.
(81) Dresco, P. A.; Zaitsev, V. S.; Gambino, R. J.; Chu, B. *Langmuir* **1999**, *15*, 1945.
(82) O'Connor, C. J.; Seip, C.; Sangregorio, C.; Carpenter, E.; Li, S.; Irvin, G.; John, V. T. *Mol. Cryst. Liq. Cryst.* **1999**, *335*, 423.
(83) Lopez-Perez, J. A.; Lopez-Quintela, M. A.; Mira, J.; Rivas, J. *IEEE Trans. Magn.* **1997**, *33*, 4359.
(84) Santra, S.; Tapec, R.; Theodoropoulou, N.; Dobson, J.; Hebard, A.; Tan, W. *Langmuir* **2001**, *17*, 2900–2906.
(85) Gobe, M.; Kon-No, K.; Kandori, K.; Kitahara, A. *J. Colloid Interface Sci.* **1983**, *93*, 293.
(86) Liz, L.; Lopez-Quintela, M. A.; Mira, J.; Rivas, J. *J. Mater. Sci.* **1994**, *29*, 3797.
(87) Meldrum, F. C.; Heywood, B. R.; Mann, S. *Science* **1992**, *257*, 522.
(88) Dickson, D. P. E.; Walton, S. A.; Mann, S.; Wong, K. *Nanostruct. Mater.* **1997**, *9*, 595.
(89) Wong, K. K. W.; Douglas, T.; Gider, S.; Awschalom, D. D.; Mann, S. *Chem. Mater.* **1998**, *10*, 279.
(90) Uchida, M.; Flenniken, M. L.; Allen, M.; Willits, D. A.; Crowley, B. E.; Brumfield, S.; Willis, A. F.; Jackiw, L.; Jutila, M.; Young, M. J.; Douglas, T. *J. Am. Chem. Soc.* **2006**, *128* (51), 16626.
(91) Strable, E.; Bulte, J. W. M.; Moskowitz, B.; Vivekanandan, K.; Allen, M.; Douglas, T. *Chem. Mater.* **2001**, *13*, 2201.
(92) Bonacchi, D.; Caneschi, A.; Dorignac, D.; Falqui, A.; Gatteschi, D.; Rovai, D.; Sangregorio, C.; Sessoli, R. *Chem. Mater.* **2004**, *16*, 2016.
(93) Hou, Y.; Kondoh, H.; Shimojo, M.; Sako, E. O.; Ozaki, N.; Kogure, T. *J. Phys. Chem. B* **2005**, *109*, 4845.
(94) Sangregorio, C.; Wiemann, J. K.; O'Connor, C. J.; Rosenzweig, Z. *J. Appl. Phys.* **1999**, *85*, 5699.
(95) De Cuyper, M.; Joniau, M. *Langmuir* **1991**, *7*, 647.
(96) Bulte, J. W. M.; Douglas, T.; Witwer, B.; Zhang, S.-C.; Strable, E.; Lewis, B. K.; Zywicke, H.; Miller, B.; van Gelderen, P.; Moskowitz, B. M.; Duncan, I. D.; Frank, J. A. *Nat. Biotechnol.* **2001**, *19* (12), 1141.
(97) Pileni, M. P.; Duxin, N. *Chem. Innov.* **2000**, *30*, 25.
(98) Inouye, K.; Endo, R.; Otsuka, Y.; Miyashiro, K.; Kaneko, K.; Ishikawa, T. *J. Phys. Chem.* **1982**, *86*, 1465.
(99) Pinelli, M. P.; Feltin, N.; Moumen, N. *Scientific and Clinical Applications of Magnetic Carriers*; Plenum Press: New York, 1997; p 117.
(100) Lee, Y.; Lee, J.; Bae, C. J.; Park, J. G.; Noh, H. J.; Park, J. H.; Hyeron, J. H. *Adv. Funct. Mater.* **2005**, *3*, 503.
(101) Deng, Y.; Wang, L.; Yang, W.; Fu, S.; Elaissari, A. *J. Magn. Magn. Mater.* **2003**, *257*, 69.
(102) Pillai, V.; Kumar, P.; Hou, M. J.; Ayyub, P.; Shah, D. O. *Adv. Colloid Interface Sci.* **1995**, *55*, 241.
(103) Seip, C. T.; Carpenter, E. E.; O'Connor, C. J.; John, V. T.; Li, S. C. *IEEE Trans. Magn.* **1998**, *34*, 1111.
(104) Pileni, M. P. *J. Phys. Chem.* **1993**, *97*, 6961.
(105) Lopez-Quintela, M. A.; Tojo, C.; Blanco, M. C.; Garcia-Rio, L.; Leis, J. R. *Curr. Opin. Colloid Interface Sci.* **2004**, *9*, 264.
(106) Munshi, N.; De, T. K.; Maitra, A. *J. Colloid Interface Sci.* **1997**, *190* (2), 387.
(107) Pileni, M. P. *Nat. Mater.* **2003**, *2*, 145.
(108) Salazar-Alvarez, G. Doctoral Thesis, Stockholm, Sweden, 2004.
(109) Stecker, M. M.; Benedk, G. B. *J. Phys. Chem.* **1984**, *88*, 6519.
(110) Kandori, K.; Fukuoka, M.; Ishikawa, T. *J. Mater. Sci.* **1991**, *26*, 3313.
(111) Krishnamurti, G. S. R.; Huang, P. M. *Clays Clay Miner.* **1991**, *39*, 28.
(112) Dimitrova, G. T.; Tadros, Th.; Luckham, P. F.; Kipps, M. R. *Langmuir* **1996**, *12*, 315.
(113) Vidal-Vidal, J.; Rivas, J.; Lopez-Quintela, M. A. *Colloids Surf., A* **2006**, *288*, 44.
(114) Lopez-Perez, J. A.; Lopez-Quintela, M. A.; Mira, J.; Rivas, J.; Charles, S. W. *J. Phys. Chem. B* **1997**, *101*, 8045.
(115) Jia, Z.; Yujun, W.; Yangcheng, L.; Jingyu, M.; Guangsheng, L. *React. Funct. Polym.* **2006**, *66*, 1552.
(116) De Cuyper, M.; Joniau, M. *Eur. Biophys. J.* **1988**, *15*, 311.
(117) Rocha, F. M.; Cristina de Pinho, S.; Zollner, R. L.; Santana, M. H. A. *J. Magn. Magn. Mater.* **2001**, *225*, 101.
(118) Bulte, J. W. M.; de Cuyper, M.; Despres, D.; Frank, J. A. *J. Magn. Magn. Mater.* **1999**, *194* (1−3), 204.
(119) Pauser, S.; Reszka, R.; Wagner, S.; Wolf, K. J.; Buhr, H. J.; Berger, G. *Anticancer Drug Res.* **1997**, *12* (2), 125.
(120) Shindai, M.; Suzuki, M.; Iijima, S.; Kobayashi, T. *Biotechnol. Appl. Biochem.* **1994**, *21*, 125.
(121) Bouhon, I. A.; Shinkai, M.; Honda, H.; Kobayashi, T. *Cytotechnology* **1997**, *25*, 231.
(122) Ito, A.; Ino, K.; Kobayashi, T.; Honda, H. *Biomaterials* **2005**, *26* (31), 6185.
(123) Gonzales, M.; Hrishnan, K. M. *J. Magn. Magn. Mater.* **2005**, *293*, 265.
(124) Lesieur, S.; Grabiele-Maldelmont, C.; Menager, V.; Cabuil, V.; Dadhi, D.; Pierrot, P.; Edwards, K. *J. Am. Chem. Soc.* **2003**, *125* (18), 5266.
(125) Giri, J.; Thakurta, S. G.; Bellare, J.; Nigam, A. K.; Bahadur, D. *J. Magn. Magn. Mater.* **2005**, *293*, 62.
(126) Nobuto, H.; Sugita, T.; Kubo, T.; Shimose, S.; Yasunaga, Y.; Murakami, T.; Ochi, M. *Int. J. Cancer* **2004**, *109* (4), 627.
(127) Domingo, J. C.; Mercadal, M.; Petriz, J.; Garcia, J.; Madariaga, M. A. *Cell. Mol. Biol. Lett.* **1999**, *4*, 583.
(128) Sangregorio, C.; Wieman, J. K.; O'Connor, C.; Rosenzweig, Z. *J. Appl. Phys.* **1999**, *85* (8), 5699.
(129) Mann, S.; Hannigton, J. P. *J. Colloid Interface Sci.* **1987**, *122* (2), 326.
(130) Martina, M. S.; Fortin, J. P.; Menager, C.; Clement, O.; Barratt, G.; Grabielle-Madelmont, C.; Gazeau, F.; Cabuil, V.; Lesieur, S. *J. Am. Chem. Soc.* **2005**, *127* (30), 10676.
(131) Peira, E.; Marzola, P.; Podio, V.; Aime, S.; Sbarbati, A.; Gasco, M. R. *J. Drug Targeting* **2003**, *11* (1), 19.
(132) Sukhorukov, G. B.; Donath, E.; Davis, S.; Lichtenfeld, H.; Caruso, F.; Popov, V. I.; Mohwald, H. *Polym. Adv. Technol.* **1998**, *9*, 759.
(133) Donath, E.; Sukhorukov, G. B.; Caruso, F.; Davis, S.; Mohwald, H. *Angew. Chem., Int. Ed.* **1998**, *37*, 2202.
(134) Shchukin, D. G.; Sukhorukov, G. B. *Adv. Mater.* **2004**, *16*, 671.
(135) Radtchenko, I. L.; Sukhorukov, G. B.; Leporatti, S.; Khomutov, G. B.; Donath, E.; Mohwald, H. *J. Colloid Interface Sci.* **2000**, *230*, 272.
(136) Matijevic, E.; Scheiner, P. *J. Colloid Interface Sci.* **1978**, *60*, 509.
(137) Lisy, M.-C.; Hartung, A.; Lang, C.; Schüler, D.; Richter, W.; Reichenbach, J. R.; Kaiser, W. A.; Hilger, I. *Invest. Radiol.* **2007**, *42*, 235.
(138) Hyeon, T.; Seong Lee, S.; Park, J.; Chung, Y.; Na, H. B. *J. Am. Chem. Soc.* **2001**, *123*, 12798.
(139) Butter, K.; Kassapidou, K.; Vroege, G. J.; Philipse, A. P. *J. Colloid Interface Sci.* **2005**, *287*, 485.
(140) Mao, B.; Kang, Z.; Wang, E.; Lian, S.; Gao, L.; Tian, C.; Wang, C. *Mater. Res. Bull.* **2006**, *41*, 2226.
(141) Zhu, H.; Yang, D.; Zhu, L. *Surf. Coat. Technol.* **2007**, *201*, 5870.
(142) Giri, S.; Samanta, S.; Maji, S.; Ganguli, S.; Bhaumik, A. *J. Magn. Magn. Mater.* **2005**, *285*, 296.
(143) Wang, J.; Sun, J.; Sun, Q.; Chen, Q. *Mater. Res. Bull.* **2003**, *38*, 1113.
(144) Lian, S.; Kang, Z.; Wang, E.; Jiang, M.; Hu, C.; Xu, L. *Solid State Commun.* **2003**, *127*, 605.
(145) Hyeon, T.; Lee, S. S.; Park, J.; Chung, Y.; Na, H. B. *J. Am. Chem. Soc.* **2001**, *123*, 12798.
(146) Chen, D.; Xu, R. *Mater. Res. Bull.* **1998**, *33*, 1015.
(147) Zheng, Y.-H.; Cheng, Y.; Bao, F.; Wang, Y.-S. *Mater. Res. Bull.* **2006**, *41* (3), 525.
(148) Sato, S.; Murakata, T.; Yanagi, H.; Miyasaka, F.; Iwaya, S. *J. Mater. Sci.* **1994**, *29*, 5657.
(149) Woo, K.; Hong, J.; Ahn, J.-P. *J. Magn. Magn. Mater.* **2005**, *293*, 177.
(150) Sun, S.; Zeng, H.; Robinson, D. B.; Raoux, S.; Rice, P. M.; Wang, S. X.; Li, G. *J. Am. Chem. Soc.* **2004**, *126*, 273.
(151) Park, J.; Lee, E.; Hwang, N. M.; Kang, M.; Kim, S. C.; Hwang, J. G.; Park, G.; Noh, H. J.; Kim, J. H.; Park, J.; Hyeron, H. *Angew. Chem., Int. Ed.* **2005**, *44*, 123.
(152) Jana, N. R.; Chen, Y.; Peng, X. *Chem. Mater.* **2004**, *16*, 3931.
(153) Park, J.; An, K.; Hwang, Y.; Park, J. G.; Noh, H. J.; Kim, J. Y.; Park, J. H.; Hwang, N. M.; Hyeron, J. H. *Nat. Mater.* **2004**, *3*, 891.

(154) Li, Z.; Choi, C. J.; You, J. H.; Kim, B.; Zhang, Z. D. *J. Magn. Magn. Mater.* **2004**, *283*, 8.

(155) Li, Z.; Chen, H.; Bao, H. B.; Gao, M. Y. *Chem. Mater.* **2004**, *16*, 1391.

(156) Li, Z.; Sun, Q.; Gao, M. *Angew. Chem., Int. Ed.* **2004**, *44* (1), 123.

(157) Wan, J.; Cai, W.; Feng, J.; Meng, X.; Liu, E. *J. Mater. Chem.* **2007**, *17*, 1188.

(158) Li, Z.; Wei, L.; Gao, M.; Lei, H. *Adv. Mater.* **2005**, *8*, 1001.

(159) Hu, F. Q.; Wei, Z.; Zhou, Z.; Ran, Y. L.; Li, Z.; Gao, M. Y. *Chem. Mater.* **2006**, *252*, 1.

(160) Jun, Y. W.; Huh, Y. M.; Choi, J. S.; Lee, J. H.; Song, H. T.; Kim, S.; Yoon, S.; Kim, K. S.; Shin, J. S.; Suh, J. S.; Cheon, J. *J. Am. Chem. Soc.* **2005**, *127* (16), 5732.

(161) Dai, Z.; Meiser, F.; Möhwald, H. *J. Colloid Interface Sci.* **2005**, *28* (1), 298.

(162) Durães, L.; Costa, B. F. O.; Vasques, J.; Campos, J.; Portugal, A. *Mater. Lett.* **2005**, *59* (7), 859.

(163) Ismail, A. A. *Appl. Catal., B* **2005**, *58*, 115.

(164) Liu, X. Q.; Tao, S. W.; Shen, Y. S. *Sens. Actuators, A* **1997**, *40*, 161.

(165) Kojima, K.; Miyazaki, M.; Mizukami, F.; Maeda, K. *J. Sol-Gel Sci. Technol.* **1997**, *8*, 77.

(166) Cannas, C.; Gatteschi, D.; Musinu, A.; Piccaluga, G.; Sangregorio, C. *J. Phys. Chem.* **1998**, *102*, 7721.

(167) Ennas, G.; Musinu, A.; Piccaluga, G.; Zedda, D.; Gatteschi, D.; Sangregorio, C.; Stanger, J. L.; Concas, G.; Spano, G. *Chem. Mater.* **1998**, *10*, 495.

(168) Brinker, C. J.; Sherrer, G. W. *Sol−Gel Science*; Academic Press: New York, 1990.

(169) da Costa, G. M.; De Grave, E.; de Bakker, P. M. A.; Vandeberghe, R. E. *J. Solid State Chem.* **1994**, *113*, 405.

(170) Del Monte, F.; Morales, M. P.; Levy, D.; Fernandez, A.; Ocana, M.; Roig, A.; Molins, E.; O'Grady, K.; Serna, C. *Langmuir* **1997**, *13*, 3627.

(171) Raileanu, M.; Crisan, M.; Petrache, C.; Crisan, D.; Jitianu, A.; Zaharescu, M.; Predoi, D.; Kuncser, V.; Filoti, G. *Rom. J. Phys.* **2005**, *50* (5−6), 595.

(172) Chaneac, C.; Tronc, E.; Jolivet, J. P. *Nanostruct. Mater.* **1995**, *6*, 715.

(173) Niznansky, D.; Rehspringer, J. L.; Drillon, M. *IEEE Trans. Magn.* **1994**, *30*, 821.

(174) Bentivegna, F.; Ferré, J.; Nyvlt, M.; Jamet, J. P.; Imhoff, D.; Canva, M.; Brun, A.; Veillet, P.; Visnovsky, S.; Chaput, F.; Boilot, J. P. *J. Appl. Phys.* **1998**, *83*, 7776.

(175) Solinas, S.; Piccaluga, G.; Morales, M. P.; Serna, C. J. *Acta Mater.* **2001**, 2805.

(176) Raileanu, M.; Crisan, M.; Petrache, C.; Crisan, D.; Zaharescu, M. *J. Optoelectron. Adv. Mater.* **2003**, *5* (3), 693.

(177) Fievet, F.; Lagier, J. P.; Blin, B.; Beaudoin, B.; Figlarz, M. *Solid State Ionics* **1989**, *198*, 32.

(178) Tzitzios, V. K.; Petridis, D.; Zafiropoulou, I.; Hadjipanayis, G.; Niarchos, D. *J. Magn. Magn. Mater.* **2005**, *294* (2), e95.

(179) Chow, G. M.; Kurihara, L. K.; Kemner, K. M.; Schoen, P. E.; Elam, W. T.; Ervin, A.; Keller, S.; Zhang, Y.D.; Budnick, J.; Ambrose, T. *J. Mater. Res.* **1995**, *10*, 1546.

(180) Chow, G. M.; Kurihara, L. K.; Schoen, P. E. U.S. Patent 6,436,167, 2002; *Chem. Abstr.* 2003, *137*, 173223.

(181) Viau, G.; Ravel, F.; Acher, O.; Fiévet-Vincent, F.; Fiévet, F. *J. Appl. Phys.* **1994**, *76*, 6570.

(182) Viau, G.; Ravel, F.; Acher, O.; Fiévet-Vincent, F.; Fiévet, F. *J. Magn. Magn. Mater.* **1995**, *140−144*, 377.

(183) Viau, G.; Fiévet-Vincent, F.; Fiévet, F. *J. Mater. Chem.* **1996**, *6*, 1047.

(184) Viau, G.; Fiévet-Vincent, F.; Fiévet, F. *Solid State Ionics* **1996**, *84*, 259.

(185) Viau, G.; Fiévet-Vincent, F.; Fiévet, F.; Toneguzzo, P.; Ravel, F.; Acher, O. *J. Appl. Phys.* **1997**, *81*, 2749.

(186) Toneguzzo, P.; Acher, O.; Viau, G.; Fiévet-Vincent, F.; Fiévet, F. *J. Appl. Phys.* **1997**, *81*, 5546.

(187) Toneguzzo, P.; Viau, G.; Acher, O.; Fiévet-Vincent, F.; Fiévet, F. *Adv. Mater.* **1998**, *10*, 1032.

(188) Toneguzzo, P.; Acher, O.; Viau, G.; Pierrard, A.; Fiévet-Vincent, F.; Fiévet, F.; Rosenman, I. *IEEE Trans. Magn.* **1999**, *35*, 3469.

(189) Mercier, D.; Lévy, J.-C.S.; Viau, G.; Fiévet-Vincent, F.; Fiévet, F.; Toneguzzo, P.; Acher, O. *Phys. Rev. B: Condens. Matter Mater. Phys.* **2000**, *62*, 532.

(190) Viau, G.; Toneguzzo, P.; Pierrard, A.; Acher, O.; Fiévet-Vincent, F.; Fiévet, F. *Scr. Mater.* **2001**, *44*, 2263.

(191) Yu, S.; Chow, G. M. *J. Nanosci. Nanotechnol.* **2006**, *6* (7), 2135.

(192) Giri, A. K.; Chowdary, K. M.; Majetich, S. A. *Mater. Phys. Mech.* **2000**, *1*, 1.

(193) Hegde, M. S.; Larcher, D.; Dupont, L.; Beaudoin, B.; Tekaia-Elhsissen, K.; Tarascon, J. M. *Solid State Ionics* **1997**, *93*, 33.

(194) Saravanan, P.; Jose, T. A.; Thomas, J. P.; Kulkarni, G. U. *Bull. Mater. Sci.* **2001**, *24*, 515.

(195) Jungk, H. O.; Feldmann, C. *J. Mater. Res.* **2000**, *15*, 2244.

(196) Feldmann, C. *Adv. Mater.* **2001**, *13*, 1301.

(197) Bianco, A.; Gusmano, G.; Montanari, R.; Montesperelli, G.; Traversa, E. *Mater. Lett.* **1994**, *19*, 263.

(198) Bianco, A.; Gusmano, G.; Montanari, R.; Montesperelli, G.; Traversa, E. *Thermochim. Acta* **1995**, *269−270*, 117.

(199) Kurihara, L. K.; Chow, G. M.; Schoen, P. E. *Nanostruct. Mater.* **1995**, *5*, 607.

(200) Ammar, S.; Helfen, A.; Jouini, N.; Fiévet, F.; Rosenman, I.; Villain, F.; Molinié, P.; Danot, M. *J. Mater. Chem.* **2001**, *11*, 186.

(201) Yu, W.; Wang, Y.; Liu, H.; Zheng, W. *J. Mol. Catal. A: Chem.* **1996**, *112*, 105.

(202) Aayyappan, S.; Subbanna, G. N.; Srinivasa Goplan, R.; Rao, C. N. R. *Solid State Ionics* **1996**, *4*, 271.

(203) Kooli, F.; Rives, V.; Jones, W. *Chem. Mater.* **1997**, *9*, 2231.

(204) Yamaguchi, T.; Kitajima, K. *J. Mater. Sci.* **1998**, *33*, 653.

(205) Toneguzzo, P.; Viau, G.; Acher, O.; Guillet, F.; Bruneton, E.; Fiévet-Vincent, F.; Fiévet, F. *J. Mater. Sci.* **2000**, *35*, 3767.

(206) Poul, L.; Jouini, N.; Fiévet, F. *Chem. Mater.* **2000**, *12*, 3123.

(207) Wu, M.; He, H.; Zhao, Z.; Yao, X. *J. Phys. D: Appl. Phys.* **2000**, *33*, 2927.

(208) Elumalai, P.; Vasan, H. N.; Verelst, M.; Lecante, P.; Carles, V.; Tailhades, P. *Mater. Res. Bull.* **2002**, *37*, 353.

(209) Teranishi, T.; Miyake, M. *Chem. Mater.* **1999**, *11*, 3414.

(210) Kurihara, L. K.; Lewis, D.; Jung, A. M.; Fliflet, A. W.; Bruce, R. W. *Structure and Mechanical Properties in Nanophase Materials*; Mayo, M. J., Weertman, J., Eds.; Materials Research Society: Warrendale, PA, 2001; B6.15−6.21.

(211) Kurihara, L. K.; Bruce, R. W.; Fliflet, A.; Lewis, D. U.S. Patent 4,025,635, 2004; *Chem. Abstr.* 2005, *140*, 185634.

(212) Jézéquel, D.; Guenot, J.; Jouini, N.; Fiévet, F. *J. Mater. Res.* **1995**, *10*, 77.

(213) Fiévet, F.; Lagier, J. P.; Blin, B.; Beaudoin, B.; Figlarz, M. *Solid State Ionics* **1989**, *32−33*, 198.

(214) Cai, W.; Wan, J. *J. Colloid Interface Sci.* **2007**, *305*, 366.

(215) Sra, A. K.; Ewers, T. D.; Schaak, R. E. *Chem. Mater.* **2005**, *17*, 758.

(216) Joseyphus, R. J.; Kodama, D.; Matsumoto, T.; Sato, Y.; Jeyadevan, B.; Tohji, K. *J. Magn. Magn. Mater.* **2007**, *310* (2), 2393.

(217) Merikhi, J.; Jungk, H.-O.; Feldmann, C. *J. Mater. Chem.* **2000**, *10*, 1311.

(218) Reetz, M. T.; Helbig, W.; Quasick, S. A. *Active Metals, Preparation, Characterization, Applications*; Furster, A., Ed.; VCH: Weinheim, Germany, 1996.

(219) Pascal, C.; Pascal, J. L.; Favier, F.; Elidrissi Moubtassim, M. L.; Payen, C. *Chem. Mater.* **1999**, *11*, 141.

(220) Kahn, H. R.; Petrikowski, K. *J. Magn. Magn. Mater.* **2000**, *215−216*, 526.

(221) Pecharroman, C.; Gonzalez-Carreno, T.; Iglesias, J. E. *Phys. Chem. Miner.* **1995**, *22*, 21.

(222) Gonzalez-Carreno, T.; Morales, M. P.; Gracia, M.; Serna, C. J. *Mater. Lett.* **1993**, *18*, 151.

(223) Veintemillas-Vendaguer, S.; Morales, M. P.; Serna, C. J. *Mater. Lett.* **1998**, *35*, 227.

(224) Morales, M. P.; Bomati-Miguel, O.; Perez de Alejo, R.; Ruiz-Cabello, J.; Veintemillas-Vendaguer, S.; Ogrady, K. *J. Magn. Magn. Mater.* **2003**, *266*, 102.

(225) Veintemillas-Vendaguer, S.; Morales, M. P.; Bomati-Miguel, O.; Batista, C.; Zhao, X.; Bonville, P.; Perez de Alejo, R.; Ruiz-Cabello, J.; Santos, M.; Tendillo-Cortijo, J.; Ferreiros, J. *J. Phys.* **2004**, *37*, 2054.

(226) Alexandrescu, R.; Morjan, I.; Voicu, I.; Dumitrache, F.; Albu, L.; Soare, I.; Prodan, G. *Appl. Surf. Sci.* **2005**, *248* (1−4), 138.

(227) Julian-Lopez, B.; Boissière, C.; Chanéac, C.; Grosso, D.; Vasseur, S.; Miraux, S.; Duguet, E.; Sanchez, C. *J. Mater. Chem.* **2007**, *17*, 1563.

(228) Osuna, J.; de Caro, D.; Amiens, C.; Chaudret, B.; Snoeck, E.; Respaud, M.; Broto, J. M.; Fert, A. *J. Phys. Chem.* **1996**, *10*, 14571.

(229) Verelst, M.; Ely, T. O.; Amiens, C.; Snoeck, E.; Lecante, P.; Mosset, A.; Respaud, M.; Broto, J. M.; Chaudret, B. *Chem. Mater.* **1999**, *11*, 2702.

(230) Dinega, D. P.; Bawendi, M. G. *Angew. Chem., Int. Ed.* **1999**, *38*, 1788.

(231) Puntes, V. F.; Krishnan, K. M.; Alivisatos, A. P. *Science* **1999**, *291*, 2115.

(232) Puntes, V. F.; Krishnan, K. M.; Alivisatos, A. P. *Top. Catal.* **2002**, *19*, 145.

(233) Puntes, V. F.; Krishnan, K. M.; Alivisatos, A. P. *Appl. Phys. Lett.* **2001**, *78*, 2187.

(234) Yin, J. S.; Wang, Z. L. *Phys. Rev. Lett.* **1997**, *79*, 2570.

(235) Rotstein, H. G.; Tannenbaum, R. *J. Phys. Chem. B* **2002**, *106*, 146.

(236) Ely, T. O.; Amiens, C.; Chaudret, B.; Snoeck, E.; Varest, M.; Respaud, M.; Broto, J. M. *Chem. Mater.* **1999**, *11*, 526.

(237) Rozenfeld, O.; Koltypin, Y.; Bamnolker, H.; Margel, S.; Gedanken, A. *Langmuir* **1994**, *10*, 3919.

(238) Sidorov, S. N.; Bronstein, L. M.; Davankov, V. A.; Tsyurupa, M. P.; Solodovnikov, S. P.; Valetsky, P. M.; Wilder, E. A.; Spontak, R. J. *Chem. Mater.* **1999**, *11*, 3210.

(239) Park, S. J.; Kim, S.; Lee, S.; Khim, Z. G.; Char, K.; Hyeon, T. *J. Am. Chem. Soc.* **2000**, *122*, 8581.

(240) Abu Mukh-Qasem, R.; Gedanken, A. *J. Colloid Interface Sci.* **2005**, *284* (2), 489.

(241) Kim, E. H.; Lee, H. S.; Kwak, B. K.; Kim, B.-K. *J. Magn. Magn. Mater.* **2005**, *289*, 328.

(242) Suslick, K. S.; Choe, S. B.; Cichowlas, A. A.; Grinstaff, M. W. *Nature* **1991**, *353*, 414.

(243) Suslick, K. S.; Hyeon, T.; Fang, M. *Chem. Mater.* **1996**, *8*, 2172.

(244) Suslick, K. S.; Fang, M.; Hyeon, T. *J. Am. Chem. Soc.* **1996**, *118*, 11960.

(245) Suslick, K. S.; Hyeon, T.; Fang, M.; Cichowlas, A. A. *Mater. Sci. Eng., A* **1995**, *204*, 186.

(246) Bellissent, R.; Galli, G.; Hyeon, T.; Migliardo, P.; Parette, G.; Suslick, K. S. *J. Non-Cryst. Solids* **1996**, *205−207*, 656.

(247) Shafi, K. V. P. M.; Gedanken, A.; Goldfarb, R. B.; Felner, I. *J. Appl. Phys.* **1997**, *81*, 6901.

(248) Katabi, G.; Koltypin, Y.; Cao, X.; Gedanken, A. *J. Cryst. Growth* **1996**, *166*, 760.

(249) Katabi, G.; Prozorov, T.; Koltypin, Y.; Cohen, H.; Sukenik, C. N.; Ulman, A.; Gedanken, A. *Langmuir* **1997**, *13*, 6151.

(250) Ramesh, S.; Cohen, Y.; Aurbach, D.; Gedanken, A. *Chem. Phys. Lett.* **1998**, *287*, 461.

(251) Gibson, C. P.; Putzer, K. J. *Science* **1995**, *267*, 1338.

(252) Koltypin, Y.; Katabi, G.; Cao, X.; Prozorov, T.; Gedanken, A. *J. Non-Cryst. Solids* **1996**, *201*, 159.

(253) Shafi, K. V. P. M.; Gedanken, A.; Prozorov, T. *J. Mater. Chem.* **1998**, *8*, 769.

(254) Katabi, G.; Koltypin, Y.; Rothe, J.; Hormes, J.; Felner, I.; Cao, X.; Gedanken, A. *Thin Solid Films* **1998**, *333*, 41.

(255) Shafi, K. V. P. M.; Koltypin, Y.; Gedanken, A.; Prozorov, R.; Balogh, J.; Lendvai, J.; Felner, I. *J. Phys. Chem. B* **1997**, *101*, 6409.

(256) Shafi, K. V. P. M.; Ulman, A.; Yari, X.; Yang, N. L.; Estournes, C.; White, H.; Rafailovich, M. *Langmuir* **2001**, *17*, 5093.

(257) Kumar, R. V.; Koltypin, Y.; Cohen, Y. S.; Cohen, Y.; Aurbach, D.; Palchik, O.; Felner, I.; Gedanken, A. *J. Mater. Chem.* **2000**, *10*, 1125.

(258) Vijayakumar, R.; Diamant, Y.; Gedanken, A. *Chem. Mater.* **2000**, *12*, 2301.

(259) Vijayakumar, R.; Koltypin, Yu.; Felner, I.; Gedanken, A. *Mater. Sci. Eng., A* **2000**, *286*, 101.

(260) Derjaguin, B. V.; Landau, L. *Acta Physicochim. URSS* **1941**, *14*, 633.

(261) Verwey, E. J. W.; Overbeek, J. T. G. *Theory of the Stability of Lyophobic Colloids*; Elsevier: Amsterdam, The Netherlands, 1948.

(262) Vincent, B.; Edwards, J.; Emment, S.; Jones, A. *Colloids Surf.* **1986**, *18*, 261.

(263) Napper, D. H. *J. Colloid Interface Sci.* **1970**, *32*, 106.

(264) Fritz, G.; Schadler, V.; Willenbacher, N.; Wagner, N. J. *Langmuir* **2002**, *18*, 6381.

(265) Ortega-Vinusea, J. L.; Martin-Rodrigez, A.; Hidalgo-Alvarez, R. *J. Colloid Interface Sci.* **1996**, *184*, 259.

(266) Kobayashi, M.; Skarba, M.; Galletto, P.; Cakara, D.; Borbovec, M. *J. Colloid Interface Sci.* **2005**, *292*, 139.

(267) Baudry, J.; Bertrand, E.; Rouzeau, C.; Greffier, O.; Koenig, A.; Dreyfus, R.; Cohen-Tannoudji, L.; Goubault, C.; Bressy, L.; Vincent, L.; Lequeux, N.; Bibette, J. *Ann. Chim. (Paris)* **2004**, *29* (1), 97.

(268) Mylon, S. E.; Loon Chen, K.; Elimelech, M. *Langmuir* **2004**, *20*, 9000.

(269) Elimelech, J. H. *J. Colloid Interface Sci.* **1992**, *154*, 1.

(270) Holthoff, H.; Egelhaaf, S. U.; Borkovec, M.; Schurtenberger, P.; Sticher, H. *Langmuir* **1996**, *12*, 5541.

(271) Holthoff, H.; Borkovec, M.; Schurtenberger, P. *J. Colloid Interface Sci.* **1997**, *192* (2), 463.

(272) Lattuada, M.; Sandkuhler, P.; Wu, H.; Sefcik, J.; Morbidelli, M. *Adv. Colloid Interface Sci.* **2003**, *103* (1), 33.

(273) Bloomfield, V. A. *Biopolymers* **2000**, *54* (3), 168.

(274) Lefebure, S.; Dubois, E.; Cabuil, V.; Neveu, S.; Massart, R. *J. Mater. Res.* **1998**, *13*, 2975.

(275) Bacri, J.-C.; Perzynski, R.; Salin, D. *J. Magn. Magn. Mater.* **1990**, *85*, 27.

(276) Cornell, R. M.; Schertmann, U. *The Iron Oxides: Structure, Properties, Reactions, Occurrence and Uses*; VCH Publishers: Weinheim, Germany, 1996.

(277) Sahoo, Y.; Pizem, H.; Fried, T.; Golodnitsky, D.; Burstein, L.; Sukenik, C. N.; Markovich, G. *Langmuir* **2001**, *17*, 7907.

(278) Sahoo, Y.; Goodarzi, A.; Swihart, M. T.; Ohulchanskyy, T. Y.; Kaur, N.; Furlani, E. P.; Prasad, P. N. *J. Phys. Chem. B* **2005**, *109*, 3879.

(279) Wagner, S.; Schnorr, J.; Pilgrimm, H.; Hamm, B.; Taupitz, M. *Invest. Radiol.* **2002**, *37*, 167.

(280) Taupitz, M.; Wagner, S.; Schnorr, J.; Kravec, I.; Pilgrimm, H.; Bergmann-Fritsch, H.; Hamm, B. *Invest. Radiol.* **2004**, *39*, 394.

(281) Huang, P. M.; Wang, M. K. In *Advances in Geoecology*; Auerswald, K., Stanjek, H., Bigham, J. M., Eds.; International Development Centre: Ottawa, Canada, 1997; Vol. 30, p 241.

(282) Liu, C.; Huang, P. M. *Soil Sci. Soc. Am. J.* **1999**, *63*, 65.

(283) Kodama, H.; Schnitzer, M. *Geoderma* **1977**, *19*, 279.

(284) Kandori, K.; Kawashima, Y.; Ishikawa, T. *J. Colloid Interface Sci.* **1992**, *125*, 284.

(285) Kandori, K.; Kawashima, Y.; Ishikawa, T. *J. Mater. Sci.* **1991**, *26*, 3313.

(286) Denizot, B.; Tanguy, G.; Hindre, F.; Rump, E.; LeJeune, J.-J.; Jallet, P. *J. Colloid Interface Sci.* **1999**, *209*, 66.

(287) Portet, D.; Denizot, B.; Rump, E.; LeJeune, J.-J.; Jallet, P. *J. Colloid Interface Sci.* **2001**, *238*, 37.

(288) Cousin, F.; Dubois, E.; Cabuil, V. *Phys. Rev. E: Stat. Phys., Plasmas, Fluids, Relat.* **2003**, *68*, 021405.

(289) Cousin, F.; Dubois, E.; Cabuil, V.; Boué, F.; Perzynski, R. *Braz. J. Phys.* **2001**, *31* (3), 350.

(290) Cousin, F.; Dubois, E.; Cabuil, V. *J. Chem. Phys.* **2001**, *115* (13), 6051.

(291) Cabuil, V. *Curr. Opin. Colloid Interface Sci.* **2000**, *5*, 44.

(292) Dubois, E.; Perzynski, R.; Boué, F.; Cabuil, V. *Langmuir* **2000**, *16*, 5617.

(293) Meriguet, G.; Cousin, F.; Dubois, E.; Boué, F.; Cebers, A.; Farago, B.; Perzynski, R. *J. Phys. Chem. B* **2006**, *110*, 4378.

(294) Portet, D.; Denizot, B.; Rump, E.; Hindre, F.; LeJeune, J.-J.; Jallet, P. *Drug Dev. Res.* **2001**, *54*, 173.

(295) Mutin, P. H.; Guerrero, G.; Vioux, A. *C. R. Chim.* **2003**, *6*, 1153.

(296) Kreller, D. I.; Gibson, G.; Novak, W.; Van Loon, G. W.; Hugh Horton, J. *Colloids Surf., A* **2003**, *212*, 249.

(297) Yee, C.; Kataby, G.; Ulman, G.; Prozorov, T.; White, H.; King, A.; Rafailovich, M.; Sokolov, J.; Gedanken, A. *Langmuir* **1999**, *15*, 7111.

(298) Tejedor-Tejedor, M. I.; Anderson, M. A. *Langmuir* **1990**, *6* (3), 602.

(299) Persson, P.; Nilsson, N.; Sjöberg, S. *J. Colloid Interface Sci.* **1996**, *177*, 263.

(300) Mohapatra, S.; Pramanik, N.; Ghosh, S. K.; Pramanik, P. *J. Nanosci. Nanotechnol.* **2006**, *6* (3), 823.

(301) Roberts, D.; Zhu, W. L.; Fromenn, C. M.; Rosenzweig, Z. *J. Appl. Phys.* **2000**, *87*, 6208.

(302) Zhang, C.; Wangler, B.; Morgenstern, B.; Zentgraf, H.; Eisenhut, M.; Untenecker, H.; Kruger, R.; Huss, R.; Seliger, C.; Semmler, W.; Kiessling, F. *Langmuir* **2007**, *23* (3), 1427.

(303) Mulvaney, P.; Liz-Marzan, L. M.; Giersig, M.; Ung, T. *J. Mater. Chem.* **2000**, *10*, 1259.

(304) Tartaj, P.; Gonzalez-Carreno, T.; Serna, C. J. *Langmuir* **2002**, *18*, 4556.

(305) Tartaj, P.; Gonzalez-Carreno, T.; Serna, C. J. *Adv. Mater.* **2001**, *13*, 1620.

(306) Santra, S.; Tapec, R.; Theodoropoulou, N.; Dobson, J.; Hebard, A.; Tan, W. *Langmuir* **2001**, *17*, 2900.

(307) Chen, M.; Yamamuro, S.; Farrell, D.; Majetich, S. A. *J. Appl. Phys.* **2003**, *93*, 7551.

(308) Lin, J.; Zhou, W.; Kumbhar, A.; Fang, J.; Carpenter, E. E.; O'Connor, C. J. *J. Solid State Chem.* **2001**, *159*, 26.

(309) Zhou, W. L.; Carpenter, E. E.; Lin, J.; Kumbhar, A.; Sims, J.; O'Connor, C. J. *Eur. Phys. J. D* **2001**, *16*, 289.

(310) Morawski, A. M.; Winter, P. M.; Crowder, K. C.; Caruthers, S. D.; Fuhrlop, R. W.; Scott, M. J.; Robertson, J. D.; Abendschein, D. R.; Lanza, G. M.; Wickline, S. A. *Magn. Reson. Med.* **2004**, *51*, 480.

(311) Shepherd, P. G.; Popplewell, J.; Charles, S. W. *J. Phys. D: Appl. Phys.* **1970**, *3*, 1985.

(312) Xu, H. K.; Sorensen, C. M.; Klabunde, K. J.; Hadjipanayis, G. C. *J. Mater. Res.* **1992**, *7*, 712.

(313) Alcala, M. D.; Real, C. *Solid State Ionics* **2006**, *177*, 955.

(314) Gushikem, Y.; Rosatto, S. S. *J. Braz. Chem. Soc.* **2001**, *12*, 695.

(315) Woo, K.; Hong, J.; Ahn, J.-P. *J. Magn. Magn. Mater.* **2005**, *293*, 177.

(316) van Ewijk, G. A.; Vroege, G. J.; Philipse, A. P. *J. Magn. Magn. Mater.* **1999**, *201*, 31.

(317) Bruce, I. J.; Taylor, J.; Todd, M.; Davies, M. J.; Borioni, E.; Sangregorio, C.; Sen, T. *J. Magn. Magn. Mater.* **2004**, *284*, 145.

(318) Ma, D.; Guan, J.; Normandin, F.; Denommee, S.; Enright, G.; Veres, T.; Simard, B. *Chem. Mater.* **2006**, *18*, 1920.

(319) Yu, J. H.; Lee, C.-W.; Im, S.-S.; Lee, J.-S. *Rev. Adv. Mater. Sci.* **2003**, *4*, 55.

(320) Lesnikovich, A. E.; Shunkevich, T. M.; Naumenko, V. N.; Vorobyova, S. A.; Baykov, M. W. *J. Magn. Magn. Mater.* **1990**, *17*, 7907.

(321) Sun, Y.; Duan, L.; Guo, Z.; DuanMu, Y.; Ma, M.; Xu, L.; Zhang, Y.; Gu, N. *J. Magn. Magn. Mater.* **2005**, *285*, 65.

(322) Hahn, F. F.; Stark, D. D.; Lewis, J.; Saini, S.; Elizondo, G.; Weissleder, R.; Fretz, C. J.; Ferrucci, J. T. *Radiology* **1990**, *175*, 695.

(323) Haldemann-Heusler, R. C.; Wight, E.; Marincek, B. J. *Magn. Reson. Imaging* **1995**, *4*, 385.

(324) Johnson, W. K.; Stoupis, C.; Torres, G. M.; Rosenberg, E. B.; Ros, R. R. *Magn. Reson. Imaging* **1996**, *14*, 43.

(325) Stöber, W.; Fink, A.; Bohn, E. *J. Colloid Interface Sci.* **1968**, *26*, 62.

(326) Philipse, A. P.; van Bruggen, M. P. B.; Pathmamanoharan, C. *Langmuir* **1994**, *10*, 92.

(327) Lu, Y.; Yin, Y.; Mayers, B. T.; Xia, Y. *Nano. Lett.* **2002**, *2*, 183.

(328) Deng, Y.-H.; Wang, C.-C.; Hu, J.-H.; Yang, W.-L.; Fu, S.-K. *Colloids Surf., A* **2005**, *262*, 87.

(329) Barnakov, Y. A.; Yu, M. H.; Rosenzweig, Z. *Langmuir* **2005**, *21*, 7524.

(330) Im, S. H.; Herricks, T.; Lee, Y. T.; Xia, Y. *Chem. Phys. Lett.* **2005**, *40* (1−3), 19.

(331) Butterworth, M. D.; Bell, S. A.; Armes, S. P.; Simpson, A. W. *J. Colloid Interface Sci.* **1996**, *183*, 91.

(332) Liu, X.; Xing, J.; Guan, Y.; Shan, G.; Liu, H. *Colloids Surf., A* **2004**, *238*, 127.

(333) Tartaj, P.; Serna, C. J. *J. Am. Chem. Soc.* **2003**, *125*, 15754.

(334) Tartaj, P.; Serna, C. J. *Chem. Mater.* **2002**, *14*, 4396.

(335) Gao, X.; Yu, K. M. K.; Tamb, K. Y.; Tsang, S. C. *Chem. Comm.* **2003**, 2298.

(336) Yang, H.-H.; Zhang, S.-Q.; Chen, X.-L.; Zhuang, Z.-X.; Xu, J.-G.; Wang, X.-R. *Anal. Chem.* **2004**, *76*, 1316.

(337) Ulman, A. *Chem. Rev.* **1996**, *96*, 1533.

(338) Liu, Q.; Finch, J. A.; Egerton, R. *Chem. Mater.* **1998**, *10*, 3936.

(339) Mornet, S.; Portier, J.; Duguet, E. *J. Magn. Magn. Mater.* **2005**, *293*, 127.

(340) del Campo, A.; Sen, T.; Lellouche, J.-P.; Bruce, I. J. *J. Magn. Magn. Mater.* **2005**, *293*, 33.

(341) Yamaura, M.; Camilo, R. L.; Sampaio, L. C.; Macedo, M. A.; Nakamuro, M.; Toma, H. E. *J. Magn. Magn. Mater.* **2004**, *279*, 210.

(342) Chagnon, M. S.; Groman, E. V.; Josephson, L.; Whitehead, R. A. Eur. Pat. Appl. EP 125995, 1994; *Chem Abstr.* **1985**, *102*, 58899.

(343) Lyon, J. L.; Fleming, D. A.; Stone, B.; Schiffer, P.; Willians, M. E. *Nano. Lett.* **2004**, *4*, 719.

(344) Kim, J.; Park, S.; Lee, J. E.; Jin, S. M.; Lee, J. H.; Lee, I. S.; Yang, I.; Kim, J. S.; Kim, S. K.; Cho, M. H.; Hyeon, T. *Angew. Chem., Int. Ed.* **2006**, *45* (46), 7754.

(345) Palmacci, S.; Josephson, L.; Groman, E. V. U.S. Patent 5,262,176, 1995; *Chem. Abstr.* **1996**, *122*, 309897.

(346) Hafeli, U.; Schütt, W.; Teller, J.; Zbrorowski, M. *Scientific and Clinical Applications of Magnetic Carriers*; Plenum Press: New York, 1997.

(347) Arshady, R. *Radiolabeled and Magnetic Particles in Medicine and Biology*; Critrus Books: London, U.K., 2001; Vol. 3.

(348) Okassa, L. N.; Marchais, H.; Douziech-Eyrolles, L.; Cohen-Jonathan, S.; Souce, M.; Dubois, P.; Chourpa, I. *Int. J. Pharm.* **2005**, *302* (1−2), 187.

(349) Zhang, Y.; Kohler, N.; Zhang, M. *Biomaterials* **2002**, *23*, 1553.

(350) Lacava, L. M.; Lacava, Z. G. M.; Da Silva, M. F.; Silva, O.; Chaves, S. B.; Azevedo, R. B.; Pelegrini, F.; Gansau, C.; Buske, N.; Sabolovic, D.; Morais, P. C. *Biophys. J.* **2001**, *80*, 2483.

(351) Groman, E. V.; Josephson, L.; Lewis, J. M. PCT Int. Appl. WO 8800060, 1988; *Chem. Abstr.* **1989**, *109*, 69622.

(352) Berry, C.; Wells, S.; Charles, S.; Curtis, A. S. G. *Biomaterials* **2003**, *23*, 4551.

(353) Lee, K. M.; Kim, S.-G.; Kim, W.-S.; Kim, S. S. *Korean J. Chem. Eng.* **2002**, *19*, 480.

(354) Laurent, S.; Nicotra, C.; Gossuin, Y.; Roch, A.; Ouakssim, A.; Vander Elst, L.; Cornant, M.; Soleil, P.; Muller, R. N. *Phys. Status Solidi* **2004**, *12*, 3644.

(355) Gamarra, L. F.; Brito, G. E. S.; Pontuschka, W. M.; Amaro, E.; Parma, A. H. C.; Goya, G. F. *J. Magn. Magn. Mater.* **2005**, *289*, 439.

(356) Molday, R. S.; MacKenzie, D. *J. Immunol. Methods* **1982**, *52*, 353.

(357) Paul, K. G.; Frigo, T. B.; Groman, J. Y.; Groman, E. V. *Bioconjugate Chem.* **2004**, *15*, 394.

(358) Pardoe, H.; Chua-anusorn, W.; St. Pierre, T. G.; Dobson, J. *J. Magn. Magn. Mater.* **2001**, *225*, 41.

(359) Jung, C. W. *Magn. Reson. Imaging* **1995**, *13*, 675.

(360) Bautista, M. C.; Bomati-Miguel, O.; Morales, M. P.; Serna, C. J.; Veintemillas-Verdaguer, S. *J. Magn. Magn. Mater.* **2005**, *293*, 20.

(361) Fournier, C.; Leonard, M.; Le Coq-Leonard, I.; Delacherie, E. *Langmuir* **1995**, *11*, 2344.

(362) Duguet, E.; Mornet, S.; Portier, J. French Patent FR2855315, 2004; *Chem. Abstr.* 2005, *141*, 405023.

(363) Mornet, S.; Vasseur, S.; Grasset, F.; Duguet, E. *J. Mater Chem.* **2004**, *14*, 2161.

(364) Kim, D. K.; Zhang, Y.; Kehr, J.; Klason, T.; Bjelke, B.; Muhammed, M. *J. Magn. Magn. Mater.* **2001**, *225*, 256.

(365) Tamaura, Y.; Takahasi, K.; Kodera, Y.; Saito, Y.; Inada, Y. *Biotechnol. Lett.* **1986**, *8*, 877.

(366) Shultz, M. D.; Calvin, S.; Fatouros, P. P.; Morrison, S. A.; Carpenter, E. E. *J. Magn. Magn. Mater.* **2007**, *311*, 464.

(367) Butterworth, M. D.; Illum, L.; Davis, S. S. *Colloids Surf., A* **2001**, *179*, 93.

(368) Ding, X. B.; Sun, Z. H.; Wan, G. X.; Jiang, Y. Y. *React. Funct. Polym.* **1998**, *38*, 11.

(369) Gupta, A. K.; Curtis, A. S. *J. Mater. Sci. Mater. Med.* **2004**, *15*, 493.

(370) Kohler, N.; Fryxell, G. E.; Zhang, M. *J. Am. Chem. Soc.* **2004**, *126*, 7206.

(371) Zhang, Y.; Kohler, N.; Zhang, M. *Biomaterials* **2002**, *23*, 1553.

(372) Tiefenauer, L. X.; Tschirky, A.; Kühne, G.; Andres, R. Y. *Magn. Reson. Imaging* **1996**, *14*, 391.

(373) Moghimi, S. M.; Hunter, A. C.; Murray, J. C. *Pharmacol. Rev.* **2001**, *53*, 283.

(374) Bjornerud, A.; Johansson, L. O.; Ahlstrom, H. K. *Magn. Reson. Mater. Phys., Biol. Med.* **2001**, *12*, 99.

(375) Koenig, S. H.; Kellar, K. E.; Fujii, D. K.; Gunther, W. H.; Briley-Saebo, K.; Spiller, M. *Acad. Radiol.* **2002**, *9* (Supplement 1), S5.

(376) Kellar, K. E.; Fujii, D. K.; Gunther, W. H.; Briley-Saebo, K.; Bjornerod, A.; Spiller, M.; Koenig, S. H. *Acad. Radiol* **2002**, *9* (Supplement 1), S34.

(377) Kellar, K. E.; Fujii, D. K.; Gunther, W. H.; Briley-Saebo, K.; Bjornerud, A.; Spiller, M.; Koenig, S. H. *J. Magn. Reson. Imaging* **2000**, *11* (5), 488.

(378) Kellar, K. E.; Fujii, D. K.; Gunther, W. H.; Briley-Saebo, K.; Spiller, M.; Koenig, S. H. *Magn. Reson. Mater. Phys., Biol. Med.* **1999**, *8* (3), 207.

(379) Ya ci Acar, H.; Garaas, R. S.; Syud, F.; Bonitatebus, P.; Kulkarni, A. M. *J. Magn. Magn. Mater.* **2005**, *293*, 1–7.

(380) Kumagai, M.; Imai, Y.; Nakamura, T.; Yamasaki, Y.; Sekino, M.; Ueno, S.; Hanaoka, K.; Kikuchi, K.; Nagano, T.; Kaneko, E.; Shimokado, K.; Kataoka, K. *Colloids Surf., B* **2007**, *56* (1−2), 174.

(381) Yokoi, H.; Kantoh, T. *Bull. Chem. Soc. Jpn.* **1993**, *66*, 1536.

(382) Sairam, M.; Naidu, B. V. K.; Nataraj, S. K.; Sreedhar, B.; Aminabhavi, T. M. *J. Membr. Sci.* **2006**, *283*, 65.

(383) Schöpf, B.; Neuberger, T.; Schulze, K.; Petri, A.; Chastellain, M.; Hofmann, M.; Hofmann, H.; von Rechenberg, B. *J. Magn. Magn. Mater.* **2005**, *293*, 411.

(384) Xue, B.; Sun, Y. *J. Chromatogr., A* **2001**, *921*, 109.

(385) Lee, J.; Isobe, T.; Senna, M. *J. Colloid Interface Sci.* **1996**, *177*, 490.

(386) Chastellain, M.; Petri, A.; Hofmann, H. *J. Colloid Interface Sci.* **2004**, *278*, 353.

(387) Osada, Y.; Gong, J. *Polymer Gels Adv. Mater.* **1998**, *10*, 827.

(388) Albornoz, C.; Jacobo, S. E. *J. Magn. Magn. Mater.* **2006**, *305*, 12.

(389) Nishio, Y.; Yamada, A.; Ezaki, K.; Miyashita, Y.; Furukawa, H.; Horie, K. *Polymer* **2004**, *45*, 7129.

(390) Llanes, F.; Ryan, D. H.; Marchessault, R. H. *Int. J. Biol. Macromol.* **2000**, *27*, 35.

(391) Finotelli, P. V.; Morales, M. A.; Rocha-Leão, M. H.; Baggio-Saitovich, E. M.; Rossi, A. M. *Mater. Sci. Eng.* **2004**, *24*, 625.

(392) Kroll, E.; Winnik, F. M.; Ziolo, R. F. *Chem. Mater.* **1996**, *8*, 1594.

(393) Ma, H.-L.; Qi, X.-R.; Maitani, Y.; Nagai, T. *Int. J. Pharmaceut.* **2006**, doi: 10.1016/j.ijpharm.2006.10.006.

(394) Morales, M. A.; Finotelli, P. V.; Coaquira, J. A. H.; Rocha-Leão, M. H. M.; Diaz-Aguila, C.; Baggio-Saitovich, E. M.; Rossi, A. M. *Mater. Sci. Eng., C* **2007**, doi: 10.1016/j.msee.2006.12.016.

(395) Jia, Z.; Yujun, W.; Yangcheng, L.; Jingyu, M.; Guangsheng, L. *React. Funct. Polym.* **2006**, *66*, 1552.

(396) Sipos, P.; Berkesi, O.; Tombacz, E.; St. Pierre, T. G.; Webb, J. *J. Inorg. Biochem.* **2003**, *95*, 55.

(397) Bhattarai, S. R.; Bahadur, K. C.; Aryal, S.; Khill, M. S.; Kim, H. Y. *Carbohydr. Polym.* **2007**, doi: 10.016/j.carbpol.2007.01.006.

(398) Kim, E. H.; Ahn, Y.; Lee, H. S. *J. Alloys Compd.* **2006**, doi: 10.1016/j.allcom.2006.08.311.

(399) Kim, E. H.; Lee, H. S.; Kwak, B. K.; Kim, B.-K. *J. Magn. Magn. Mater.* **2005**, *289*, 328.

(400) Lee, H. S.; Kim, E. H.; Shao, H.; Kwak, B. K. *J. Magn. Magn. Mater.* **2005**, *293*, 102.

(401) Mendenhall, G. D.; Geng, Y.; Hwang, J. *J. Colloid Interface Sci.* **1996**, *184*, 519.

(402) Wormuth, K. *J. Colloid Interface Sci.* **2001**, *241*, 366.

(403) Liu, H.-L.; Ko, S. P.; Wu, J.-H.; Jung, M.-H.; Min, J. H.; Lee, J. H.; An, B. H.; Kim, Y. K. *J. Magn. Magn. Mater.* **2006**, doi: 10.1016/j.jmmm.2006.10.776.

(404) Lee, H. Y.; Lim, N. H.; Seo, J. A.; Khang, G.; Kim, J.; Lee, H. B.; Cho, S. H. *Polymer* **2005**, *29*, 266.

(405) Iijima, M.; Yonemochi, Y.; Tsukada, M.; Kamiya, H. *J. Colloid Interface Sci.* **2006**, *298*, 202.

(406) Fahlvik, A. K.; Holtz, E.; Schröder, U.; Klaveness, J. *Invest. Radiol.* **1990**, *25*, 793.

(407) Kellar, K. E.; Fujii, D. K.; Wolfgang, H.; Gunther, W. H.; Briley-Saebo, K.; Spiller, M.; Koening, S. H. *Magn. Reson. Mater. Phys., Biol. Med.* **1999**, *8*, 207.

(408) Kim, D. K.; Mikhaylova, M.; Wang, F. H.; Kehr, J.; Bjelke, B.; Zhang, Y.; Tsakalakos, T.; Muhammed, M. *Chem. Mater.* **2003**, *15*, 4343.

(409) Kim, D. K.; Mikhaylova, M.; Zhang, Y.; Tsakalakos, T.; Muhammed, M. *Chem. Mater.* **2003**, *15*, 1617.

(410) Arias, J. L.; Gallardo, V.; Gomez-Lopera, S. A.; Delgado, A. V. *J. Biomed. Nanotechnol.* **2005**, *1*, 214.

(411) Gomez-Lopera, S. A.; Arias, J. L.; Gallardo, V.; Delgado, A. V. *Langmuir* **2006**, *22*, 2816.

(412) Arias, J. L.; López-Viota, M.; Ruiz, M. A.; López-Viota, J.; Delgado, A. V. *Int. J. Pharm.* **2007**, doi: 10.1016/j.ijpharm.2007.02.028.

(413) Flesch, C.; Delaite, C.; Dumas, P.; Bourgeaut-Lami, E.; Duguet, E. *J. Polym. Sci., Part A: Polym. Chem.* **2004**, *42*, 6011.

(414) Flesch, C.; Bourgeaut-Lami, E.; Mornet, S.; Duguet, E.; Delaite, C.; Dumas, P. *J. Polym. Sci., Part A: Polym. Chem.* **2005**, *43*, 3221.

(415) Lawaczeck, R.; Menzel, M.; Pietsch, H. *Appl. Organomet. Chem.* **2004**, *18*, 506.

(416) Reimer, P.; Weissleder, R.; Lee, A. S.; Wittenberg, J.; Brady, T. J. *Radiology* **1990**, *177*, 729.

(417) Weissleder, R.; Reimer, P.; Lee, A. S.; Wittenberg, J.; Brady, T. J. *Am. J. Roentgenol.* **1990**, *155*, 1161.

(418) Reimer, P.; Weissleder, R.; Wittenberg, J.; Brady, T. J. *Radiology* **1992**, *182*, 565.

(419) Josephson, L.; Groman, E. V.; Menz, E.; Lewis, J. M.; Bengele, H. *Magn. Reson. Imaging* **1990**, *8*, 637.

(420) Groman, E. V.; Enriquez, P. M.; Jung, C.; Josephson, L. *Bioconjugate Chem.* **1994**, *5* (6), 547.

(421) Arbab, A. S.; Bashaw, L. A.; Miller, B. R.; Jordan, E. K.; Lewis, B. K.; Kalish, H.; Frank, J. A. *Radiology* **2003**, *229*, 838.

(422) Edward, A.; Alina, M.; Eric, A.; Wayne, F.; Kay, C. *J. Biomed. Mater. Res.* **2004**, *70*, 506.

(423) Kopke, R. D.; Wassel, R. A.; Mondalek, F. *Audiol. Neuro-Otol.* **2006**, *11*, 123.

(424) Moeser, G. D.; Green, W. H.; Laibinis, P. E.; Linse, P.; Hatton, T. A. *Langmuir* **2004**, *20*, 5223.

(425) Sun, S.; Anders, S.; Hamann, H. F.; Thiele, J. U.; Baglin, J. E. E.; Thomson, T.; Fullerton, E. E.; Murray, C. B.; Terris, B. D. *J. Am. Chem. Soc.* **2002**, *12*, 2884.

(426) Gomez-Lopera, S. A.; Plaza, R. C.; Delgado, A. V. *J. Colloid Interface Sci.* **2001**, *240*, 40.

(427) Deng, Y.; Wang, W.; Wang, C.; Fu, S. *Adv. Mater.* **2003**, *15*, 1729.

(428) Liao, M. H.; Chen, D. H. *J. Mater. Chem.* **2002**, *12*, 3654.

(429) Yu, S.; Chow, G. M. *J. Mater. Chem.* **2004**, *14*, 2781.

(430) Underhill, R. S.; Liu, G. *Chem. Mater.* **2000**, *12*, 2082.

(431) Zhang, J.; Xu, S.; Kumacheva, E. *J. Am. Chem. Soc.* **2004**, *126*, 7908.

(432) Breulmann, M.; Colfen, H.; Hentze, H.; Antonietti, M.; Walsh, D.; Mann, S. *Adv. Mater.* **1998**, *10*, 237.

(433) Ziolo, R. F.; Giannelis, E. P.; Weinstein, B. A.; O'Horo, M. P.; Ganguly, B. N.; Mehrotra, V.; Russel, M. W.; Huffman, D. R. *Science* **1992**, *257*, 219.

(434) Breulmann, M.; Davis, S. A.; Mann, S.; Hentze, H.; Antonietti, M. *Adv. Mater.* **2000**, *12*, 502.

(435) Gass, J.; Poddar, P.; Almand, J.; Srinath, S.; Srikanth, H. *Adv. Funct. Mater.* **2006**, *16*, 71.

(436) Furusawa, K.; Nagashima, K.; Anzai, C. *Colloid Polym. Sci.* **1994**, *272*, 1104.

(437) Zaitsev, V. S.; Filimonov, D. S.; Presnyakov, I. A.; Gambino, R. J.; Chu, B. *J. Colloid Interface Sci.* **1999**, *212*, 49.

(438) Arias, J. L.; Gallardo, V.; Gomez-Lopera, S. A.; Plaza, R. C.; Delgado, A. V. *J. Controlled Release* **2001**, *77*, 309.

(439) Sauzedde, F.; Elaissari, A.; Pichot, C. *Colloid Polym. Sci.* **1999**, *227*, 846.

(440) Sun, Y.; Ding, X.; Zheng, Z.; Cheng, X.; Hu, X.; Peng, Y. *Eur. Polym. J.* **2007**, *43*, 762.

(441) Pich, A.; Bhattacharya, S.; Ghosh, A.; Adler, H.-J. P. *Polymer* **2005**, *46*, 4596.

(442) Pirko, I.; Johnson, A.; Ciric, B.; Gamez, J.; Macura, S. I.; Pease, L.; Rodriguez, M. *FASEB J.* **2004**, *18*, 179.

(443) Weissleder, R.; Lee, A. S.; Khaw, B. A.; Shen, T.; Brady, T. J. *Radiology* **1992**, *182*, 381.

(444) Suwa, T.; Ozawa, S.; Ueda, M.; Ando, N.; Kitajima, M. *Int. J. Cancer* **1998**, *75*, 626.

(445) Wadghiri, Y. Z.; Sigurdsson, E. M.; Sadowski, M.; Elliott, J. I.; Li, Y.; Scholtzova, H.; Tang, C. Y.; Aguinaldo, G.; Pappolla, M.; Duff, K.; Wisniewski, T.; Turnbull, D. H. *Magn. Reson. Med.* **2003**, *50*, 293.

(446) Reimer, P.; Weissleder, R.; Shen, T.; Knoefel, W. T.; Brady, T. J. *Radiology* **1994**, *193*, 527.

(447) Jung, H. I.; Kettunen, M. I.; Davletov, B.; Brindle, K. M. *Bioconjugate Chem.* **2004**, *15* (5), 983.

(448) Artemov, D.; Mori, N.; Okollie, B.; Bhujwalla, Z. M. *Magn. Reson. Med.* **2003**, *49*, 403.

(449) Bulte, J. W.; Hoekstra, Y.; Kamman, R. L.; Magin, R. L.; Webb, A. G.; Briggs, R. W.; Go, K. G.; Hulstaert, C. E.; Miltenyi, S.; The, T. H.; De Leij, L. *Magn. Reson. Med.* **1992**, *25*, 148.

(450) Go, K. G.; Bulte, J. W.; de Ley, L.; The, T. H.; Kamman, R. L.; Hulstaert, C. E.; Blaauw, E. H.; Ma, L. D. *Eur. J. Radiol.* **1993**, *16* (3), 171.

(451) Sun, E. Y.; Josephson, L.; Kelly, K. A.; Weissleder, R. *Bioconjugate Chem.* **2006**, *17*, 109.

(452) Suzuki, M.; Shinkai, M.; Kamihira, M.; Kobayashi, T. *Biotechnol. Appl. Biochem.* **1995**, *21*, 335.

(453) Renshaw, P. F.; Owen, C. S.; Evans, A. E.; Leigh, J. S. *Magn. Reson. Imaging* **1986**, *4*, 351.

(454) Zhou, J.; Leuschner, C.; Kumar, C.; Hormes, J. F.; Soboyeyo, W. O. *Biomaterials* **2006**, *27*, 2001.

(455) Leuschner, C.; Kumar, C. S. S. R.; Hansel, W.; Hormes, J. *J. Biomed. Nanotechnol.* **2005**, *1*, 229.

(456) Zhang, C.; Jugold, M.; Woenne, E. C.; Lammers, T.; Morgenstern, B.; Mueller, M. M.; Zentgraf, H.; Bock, M.; Eisenhut, M.; Semmler, W.; Kiessling, F. *Cancer Res.* **2007**, *67* (4), 1555.

(457) Peng, Z. G.; Hidajat, K.; Uddin, M. S. *J. Colloid Interface Sci.* **2004**, *271*, 277.

(458) Mehta, R. V.; Upadhyay, R. V.; Charles, S. W.; Ramchand, C. N. *Biotechnol. Tech.* **1997**, *11* (7), 493.

(459) Tiefenauer, L. X.; Kuhne, G.; Andres, R. Y. *Bioconjugate Chem.* **1993**, *4*, 347.

(460) Tiefenauer, L. X.; Tschirky, A.; Kuhne, G.; Andres, R. Y. *Magn. Reson. Imaging* **1996**, *14* (4), 391.

(461) Johansson, L. O.; Bjornerud, A.; Ahlstrom, H. K.; Ladd, D. L.; Fujii, D. K. *J. Magn. Reson. Imaging* **2001**, *13*, 615.

(462) Kresse, M.; Wagner, S.; Pfefferer, D.; Lawaczeck, R.; Elste, V.; Semmler, W. *Magn. Reson. Med.* **1998**, *40*, 236.

(463) Cengelli, F.; Maysinger, D.; Tschuddi-Monnet, F.; Montet, X.; Corot, C.; Petri-Fink, A.; Hofmann, H.; Juillerat-Jeanneret, L. *J. Pharmacol. Exp. Ther.* **2006**, *318* (1), 108.

(464) Zhao, M.; Beauregard, D. A.; Loizou, L.; Davletov, B.; Brindle, K. M. *Nat. Med.* **2001**, *7*, 1241.

(465) Weissleder, R.; Lee, A. S.; Fischman, A. J.; Reimer, P.; Shen, T.; Wilkinson, R.; Callahan, R. J.; Brady, T. J. *Radiology* **1991**, *181*, 245.

(466) Toma, A.; Otsuji, E.; Kuriu, Y.; Okatomo, Y. K.; Ichikawa, D.; Hagiwara, A.; Ito, H.; Nischimura, T.; Yamagishi, H. *Br. J. Cancer* **2005**, *93*, 131.

(467) Li, M.; Xu, H.; Zuo, J.; Ji, A.; He, B. *Sci. China* **1996**, *39* (6), 577.

(468) Remsen, L. G.; McCormick, C. I.; Roman-Goldstein, S.; Nilaver, G.; Weissleder, R.; Bogdanov, A.; Hellstrom, I.; Kroll, R. A.; Neuwelt, E. A. *Am. J. Neuroradiol.* **1996**, *17*, 411.

(469) Funovics, M. A.; Kapeller, B.; Hoeller, C.; Su, H. S.; Kunstfeld, R.; Puig, S.; Macfelda, K. *Magn. Reson. Imaging* **2004**, *22*, 843.

(470) Enochs, W. S.; Schaffer, B.; Bhide, P. G.; Nossiff, N.; Papisov, M.; Bogdanov, A.; Brady, T. J.; Weissleder, R. *Exp. Neurol.* **1993**, *123*, 235.

(471) Enochs, W. S.; Weissleder, R. *J. Magn. Reson. Imaging* **1994**, *4*, 251.

(472) Petropoulos, A. E.; Schaffer, B. K.; Cheney, M. L.; Enochs, S.; Zimmer, C.; Weissleder, R. *Acta Otolaryngol.* **1995**, *115*, 512.

(473) Van Everdingen, K. J.; Enochs, W. S.; Bhide, P. G.; Nossiff, N.; Papisov, M.; Bogdanov, A.; Brady, T. J.; Weissleder, R. *Radiology* **1994**, *193*, 485.

(474) Papisov, M. I.; Bogdanov, A.; Schaffer, B.; Nossiff, N.; Shen, T.; Weissleder, R.; Brady, T. J. *J. Magn. Magn. Mater.* **1993**, *122*, 383.

(475) Hogemann, D.; Josephson, L.; Weissleder, R.; Basilion, J. P. *Bioconjugate Chem.* **2000**, *11* (6), 941.

(476) Wunderbaldinger, P.; Josephson, L.; Weissleder, R. *Acad. Radiol.* **2002**, *9* (Supplement 2), S304.

(477) Josephson, L.; Tung, C. H.; Moore, A.; Weissleder, R. *Bioconjugate Chem.* **1999**, *10*, 186.

(478) Hogemann-Savellano, D.; Bos, E.; Blondet, C.; Sato, F.; Abe, T.; Josephson, L.; Weissleder, R.; Gaudet, J.; Sgroi, D.; Peters, P. J.; Basilion, J. P. *Neoplasia* **2003**, *5* (6), 495.

(479) Kang, H. W.; Josephson, L.; Petrovsky, A.; Weissleder, R.; Bogdanov, A. J. *Bioconjugate Chem.* **2002**, *13*, 122.

(480) Schellenberger, E. A.; Bogdanov, A. J.; Hogemann, D.; Tait, J.; Weissleder, R.; Josephson, L. *Mol. Imaging* **2002**, *1*, 102.

(481) Schellenberger, E. A.; Sosnovik, D. E.; Weissleder, R.; Josephson, L. *Bioconjugate Chem.* **2004**, *15*, 1062.

(482) Sosnovik, D. E.; Schellenberger, E. A.; Nahrendorf, M.; Novikov, M. S.; Matsui, T.; Dai, G.; Reynolds, F.; Grazette, L.; Rosenzweig, A.; Weissleder, R.; Josephson, L. *Magn. Reson. Med.* **2005**, *54*, 718.

(483) Schellenberger, E. A.; Reynolds, F.; Weissleder, R.; Josephson, L. *ChemBioChem* **2004**, *5* (3), 275.

(484) Sun, C.; Sze, R.; Zhang, M. *J. Biomed. Mater. Res. A* **2006**, *78* (3), 550.

(485) Reynolds, P. R.; Larkman, D. J.; Haskard, D. O.; Hajnal, J. V.; Kennea, N. L.; George, A. J.; Edwards, A. D. *Radiology* **2006**, *241* (2), 469.

(486) Josephson, L.; Kircher, M. F.; Mahmood, U.; Tang, Y.; Weissleder, R. *Bioconjugate Chem.* **2002**, *13* (3), 554.

(487) Lewin, M.; Carlesso, N.; Tung, C. H.; Tang, X. W.; Cory, D.; Scadden, D. T.; Weissleder, R. *Nat. Biotechnol.* **2000**, *18*, 410.

(488) Zhao, M.; Kircher, M. F.; Josephson, L.; Weissleder, R. *Bioconjug. Chem.* **2002**, *13*, 840.

(489) Dodd, C. H.; Hsu, H. C.; Chu, W. J.; Yang, P.; Zhang, H. G.; Mountz, J. D.; Zinn, K.; Forder, K.; Josephson, L.; Weissleder, R.; Mountz, J. M.; Mountz, J. D. *J. Immunol. Methods* **2001**, *256* (1−2), 89.

(490) Koch, A. M.; Reynolds, F.; Merkle, H. P.; Weissleder, R.; Josephson, L. *ChemBioChem* **2005**, *6* (2), 337.

(491) Funovics, M.; Montet, X.; Reynolds, F.; Weissleder, R.; Josephson, L. *Neoplasia* **2005**, *7* (10), 904.

(492) Kircher, M. F.; Josephson, L.; Weissleder, R. *Mol. Imaging* **2002**, *1* (2), 89.

(493) Kircher, M. F.; Weissleder, R.; Josephson, L. *Bioconjugate Chem.* **2004**, *15* (2), 242.

(494) Moore, A.; Medarova, Z.; Potthast, A.; Dai, G. *Cancer Res.* **2004**, *64*, 1821.

(495) Hogemann, D.; Ntziachristos, V.; Josephson, L.; Weissleder, R. *Bioconjugate Chem.* **2002**, *13* (1), 116.

(496) Tsourkas, A.; Shinde-Patil, V. R.; Kelly, K. A.; Patel, P.; Wolley, A.; Allport, J. R.; Weissleder, R. *Bioconjugate Chem.* **2005**, *16*, 576.

(497) Montet, X.; Weissleder, R.; Josephson, L. *Bioconjugate Chem.* **2006**, *17* (4), 905.

(498) Montet, X.; Funovics, M.; Montet-Abou, K.; Weissleder, R.; Josephson, L. *J. Med. Chem.* **2006**, *49* (20), 6087.

(499) Montet, X.; Montet-Abou, K.; Reynolds, F.; Weissleder, R.; Josephson, L. *Neoplasia* **2006**, *8* (3), 214.

(500) Kelly, K. A.; Allport, J. R.; Tsourkas, A.; Shinde-Patil, V. R.; Josephson, L.; Weissleder, R. *Circ. Res.* **2005**, *96*, 327.

(501) Weissleder, R.; Kelly, K.; Sun, E. Y.; Shtatland, T.; Josephson, L. *Nat. Biotechnol.* **2005**, *23* (11), 1418.

(502) Kircher, M. F.; Mahmood, U.; King, R. S.; Weissleder, R.; Josephson, L. *Cancer Res.* **2003**, *63* (23), 8122.

(503) Sun, E. Y.; Josephson, L.; Kelly, K. A.; Weissleder, R. *Bioconjugate Chem.* **2006**, *17* (1), 109.

(504) Sun, E. Y.; Josephson, L.; Weissleder, R. *Mol. Imaging* **2006**, *5* (2), 122.

(505) Segers, J.; Laumonier, C.; Burtea, C.; Laurent, S.; Vander Elst, L.; Muller, R. N. *Bioconjugate Chem.* **2007**, *18* (4), 1251.

(506) Halbreich, A.; Roger, J.; Pons, J. N.; Da Silva, A.; Hasmonay, E.; Roudier, M.; Boynard, M.; Sestier, C.; Amri, A.; Geldwerth, D.; Fertil, B.; Bacri, J. C.; Sabolovic, D. *Scientific and Clinical Applications of Magnetic Carriers*; Hafeli, U., Schütt, W., Teller, J., Zborowski, M., Eds.; Plenum Press, New York, 1997; pp 399−417.

(507) Jun, Y. W.; Huh, Y. M.; Choi, J. S.; Lee, J. H.; Song, H. T.; Kim, S.; Yoon, S.; Kim, K. S.; Shin, J. S.; Suh, J. S.; Cheon, J. *J. Am. Chem. Soc.* **2005**, *127* (16), 5732.

(508) Huh, Y. M.; Jun, Y. W.; Song, H. T.; Kim, S.; Choi, J. S.; Lee, J. H.; Yoon, S.; Kim, J. S.; Shin, J. S.; Suh, J. S.; Cheon, J. *J. Am. Chem. Soc.* **2005**, *7*, 12387.

(509) Halbreich, A.; Sabolovic, D.; Sestier, C.; Amri, A.; Pons, J. N.; Roger, J.; Geldwerth, D. *Parasitol. Today* **1996**, *12* (7), 292.

(510) Fauconnier, N.; Pons, J. N.; Roger, J.; Bee, A. *J. Colloid Interface Sci.* **1997**, *194*, 427.

(511) Sestier, C.; Sabolovic, D.; Geldwerth, D.; Moumaris, M.; Roger, J.; Pons, J. N.; Halbreich, A. *C. R. Acad. Sci., Ser. III* **1995**, *318* (11), 1141.

(512) Roger, J.; Pons, J. N.; Massart, R.; Halbreich, A.; Bacri, J. C. *Eur. Phys. J. A* **1999**, *5*, 321.

(513) Halbreich, A.; Roger, J.; Pons, J. N.; Geldwerth, D.; Da Silva, M. F.; Roudier, M.; Bacri, J. C. *Biochimie* **1998**, *80*, 379.

(514) Lee, J. H.; Huh, Y. M.; Jun, Y. W.; Seo, J. W.; Jang, J. T.; Song, H. T.; Kim, S.; Cho, E. J.; Yoon, H. G.; Suh, J. S.; Cheon, J. *Nat. Med.* **2007**, *13* (1), 9.

(515) Cao, J.; Wang, Y.; Yu, J.; Xia, J.; Zhang, C.; Yin, D.; Hafeli, U. O. *J. Magn. Magn. Mater.* **2004**, *277*, 165.

(516) Zhang, Y.; Kohler, N.; Zhang, M. *Mater. Res. Soc. Symp. Proc.* **2001**, *676*, 981.

(517) Zhang, Y.; Zhang, J. *J. Colloid Interface Sci.* **2005**, *2832*, 352.

(518) Whitehead, R. A.; Chagnon, M. S.; Groman, E. V.; Josephson, L. Magnetic particles for use in separations, U.S. Patent 4,695,392, 1987.

(519) Arkles, B. *Chem. Tech.* **1977**, *7* (12), 766.

(520) Brandriss, S.; Margel, S. *Langmuir* **1993**, *9*, 1232.

(521) Wikstrom, P.; Mandenius, C. F.; Larsson, P. O. *J. Chromatogr.* **1988**, *455*, 105.

(522) Muller-Schulte, D.; Fussl, F.; Lueken, H.; De Cuyper, M. *Sci. Clin. Appl. Magn. Carriers* **1997**, 517.

(523) Shinkai, M.; Suzuki, M.; Iijima, S.; Kobayashi, T. *Biotechnol. Appl. Biochem.* **1994**, *21*, 125.

(524) Domingo, J. C.; Mercadal, M.; Petriz, J.; De Madariaga, M. A. *J. Microencapsulation* **2001**, *18* (1), 41.

(525) Ito, A.; Kuga, Y.; Honda, H.; Kikkawa, H.; Horiuchi, A.; Watanabe, Y.; Kobayashi, T. *Cancer Lett.* **2004**, *212* (2), 167.

(526) Ito, A.; Ino, K.; Kobayashi, T.; Honda, H. *Biomaterials* **2005**, *26* (31), 6185.

(527) Hodenius, M.; De Cuyper, M.; Desender, L.; Muller-Schulte, D.; Steigel, A.; Lueken, H. *Chem. Phys. Lipids* **2002**, *120* (1−2), 75.

(528) Nitin, N.; LaConte, L. E.; Zurkiya, O.; Hu, X.; Bao, G. *J. Biol. Inorg. Chem.* **2004**, *9*, 706.

(529) Nasongkla, N.; Bey, E.; Ren, J.; Ai, H.; Khemtong, C.; Guthi, J. S.; Chin, S. F.; Sherry, A. D.; Boothman, D. A.; Gao, J. *Nano Lett.* **2006**, *6* (11), 2427.

(530) Kaiser, R.; Miskolczy, G. *J. Appl. Phys.* **1970**, *41*, 1064.

(531) Kim, D. K.; Zhang, Y.; Voit, W.; Rao, K. V.; Muhammed, M. *J. Magn. Magn. Mater.* **2001**, *225*, 30.

(532) Thomas, G.; Hutten, A. *Nanostruct. Mater.* **1997**, *9*, 271.

(533) Ascencio, J. A.; Gutíerrez-Wing, C.; Espinosa-Pesqueira, M. E.; Marın, M.; Tehuacanero, S.; Zorrilla, C.; Jose-Yacaman, M. *Surf. Sci.* **1998**, *396*, 349.

(534) Pascal, C.; Pascal, J. L.; Favier, F.; Elidrissi Moubtassim, M. L.; Payen, C. *Chem. Mater.* **1999**, *11*, 141.

(535) Nakayama, T.; Yamamoto, T. A.; Choa, Y.-H.; Niihara, K. *J. Mater. Sci.* **2000**, *35*, 3857.

(536) Tomita, S.; Hikita, M.; Fujii, M.; Hayashi, S.; Yamamoto, K. *Chem. Phys. Lett.* **2000**, *316*, 361.

(537) Kwok, Y. S.; Zhang, X. X.; Qin, B.; Fung, K. K. *Appl. Phys. Lett.* **2000**, *77*, 3971.

(538) Zhou, W. L.; Carpenter, E. E.; Lin, J.; Kumbhar, A.; Sims, J.; O'Connor, C. J. *Eur. Phys. J. D* **2001**, *16*, 289.

(539) Teunissen, W.; De Groot, F. M. F.; Geus, J.; Stephan, O.; Tence, M.; Colliex, C. *J. Catal.* **2001**, *204*, 169.

(540) Santra, S.; Tapec, R.; Theodoropoulou, N.; Dobson, J.; Hebard, A.; Tan, W. *Langmuir* **2001**, *17*, 2900.

(541) Sun, X.-C.; Nava, N. *Nano Lett.* **2002**, *2*, 765.

(542) Brice-Profeta, S.; Arrio, M. A.; Tronc, E.; Menguy, N.; Letard, I.; Cartier dit Moulin, C.; Nogues, M.; Chaneac, C.; Jolivet, J. P.; Saintctavit, Ph. *J. Magn. Magn. Mater.* **2005**, *288*, 354.

(543) Serna, C. J.; Bodker, F.; Morup, S.; Morales, M. P.; Sandiumenge, F.; Veintemillas-Verdaguer, S. *Solid State Commun.* **2001**, *118*, 437.

(544) Morales, M. P.; Veintemillas-Verdaguer, S.; Montero, M. I.; Serna, C. J. *Chem. Mater.* **1999**, *11*, 3058.

(545) Inouye, K.; Endo, R.; Otsuka, Y.; Miyashiro, K.; Kaneko, K.; Ishikawa, T. *J. Phys. Chem.* **1982**, *86*, 1465.

(546) Rao, S.; Houska, C. R. *Acta Crystallogr., Sect. A: Found. Crystallogr.* **1986**, *42*, 6.

(547) Calvin, S.; Carpenter, E. E.; Harris, V. G. *Phys. Rev. B: Condens. Matter Mater. Phys.* **2003**, *6803* (3), 3411.

(548) Calvin, S.; Riedel, C.; Carpenter, E.; Morrison, S.; Stroud, R.; Harris, V. *J. Phys. Condens. Mater.* **2005**, *17* (41), 6393.

(549) Calvin, S.; Miller, M. M.; Goswami, R.; Cheng, S.-F.; Mulvaney, S. P.; Whitman, L. J.; Harris, V. G. *J. Appl. Phys.* **2003**, *94*, 778.

(550) Di Marco, M.; Guilbert, I.; Port, M.; Robic, C.; Couvreur, P.; Dubernet, C. *Int. J. Pharm.* **2006**, *324* (1), 37.

(551) Lindner, P.; Zemb, T. Neutrons, *X Ray and light: scattering Methods Applied to Soft Condensed Matter, Elsevier*, 2002.

(552) De Jaeger, N.; Demeye, H.; Findy, R.; Sneyer, R.; Vanderdeelen, J.; van der Meeren, P.; Laethem, M. *Part. Part. Syst. Charact.* **1991**, *8*, 179.

(553) Crangle, J. *Solid State Magnetism*; Edward Arnold: London, U.K., 1991.

(554) Dormann, J. L. *Rev. Phys. Appl.* **1981**, *16*, 275.

(555) Chantrell, R. W.; Lyberatos, A.; El-Hilo, M.; O'Grady, K. *J. Appl. Phys.* **1994**, *76*, 6407.

(556) Dormann, J. L.; Spinu, L.; Tronc, E.; Jolivet, J. P.; Lucari, F.; D'Orazio, F.; Fiorani, D. *J. Magn. Magn. Mater.* **1998**, *183*, L255.

(557) Dormann, J. L.; D'Orazio, F.; Lucari, F.; Tronc, E.; Prene, P.; Jolivet, J. P.; Fiorani, D.; Cherkaoui, R.; Nogue's, M. *Phys. Rev. B: Condens. Matter Mater. Phys.* **1996**, *53*, 21.

(558) Butler, R. F. *Paleomagnetism: Magnetics Domains to Geologic Terranes*; Blackwell Scientific Publications: Boston, MA, 1992.

(559) Rosensweig, R. E. *Ferrohydrodynamics*; Cambrige Univerity Press: New York, 1985.

(560) Bean, C. P.; Livingston, J. D. *J. Appl. Phys.* **1959**, *30*, 120S

(561) Giessen, A. A. *J. Phys. Chem. Solids* **1967**, *28* (2), 343.

(562) Panda, R. N.; Gajbhiye, N. S.; Balaji, G. *J. Alloys Compd.* **2001**, *326* (1−2), 50.

(563) Tronc, E.; Prené, P.; Jolivet, J. P.; Fiorani, D.; Testa, A. M.; Cherkaoui, R.; Noguès, M.; Dormann, J. L. *Nanostuct. Mater.* **1995**, *6*, 945.

(564) Fannin, P. C. *J. Mol. Liq.* **2004**, *114*, 79.

(565) Mendonca Dias, M. H.; Lauterbur, P. C. *Magn. Reson. Med.* **1986**, *3*, 328.

(566) Muller, R. N.; Roch, A.; Colet, J. M.; Ouakssim, A.; Gillis, P. *The Chemistry of Contrast Agents in Medical Magnetic Resonance Imaging*; Merbach, A. E., Toth, E., Eds.; Wiley: New York, 2001; Chapter 10, pp 417−435.

(567) Freed, J. H. *J. Chem. Phys.* **1978**, *68*, 4034.

(568) Hwang, L.-P.; Freed, J. H. *J. Chem. Phys.* **1975**, *63*, 118.

(569) Ayant, Y.; Belorizly, E.; Alizon, J.; Gallice, J. *J. Phys. (Paris)* **1975**, *36*, 991.

(570) Pfeifer, H. *Ann. Phys. (Berlin)* **1961**, *8*, 1.

(571) Roch, A.; Muller, R. N.; Gillis, P. *J. Magn. Reson. Imaging* **2001**, *14*, 94.

(572) Gueron, M. *J. Magn. Reson.* **1975**, *19*, 58.

(573) Roch, A.; Muller, R. N. *Proc. 11th Annu. Meet. Soc. Magn. Reson. Med.* **1992**, *11*, 1447.

(574) Roch, A.; Gillis, P.; Ouakssim, A.; Muller, R. N. *J. Magn. Magn. Mater.* **1999**, *201*, 77.

(575) Roch, A.; Muller, R. N.; Gillis, P. *J. Chem. Phys.* **1999**, *110*, 5403.

(576) Koenig, S. H.; Kellar, K. *Magn. Reson. Med.* **1995**, *34*, 227.

(577) Kellar, K. E.; Fuji, D. K.; Gunther, W. H. H.; Briley-Saebo, K.; Bjornerud, A.; Spiller, M.; Koening, S. H. *Magn. Reson. Mater. Phys. Biol. Med.* **1999**, *8*, 207.

(578) Kellar, K. E.; Fuji, D. K.; Gunther, W. H. H.; Briley-Saebo, K.; Bjornerud, A.; Spiller, M.; Koening, S. H. *J. Magn. Reson. Imaging* **2000**, *11*, 488.

(579) Muller, R. N.; Vallet, P.; Maton, F.; Roch, A.; Goudemant, J. F.; Vander Elst, L.; Gillis, P.; Peto, S. *Invest. Radiol.* **1990**, *22*, S34.

(580) Ouakssim, A.; Fastrez, S.; Roch, A.; Laurent, S.; Gossuin, Y.; Pierart, C.; Vander Elst, L.; Muller, R. N. *J. Magn. Magn. Mater.* **2004**, *272*, e1711.

(581) Muller, R. N.; Vander Elst, L.; Roch, A.; Peters, J. A.; Csajbok, E.; Gillis, P.; Gossuin, Y. *Adv. Inorg. Chem.* **2005**, *57*, 239.

(582) Roch, A.; Gossuin, Y.; Gillis, P.; Muller, R. N. *J. Magn. Magn. Mater.* **2005**, *293*, 532.

(583) Roch, A.; Bach-Gansmo, T.; Muller, R. N. *Magn. Reson. Mater. Phys. Biol. Med.* **1993**, *1*, 83.

(584) Weisskoff, R. M.; Zuo, C. S.; Boxeman, J. L.; Rosen, B. R. *Magn. Reson. Med.* **1994**, *31*, 601.

(585) Brown, R. J. S. *Phys. Rev.* **1961**, *121*, 1379.

(586) Jensen, J. H.; Chandra, R. *Magn. Reson. Med.* **2000**, *44*, 144.

(587) Brooks, R. A.; Moiny, F.; Gillis, P. *Magn. Reson. Med.* **2001**, *45*, 1014.

(588) Shen, T.; Weissleder, R.; Papisov, M.; Bogdanov, A.; Brady, T. J. *Magn. Reson. Med.* **1993**, *29*, 599.

(589) Weissleder, R.; Lee, A. S.; Khaw, B. A.; Shen, T.; Brady, T. J. *Radiology* **1992**, *182*, 381.

(590) Montet, X.; Weissleder, R.; Josephson, L. *Bioconjugate Chem.* **2006**, *17* (4), 905.

(591) Wang, Y.-X. J.; Hussain, S. M.; Krestin, G. P. *Eur. Radiol.* **2001**, *11*, 2319.

(592) Li, W.; Tutton, S.; Vu, A. T.; Pierchala, L.; Li, B.; Lewis, J.; Prasad, P. V.; Edelman, R. R. *J. Magn. Reson. Imaging* **2005**, *21*, 46.

(593) McLachlan, S. J.; Morris, M. R.; Lucas, M. A.; Fisco, R. A.; Eakins, M. N.; Fowler, D. R.; Scheetz, R. B. *J. Magn. Reson. Imaging* **1994**, *43*, 301.

(594) Reimer, P.; Marx, C.; Rummeny, E. J.; Müller, M.; Lentschig, M.; Balzer, T.; Dietl, K. H.; Sulkowski, U.; Berns, T.; Shamsi, K.; Peters, P. E. *J. Magn. Reson. Imaging* **1997**, *7*, 945.

(595) Simon, G. H.; von Vopelius-Feldt, J.; Fu, Y.; Schlegel, J.; Pinotek, G.; Wendland, M. F.; Chen, M. H.; Daldrup-Link, H. E. *Invest. Radiol.* **2006**, 41.

(596) Laumonier, C.; Segers, J.; Laurent, S.; Michel, A.; Coppée, F.; Belayew, A.; Vander Elst, L.; Muller, R. N. *J. Biomol. Screening* **2006**, *11* (5), 537.

(597) Montet, X.; Montet-Abou, K.; Reynolds, F.; Weissleder, R.; Josephson, L. *Neoplasia* **2006**, *8* (3), 214.

(598) Arbab, A. S.; Yocum, G. T.; Kalish, H.; Jordan, E. K.; Anderson, S. A.; Khakoo, A. Y.; Read, E. J.; Frank, J. A. *Blood* **2004**, *104* (4), 1217.

(599) Kalish, H.; Arbab, A. S.; Miller, B. R.; Lewis, B. K.; Zywicke, H. A.; Bulté, J. W. M.; Bryan, L. H.; Frank, J. A. *Magn. Reson. Med.* **2003**, *50*, 275.

(600) Schulze, E.; Ferrucci, J. T.; Poss, K.; Lapointe, L.; Bogdanova, A.; Weissleder, R. *Invest. Radiol.* **1995**, *30*, 604.

(601) Moore, A.; Marecos, E.; Bogdanov, A.; Weissleder, R. *Radiology* **2000**, *214*, 568.

(602) Sipe, J. C.; Filippi, M.; Martino, G.; Furlan, R.; Rocca, M. A.; Rovaris, M.; Bergami, A.; Zyroff, J.; Scotti, G.; Comi, G. *Magn. Reson. Imaging* **1999**, *17*, 1521.

(603) Zhao, M.; Beauregard, D. A.; Loizou, L.; Davletov, B.; Brindle, K. M. *Nat. Med.* **2001**, *7*, 1241.

(604) Frankel, A. D.; Pabo, C. O. *Cell* **1988**, *55*, 1189.

(605) Koch, A. M.; Reynolds, F.; Kircher, M. F.; Merkle, H. P.; Weissleder, R.; Josephson, L. *Bioconjugate Chem.* **2003**, *14*, 1115.

(606) Zhao, M.; Kircher, M. F.; Josephson, R.; Weissleder, R. *Bioconjugate Chem.* **2002**, *13*, 840.

(607) Stella, B.; Arpicco, S.; Peracchia, M. T.; Desmaële, D.; Hoebeke, J.; Renoir, M.; D'Angelo, J.; Cattel, L.; Couvreur, P. *J. Pharm. Sci.* **2000**, *11*, 145.

(608) Zhang, Y.; Kohler, N.; Zhang, M. *Biomaterials* **2002**, *23*, 1553.

(609) Bulte, J. W. *Methods Mol. Med.* **2006**, *124*, 419.

(610) Kohler, N.; Sun, C.; Wang, J.; Zhang, M. *Langmuir* **2005**, *21* (19), 8858.

(611) Petri-Fink, A.; Chastellain, M.; Juillerat-Jeanneret, L.; Ferrari, A.; Hofmann, H. *Biomaterials* **2005**, *26* (15), 2685.

(612) Quinti, L.; Weissleder, R.; Tung, C. H. *Nano Lett.* **2006**, *6* (3), 488.

(613) Perez, J. M.; Josephson, L.; Weissleder, R. *ChemBioChem* **2004**, *5* (3), 261.

(614) Perez, J. M.; O'Loughin, T.; Simeone, F. J.; Weissleder, R.; Josephson, L. *J. Am. Chem. Soc.* **2002**, *124* (12), 2856.

(615) Perez, J. M.; Josephson, L.; O'Loughlin, T.; Hogemann, D.; Weissleder, R. *Nat. Biotechnol.* **2002**, *20* (8), 816.

(616) Josephson, L.; Perez, J. M.; Weissleder, R. *Angew. Chem., Int. Ed.* **2001**, *40* (17), 3204.

(617) Zhao, M.; Josephson, L.; Tang, Y.; Weissleder, R. *Angew. Chem., Int. Ed.* **2003**, *42* (12), 1375.

(618) Perez, J. M.; Simeone, F. J.; Saeki, Y.; Josephson, L.; Weissleder, R. *J. Am. Chem. Soc.* **2003**, *125* (34), 10192.

(619) Grimm, J.; Perez, J. M.; Josephson, L.; Weissleder, R. *Cancer Res.* **2004**, *64* (2), 639.

(620) Harris, T. J.; von Maltzahn, G.; Derfus, A. M.; Ruoslahti, E.; Bhatia, S. N. *Angew. Chem., Int. Ed.* **2006**, *45* (19), 3161.

(621) Harris, T. J.; Maltzahn, G.; Derfus, A. M.; Ruoslahti, E.; Bhatia, S. N. *Angew. Chem., Int. Ed.* **2006**, *45*, 3161.

(622) Atanasijevic, T.; Shusteff, M.; Fam, P.; Jasanoff, A. *Proc. Natl. Acad. Sci. U.S.A.* **2006**, *103* (40), 14707.

(623) Sun, E. Y.; Weisseleder, R.; Josephson, L. *Small* **2006**, *2*, 1144.

(624) Tsourkas, A.; Hofstetter, O.; Hofstetter, H.; Weissleder, R.; Josephson, L. *Angew. Chem., Int. Ed.* **2004**, *43* (18), 2395.

(625) Moore, A.; Basilion, J. P.; Chiocca, E. A.; Weissleder, R. *Biochim. Biophys. Acta* **1998**, *1402*, 239.

(626) Moore, A.; Josephson, L.; Bhorade, R. M.; Basilion, J. P.; Weissleder, R. *Radiology* **2001**, *221*, 244.

(627) Weissleder, R.; Moore, A.; Mahmood, U.; Bhorade, R.; Benveniste, H.; Chiocca, E. A.; Basilion, J. P. *Nat. Med.* **2000**, *6*, 351.

(628) Cerdan, S.; Lotscher, H. R.; Kunnecke, B.; Seelig, J. *Magn. Reson. Med.* **1989**, *12*, 151.

(629) Kelly, K. A.; Nahrendorf, M.; Yu, A. M.; Reynolds, F.; Weissleder, R. *Mol. Imaging* **2006**, *8*, 201.

(630) Sonvico, F.; Mornet, S.; Vasseur, S.; Dubernet, C.; Jaillard, D.; Degrouard, J.; Hoebeke, J.; Duguet, E.; Colombo, P.; Couvreur, P. *Bioconjugate Chem.* **2005**, *16*, 1181.

(631) Gao, Y. *Nanotechnologies for the Life Sciences*; Kumar, C., Ed.; Wiley: New York, 2005; Vol. 1, Chapter 3: Biofunctionalization of Nanomaterials.

(632) Safarik, I.; Safarikova, M. *Biomagn. Res. Technol.* **2004**, *2* (1), 7.

(633) Fan, J.; Lu, J.; Xu, R.; Jiang, R.; Gao, Y. *J. Colloid Interface Sci.* **2003**, *266*, 215.

(634) Xu, C.; Xu, K.; Gu, H.; Zheng, R.; Liu, H.; Zhang, X.; Guo, Z.; Xu, B. *J. Am. Chem. Soc.* **2004**, *126*, 9938.

(635) Gu, H.; Ho, P. L.; Tsang, K. W. T.; Wang, L.; Xu, B. *J. Am. Chem. Soc.* **2003**, *125*, 15702.

(636) Chen, D. W.; Liao, M. H. *J. Mol. Catal. B: Enzym.* **2002**, *16*, 283.

(637) Kumar, C. S. S. R.; Leuschner, C.; Doomes, E. E.; Henry, L.; Juban, M.; Hormes, J. *J. Nanosci. Nanotechol.* **2004**, *4*, 245.

(638) Ho, K.-C.; Tsai, P.-J.; Lin, Y.-S.; Chen, Y.-C. *Anal. Chem.* **2004**, *76*, 7162.

(639) Bourlinos, A. B.; Bakandritos, A.; Georgakilas, V.; Petridis, D. *Chem. Mater.* **2002**, *14*, 3226.

(640) Boai, A. K.; Das, K.; Gray, M.; Rotello, V. M. *Chem. Mater.* **2002**, *14*, 2628.

(641) Lu, J.; Fan, J.; Xu, R.; Roy, S.; Ali, N.; Gao, Y. *J. Colloid Interface Sci.* **2003**, *258*, 427.

(642) Portet, D.; Denizot, B.; Rump, E.; Lejeune, J. J.; Jallet, P. *J. Colloid Interface Sci.* **2001**, *238*, 37.

(643) Wang, Y.; Wong, J. F.; Teng, X.; Lin, X. Z.; Yang, H. *Nano Lett.* **2003**, *3*, 1555.

(644) Kohler, N.; Fryxell, G. E.; Zhang, M. *J. Am. Chem. Soc.* **2004**, *126*, 7206.

(645) Hirsch, R.; Katz, E.; Willner, I. *J. Am. Chem. Soc.* **2000**, *122*, 12053.

(646) Reddy, J. A.; Low, P. S. *Crit. Rev. Ther. Drug Carrier Syst.* **1998**, *15*, 587.

(647) Lu, Y.; Yin, Y.; Mayers, B. T.; Xia, Y. *Nano Lett.* **2002**, *2*, 183.

(648) Stöber, W.; Fink, A.; Bohn, E. *J. Colloid Interface Sci.* **1968**, *26*, 62.

(649) Gao, X.; Yu, K. M. K.; Tam, K. Y.; Tsang, S. C. *Chem. Commun.* **2003**, 2998.

(650) Bucak, S.; Jones, D. A.; Laibinis, P. E.; Hatton, T. A. *Biotechnol. Prog.* **2003**, *19*, 477.

(651) Alexiou, C.; Schmid, R. J.; Jurgons, R.; Kremer, M.; Wanner, G.; Bergemann, C.; Huenges, E.; Nawroth, T.; Arnold, W.; Parak, F. G. *Eur. Biophys. J.* **2006**, *35* (5), 446.

(652) Kohler, N.; Sun, C.; Fichtenholtz, A.; Gunn, J.; Fang, C.; Zhang, M. *Small* **2006**, *2* (6), 785.

(653) Gallo, J. M.; Varkonyi, P.; Hassan, E. E.; Groothius, D. R. *J. Pharmacokinet. Biopharm.* **1993**, *21* (5), 575.

(654) Jordan, A.; Wust, P.; Fahling, H.; John, W.; Hinz, A.; Felix, R. *Int. J. Hyperthermia* **1993**, *9*, 51.

(655) Jordan, A.; Scho1z, R.; Wust, P.; Fähling, H.; Felix, R. *J. Magn. Magn. Mater.* **1999**, *210*, 413.

(656) Moroz, P.; Jones, S. K.; Gray, B. N. *Int. J. Hyperthermia* **2002**, *18*, 267.

(657) Paulides, M. M.; Bakker, J. F.; Zwamborn, A. P. M.; van Rhoon, G. C. *Int. J. Hyperthermia* **2007**, *23* (1), 59.

(658) Sneed, P. K.; Stauffer, P. R.; McDermott, M. W.; Diederich, C. J.; Lamborn, K. R.; Prados, M. D.; Chang, S.; Weaver, K. A.; Spry, L.; Malec, M. K.; Lamb, S. A.; Voss, B.; Davis, R. L.; Wara, W. M.; Larson, D. A.; Phillips, T. L.; Gutin, P. H. *Radiat. Oncol. Biol. Phys.* **1998**, *40*, 287.

(659) Rau, B.; Wust, P.; Tilly, W.; Gellermann, J.; Harder, C.; Riess, H.; Budach, V.; Felix, R.; Schlag, P. M. *Int. J. Radiat. Oncol., Biol., Phys.* **2000**, *48*, 381.

(660) Johnson, R. H.; Robinson, M. P.; Preece, A. W.; Green, J. L.; Pothecary, N. M.; Railton, C. J. *Phys. Med. Biol.* **1993**, *38* (8), 1023.

(661) Van den Berg, C. A. T.; Bartels, L. W.; De Leeuw, A. A. C.; Lagendijk, J. J. W.; Van de Kame1, J. B. *Phys. Med. Biol.* **2004**, *49*, 5029.

(662) Rosensweig, R. E. *J. Magn. Magn. Mater.* **2002**, *252*, 370.

(663) Jordan, A.; Scholz, R.; Wust, P.; Schirra, H.; Schiestel, T.; Schmidt, H.; Felix, R. *J. Magn. Magn. Mater.* **1999**, *194*, 185.

(664) Jordan, A.; Scholz, R.; Maier-Hauff, K.; Johannsen, M.; Wust, P.; Nadobny, J.; Schirra, H.; Schmidt, H.; Deger, S.; Loening, S.; Lanksch, W.; Felix, R. *J. Magn. Magn. Mater.* **2001**, *225*, 118.

(665) Wust, P.; Gneveckow, U.; Johannsen, M.; Bohmer, D.; Henkel, T.; Kahmann, F.; Sehouli, J.; Felix, R.; Ricke, J.; Jordan, A. *Int. J. Hyperthermia* **2006**, *22*, 673.

(666) Babincova, M.; Ciemanece, P.; Altanerova, V.; Altaner, C.; Babinece, P. *Bioelectrochemistry* **2002**, *55*, 17.

(667) De Gennes, P. G. *Macromolecules* **1980**, *13*, 1069.

(668) Marinescu, G.; Patron, L.; Culita, D. C.; Neagoe, C.; Lepadatu, I.; Balint, I.; Bessais, L.; Cizmas, C. B. *J. Nanopart. Res.* **2006**, *8*, 1045.

(669) Whitesides, G. M. *Angew. Chem., Int. Ed.* **2004**, *116*, 3716.